Master's thesis

NTNU
Norwegian University of Science and Technology

Finja Tietjen

RKKY Interaction in Unconventional Superconductors

Master's thesis in Physics
Supervisor: Jacob Linder
May 2023

NTNU
Norwegian University of
Science and Technology

Finja Tietjen

RKKY Interaction in Unconventional Superconductors

Master's thesis in Physics
Supervisor: Jacob Linder
May 2023

Norwegian University of Science and Technology

NTNU
Norwegian University of
Science and Technology

Sammedrag

Med den økende interessen for ikke-konvensjonelle superledere og jakten på kontrollerbare kvantebits, har Ruderman-Kittel-Kasuya-Yosida (RKKY) vekselvirkningen, en viktig utveklslings-vekselsvirkning mellom lokale spinnmomenter mediert av ledningselektroner, blitt gjennomgående studert i forskjellige systemer, slik som vanlige metaller, konvensjonelle superledere, og normale metaller med spinn-bane-kobling (SBK).

I dette arbeidet er fokuset på å undersøke RKKY vekselvirkningen i en ikke-konvensjonell superleder, hvor inversjonssymmetrien er brutt, og dermed har en Rashba SBK. Både analytiske beregninger, ved bruk av Schrieffer-Wolff transformasjonen (SWT) og numeriske simuleringer ved hjelp av Bogoliubov-de Gennes (BdG) metoden blir brukt for å analysere vekselvirkningen.

Funnene i oppgaven viser at i ikke-konvensjonelle superledere har RKKY vekselvirkningen de forventede Heisenberg og Dzyaloshinskii-Moriya (DM) komponentene. Vi observerer også at Ising-komponenten er større enn forventet, som tyder på en innflytelse fra spesifikke egenskaper ved den ikke-konvensjonelle superledende tilstanden. Videre finner vi at egenskapene til RKKY vekselvirkningen blir mer lik den av et normalt metall, mes degenerasjonen av vekselvirkningen minskes.

Abstract

With the rising interest in unconventional superconductors and the pursuit of controllable quantum bits, the Ruderman-Kittel-Kasuya-Yosida (RKKY) interaction, an important exchange interaction between localized spins mediated by conduction electrons, has been extensively studied in various systems such as normal metals, conventional superconductors, and normal metals with spin-orbit coupling (SOC).

In this work, the focus is on investigating the RKKY interaction in unconventional superconductors, which have broken inversion symmetry and consequently Rashba-type SOC. Both analytical calculations using the Schrieffer-Wolff transformation (SWT) and numerical simulations using the Bogoliubov-de Gennes (BdG) approach are employed to analyze the interaction.

The findings reveal that in unconventional superconductors, the RKKY interaction exhibits the expected Heisenberg and Dzyaloshinskii-Moriya (DM) components. Interestingly, we observe that the Ising component is larger than anticipated, suggesting the influence of specific characteristics of the unconventional superconducting state. Furthermore, we observe that the behavior of the RKKY interaction becomes more akin to that of a normal metal, while the degeneracy of the interaction decreases.

Thank You

This thesis marks the end of my studies, first in Göttingen for my bachelor's and the last two years in Trondheim for my master's. It has been an incredible journey on which I learned not only a lot about physics, research and stress management, but I also had to opportunity to study abroad, learn new languages and get acquainted with new cultures, and grew personally a lot. All that would not have been possible all by myself, therefore I would like to thank all that have made it possible.
Jacob Linder made this thesis possible in the first place as he agreed to be my supervisor and explained all the fundamental physics to me. During the writing, he helped me to stay goal oriented and find the next logical or previously wrong step.
Jabir Ali Ouassou was always happy to discuss my code and physical intuition. That did not only help me with the details, but also restored my confidence after days or weeks of struggles.
Johanne was not only an important training partner, but also a great discussion partner. Although our topics were quite different, we explained it so often to each other that we probably could each write about the other's topic. We also made sense of the master student life together and worked out how to deal with the ups and downs.
Thank you!

The following is in German and for my family and German friends. Max und Jonas haben die ersten Entwürfe dieser Arbeit gelesen und kommentiert. Beide haben eine andere Perspektive auf das Thema als ich und konnten dadurch nochmal neue Aspekte einbringen. Dadurch haben beide nicht nur die Verständlichkeit dieser Arbeit verbessert, sondern auch die eingenommenen Perspektiven erweitert. Danke dafür!
Fast sechs Jahre zu studieren und dann den Kopf für ein so langes Projekt zu haben, erfordert, dass es Menschen gibt, die sich um einen kümmern. Meine Familie und Kim haben mich durch alle Zweifel begleitet und meine Erfolge noch mehr als ich gefeiert. Sie haben sich alle möglichen Ideen - ob gut oder schlecht - angehört und mich ernst und wahrgenommen. Dafür möchte ich euch von ganzem Herzen danken!

Contents

List of Figures

1 Introduction

The interest in the field of spintronics has been steadily increasing for several decades, further fueled by the public's fascination with quantum computing. Recent reports from the Intergovernmental Panel on Climate Change (IPCC) on global energy consumption underscore the significance of research and development in low-energy consumption for electricity, information transfer, and storage [1, 2]. Superconductors have long played a crucial role in this field due to their unique electron transport properties.

Ongoing research on the characterization of various superconductors has led to the discovery of increasingly complex and exotic materials. In particular, high-transition-temperature and heavy fermion superconductors have been extensively studied in recent decades, prompting the need for theoretical explanations of experimental findings. One distinguishing characteristic of many heavy fermion and some high-transition-temperature superconductors is their unconventional alternated gap symmetry, placing them in the category of unconventional superconductors [3, 4]. The wide range of transition temperatures exhibited by this class of superconductors holds fundamental importance for potential applications.

Simultaneously, advancements in experimental techniques for examining spin structures have allowed for the study of groundstate configurations of impurity spins in different materials. This means that predictions for groundstate spin configurations, based on the Rudermann-Kittel-Kasuya-Yosida (RKKY) interaction theory, can now be tested across a variety of materials.

When the RKKY interaction between impurity spins is understood in known materials, it can be utilized to determine the characteristics of new materials. Furthermore, the surrounding material can control the impurity spins, as the RKKY interaction is heavily dependent on the environment. This results in controllable bits of atomic-scale information, which holds promise for information transport and storage.

The recent experimental and theoretical progress in understanding unconventional superconductors has given rise to the research question addressed in this thesis: How does the RKKY interaction behave in unconventional superconductors?

Extensive studies have already been conducted on the RKKY interaction in conventional superconductors, including investigations in the presence of magnetic fields [5]. The crucial distinction between conventional and unconventional superconductors lies in the permissible pairing symmetries for Cooper pairs. Various symmetries and symmetry-breaking mechanisms are possible. For superconductors with d-wave symmetry, Aristov et al. examined the RKKY interaction and found that the spin structure is more complex in such anisotropic superconductors compared to the conventional case [6]. However, an increasing number of superconductors potentially exhibit p-wave symmetry, which has already been shown to give rise to a range of intriguing phenomena [7]. One of the most promising candidates for p-wave pairing of Cooper pairs is CePt3Si [8], where the inversion symmetry is spontaneously broken. The RKKY interaction in such non-centrosymmetric superconductors without inversion symmetry has not yet been studied, making it the focus of this thesis.

After this introduction, the thesis proceeds with an explanation of the underlying theory. The concepts of conventional and unconventional superconductivity are introduced in the framework of second quantization formalism, which is briefly derived. For unconventional superconductors, a broken symmetry is necessary, which is combined with the spin-orbit coupling (SOC) explained in subsequent sections. The next section provides an introduction to RKKY interaction, laying the foundation for the subsequent analysis. The Bogoliubov-de Gennes and Schrieffer-Wolff transform-

ations, which are the primary tools for determining the energy spectrum and effective interaction in the investigated systems, are presented in Sec. 3. Additionally, the numerical approach is outlined, along with the computed observables.
Sec. 4 examines the first of four different systems - a normal metal with RKKY interaction. This investigation, combined with the examination of RKKY interaction in conventional superconductors in Sec. 5, allows to put the chosen methods to the test. In Sec. 6, SOC is introduced to a normal metal, which enables to explore the boundaries of known RKKY interaction behaviors. By studying a normal metal with SOC, expectations for the unconventional superconductor analyzed in Sec. 7 can be developed. Here, the main focus is on RKKY interaction in a superconductor with Rashba-type SOC. Bound states resulting from the p-wave symmetry of the gap are also briefly investigated. Lastly, the obtained results are discussed in Sec. 8, which also comprises some suggests for further theoretical and experimental work.
During the course of this master's thesis, a poster was presented on DPG Spring Meeting 2023 in Dresden, where a science slam additionally presented the topic in an entertaining way. A teaser for the science slam can be found in App. G and the poster in App. F. Moreover a video about the basic concept of superconductors was created [9].
All code used in this thesis can be found on GitHub [10].

2 Theoretical Background

The following sections of this chapter are going to give an overview of the theories fundamental to this thesis. At first the indirect interaction between spins via conduction electrons (RKKY interaction) is introduced. Secondly, a brief introduction is given to 2nd quantization, which is the formalism used throughout. Then the 2nd quantization is used to give an introduction to superconductivity, which is first discussed for conventional superconductors. After that spin orbit coupling (SOC) is introduced, because it is, in combination with broken inversion symmetry, leading to unconventional superconductivity as discussed in the last section of this chapter.
Ultimately, these formalisms and concepts allow us to formulate the Hamiltonian of the system of interest.
Note that the constant $\hbar$ is set to unity throughout the entire thesis.

2.1 RKKY Interaction

The concept of the Rudermann-Kittel-Kasuya-Yosida (RKKY) interaction was firstly discussed by M. Rudermann and C. Kittel as an explanation for the broadened lines found in nuclear spin resonance experiments [11]. It was introduced as the indirect exchange coupling between magnetic moments in a metal via the direct hyperfine interaction with the conduction electrons. T. Kasuya and K. Yosida expanded this theory to localized inner d-electron interactions [12, 13].
The derivation of different characteristics of the RKKY-interaction takes a non-magnetic metal with two impurity spins, which do not directly interact with each other, as a starting point. This is schematically illustrated in Fig. 1(a), where the two large arrows with blue background represent the impurity spins and the small arrows with red background are the itinerant spins. The interactions between them are indicated by the double-tipped arrows of which the bright red one is the direct spin-spin interaction and the dark red one the RKKY interaction, which is going to derived in the following for a non-magnetic metal.
Consequently, the conduction electrons of the metal can be described by the Sommerfeld model and their spin is assumed to interact locally and directly with the impurity spins, which leads to the general expression for the RKKY interaction

$$H_{RKKY} = \sum_{i=1}^{2} J\vec{S}_i\vec{s}_i \tag{2.1}$$

where J denotes the coupling strength between the classic local spin $\vec{S}_i$ and the quantum mechanical itinerant spin $\vec{s}_i$. The itinerant spins can be expressed via fermionic creation and annihilation operators $c^{[\dagger]}$ and transformed into k-space. J is assumed to be of Heisenberg type, since direct spin-spin exchange interaction is considered. Based on that expression, the effect of the RKKY-interaction onto the system can be studied via perturbation theory.
To first order in perturbation the correction to the groundstate energy is zero, because the electron system is not spin-polarized. To second order in perturbation, there is a contribution due to the fact that excited states are taken into account. If those excited states correspond to particle-hole excitations, their contribution is not vanishing. When using the formalism of spin states and the Pauli matrices, the energy correction to the groundstate energy to second order in perturbation

theory reads

$$E_0^{(2)} = \frac{-J^2\hbar^2}{2N^2} \sum_{\substack{k,q \\ i,j}} \Theta_{k,k+q} e^{-iq(r_i - r_j)} \frac{\langle f|\vec{S}_i \cdot \vec{S}_j|f\rangle}{\epsilon(k+q) - \epsilon(k)}$$

where Θ is the Heaveside-stepfunction, $\epsilon(k)$ is the energy of the unperturbed system, N the total number of particles and $|f\rangle$ is the spin state of the itinerant electrons.
Therefore the coupling constant J is

$$J_{ij}^{RKKY} = \frac{J^2\hbar^2}{2N^2} \sum_{k,q,m_s} \sum_{i,j=1}^{2} \Theta_{k,k+q} e^{-iq(r_i - r_j)} \frac{\langle f|\vec{S}_i \cdot \vec{S}_j|f\rangle}{\epsilon(k+q) - \epsilon(k)} \tag{2.2}$$

which can be evaluated and shows an oscillatory behavior as a function of the separation $R = (r_i - r_j)$ of the impurity spins.
The oscillatory nature of this interaction can also be understood based on the electron density between the two impurity spins. When treating the impurity spins as ferromagnetic layers that enclose a non-magnetic layer representing the normal metal, it becomes clear that the wave function of the electron depends on the free plane-wave and a reflected wave. The probability of finding an electron at a certain position described by its wave function Π is therefore

$$|\Pi(x)|^2 = |\exp(ikx) + R\exp(-ikx)|^2 = 1 + R^2 + 2R\cos(2kx) \tag{2.3}$$

with the reflection coefficient R, real space coordinate x, and wave vector k. Therefore the spin-density of the electrons varies proportional to $\cos(x)$. Since the electrons are the carries of the spin information that facilitate the indirect interaction between the fixed spins, this interaction is also of oscillatory nature.
The expectation value in Eq. 2.2 can be evaluated and it is possible to explicitly study its distance dependence. In order to do so, the sum over k-space is converted into an integral in polar coordinates and zero temperature is assumed. Additionally, the energies ϵ are taken to be the free electron dispersion, which allows for an easier derivation here. This leads to

$$\begin{aligned} I_{nm} &= -\frac{J^2}{N^2} \sum_{k,k'} \Theta_{k,k'} \frac{e^{i(k-k')(r_i - r_j)}}{\epsilon_k - \epsilon_{k'}} \\ &= \frac{J^2V^2}{N^2(2\pi)^6} \int_0^{2\pi} d\alpha \int_{k_F}^{\infty} dk \int_0^{k_F} dk' \frac{-2m^*}{\hbar^2} kk' \frac{e^{i(k-k')(r_i - r_j)\cos(\alpha)}}{k^2 - k'^2} \end{aligned}$$

as the integral to solve for determining the distance dependence. The angular integral can be evaluated by using the substitution $x = \cos(\alpha)$. After that the lower boundary of the k-integral is changed to zero. That is possible, because the additional interval has a vanishing integral in combination with the k'-integral. Therefore, the k-space integral reads

$$I_{nm} = \frac{-2m^*J^2V^2}{N^2(2\pi)^6\hbar^2} \int_0^{\infty} dk \int_0^{k_F} dk' kk' \frac{\sin(k'R)\sin(kR)}{k^2 - k'^2}$$

where the short-hand notation $R = (r_i - r_j)$ is used. Now, the integral over k can be evaluated and after using a trigonometric identity, the expression takes the form

$$I_{nm} = \frac{-2m^*J^2V^2}{N^2(2\pi)^6\hbar^2} \int_0^{k_F} dk' k' \frac{\pi}{4} \sin(2k'R)$$

The remaining integral can be calculated using the implicit derivation of the sine function with respect to the distance R. Finally, the expression is rearranged such that all dependencies on the distance and the Fermi-momentum are explicit, which yields

$$\begin{aligned} I_{nm} &= \frac{-2m^* J^2 V^2}{N^2 (2\pi)^6 \hbar^2} \int_0^{k_F} dk' \frac{-\pi}{8} \frac{d}{dR} \cos(2k'R) \\ &= \frac{m^* J^2 V^2 \pi}{N^2 (2\pi)^6 \hbar^2} k_F^4 R^2 \frac{\sin(2k_F R) - 2k_F R \cos(2k_F R)}{(2k_F R)^4} \end{aligned}$$

This expression can be simplified to the proportionality

$$J_{ij} \sim \frac{\sin(R) - R\cos(R)}{R^4} \tag{2.4}$$

and Fig. 1(b) illustrates the resulting oscillation for the normalized $R = R'/(2k_F)$. It is clearly visible that the interaction strength oscillates around zero and is damped quickly. Since a positive interaction constant favors anti-parallel spin alignment, while a negative interaction constant favors parallel alignment, the impurity spins oscillate between parallel and anti-parallel alignment with their separation distance. The exact behavior of the interaction strength J_{ij} depends on the system as will be shown in the later sections.

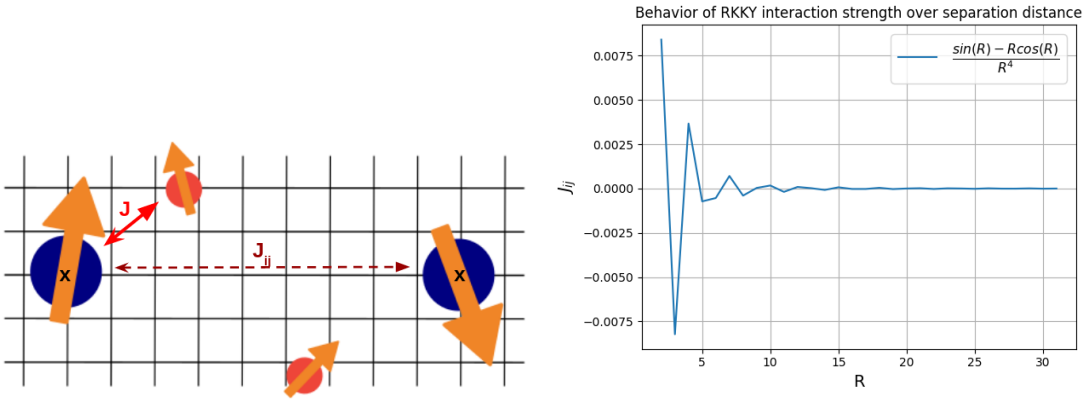

(a) (b)

Figure 1: (a) Schematic picture of RKKY interaction mechanism and (b) its oscillatory behavior. J_{ij} and R are normalized against the Fermi-energy k_F.

The oscillatory behavior has also been explicitly derived in the tight-binding approach for graphene [14], which is just one example for derivations based on different electron dispersions. Regardless of the exact electron dispersion, a damped oscillation comprised of sin and cos terms over R^n is expected, where n is the dimension of the system [15].

2.1.1 Spin Structure

The indirect interaction of spins leads to an effective interaction, which can take the same forms as direct spin interaction. Most of these interactions can be described in the framework of the Hubbard model [16], where different electron-electron interactions stem from Coulomb interaction. Depending on the approximations or restrictions applied, the Hubbard model gives rise to different spin-spin interactions.

The first one is called Heisenberg interaction and it takes the form

$$H_{\text{Heisenberg}} = \sum_{i,j} J_{ij} \mathbf{S}_i \cdot \mathbf{S}_j$$

where $\mathbf{S}_i$ denotes a classical spin and J is the interaction strength. This interaction strength is the same for all components of the spins, but might vary for the different lattice sites. It can give rise to ferromagnetic and anti-ferromagnetic order of spins, because we have $\mathbf{S}_i \cdot \mathbf{S}_j = S_{i,x}S_{j,x} + S_{i,y}S_{j,y} + S_{i,z}S_{j,z}$ and therefore the spins either try to minimize their total spin (anti-ferromagnetic) or maximize it (ferromagnetic) depending on the sign of J.
It can be seen that it is possible to have different interaction strengths for different components of the spins, which results in Ising interaction. It takes the form

$$H_{\text{Ising}} = \sum_{i,j} \mathbf{I}_{ij} \cdot (\mathbf{S}_i \cdot \mathbf{S}_j)$$

where the interaction strength $\mathbf{I}_{ij}$ itself is a vector now. Therefore the Ising interaction of spins can reflect asymmetries in the system, since each spin component gets their individual interaction strength.
In both cases, Heisenberg and Ising, the spins only interact componentwise with each other. But in more complex structures that can change and the spin components can act in arbitrary ways. That gives rise to the Dzyaloschinskii-Moriya (DM) interaction, which is based on the cross product between two spins

$$H_{\text{DM}} = \sum_{i,j} \mathbf{D}_{ij} (\mathbf{S}_i \times \mathbf{S}_j)$$

and has an interaction strength $\mathbf{D}_{ij}$ that can vary for the different components of the cross product. This type of interaction allows for twisted spin configurations and does not give rise to simple ferromagnetic or anti-ferromagnetic ordering.
Lastly, all remaining interaction types are going to be collected in a tensor in this thesis. It takes the form

$$H_{\text{remaining}} = \sum_{i,j} \mathbf{S}_i \cdot \overleftrightarrow{\Gamma}_{ij} \cdot \mathbf{S}_j$$

where $\overleftrightarrow{\Gamma} \in \mathbf{R}^{3x3}$ is the interaction strength.
The combination of this four spin-spin interaction types allows to express any kind of spin configuration including highly complex ones.

2.2 2nd Quantization

Quantum mechanics can be formulated with the Schrödinger equation and wave functions, which in combination give an accurate description of any system. For interacting many body systems like found in condensed matter systems, the wave function depends on as many variable sets as particles in the system. Therefore, it becomes extremely cumbersome to solve the wave function to a many body system, leaving even relatively simple systems nearly unsolvable.
2nd quantization resolves this problem by working with occupation numbers and their corresponding basis and operators, instead of wave functions. Its name stems from the fact, that particles are

already a description that comes out of the quantization of energy spectra and now these particles are going to be described by a formalism which is quantized even further. The full derivation is beyond the scope of this thesis and is extensively covered in textbooks [17, 18]. Nevertheless, the main concept is explained in the following.
Many particle states can be expressed as a product of single particle states $|\Psi(x)\rangle$, where x represents all quantum numbers needed to uniquely define this state. Those quantum numbers can include space $\mathbf{r}$ and spin projection σ. This notation adapts to many particle systems such that $|\Psi\rangle = |\Psi(x_1, x_2, \ldots, x_N)\rangle$ represents a state of N particles.
In quantum mechanics, indistinguishable particles are used to describe the system without actually considering each individual particle, but more their distribution over different states. There are still some differences between those particles, namely they can be distinguished into two different types: into bosons that act even under exchange of two bosons, and into fermions that pick up a minus sign when exchanging two of them. These signs do not not influence the expectation value of the wave function since it is quadratic. But this only holds true as long as the particles have different coordinates. When they have identical coordinates aka. quantum numbers, the Pauli principle applies to the fermions resulting into a wave function equaling zero when two fermions are exchanged. Bosons, however are not influenced by the Pauli exclusion principle.
This can be expressed in an occupation number basis, where the many particle states becomes

$$|\Psi\rangle = |n_{\lambda_1}, n_{\lambda_2}, n_{\lambda_3}, \ldots\rangle$$

with n being the number of particles in the quantum states defined by the set of quantum numbers λ_i. For bosons, there are none, one or more particles allowed in each state, so $n \geq 0$, But it is $n = 0, 1$ for fermions, since the Pauli exclusion principle applies.
Such states are created from vacuum by creation operators commonly denoted as $c^\dagger_\lambda$ ($\tilde{c}^\dagger_\lambda$) for fermions (bosons), which creates exactly one particle in state λ. The symbol † denotes the adjoint of the respective operator. Particles can also be destroyed by the annihilation operators c_λ ($\tilde{c}_\lambda$), which removes one particle of state λ. Any possible state can be constructed using a combination of these four operators, including systems allowing for hopping and superconductivity.
Commutation relations are an important property of quantum mechanical operators and for the fermionic particle operators in 2nd quantization formalism they are

$$\{c_{\lambda_1}, c^\dagger_{\lambda_2}\} = c_{\lambda_1} c^\dagger_{\lambda_2} + c^\dagger_{\lambda_2} c_{\lambda_1} = \delta_{\lambda_1,\lambda_2}$$
$$\{c_{\lambda_1}, c_{\lambda_2}\} = \{c^\dagger_{\lambda_1}, c^\dagger_{\lambda_2}\} = 0$$

where $\{\ldots\}$ denotes the anti-commutator.
For bosons, the commutator $[\ldots]$ is used formulate their commutation relations, which read

$$[\tilde{c}_{\lambda_1}, \tilde{c}^\dagger_{\lambda_2}] = \tilde{c}_{\lambda_1} \tilde{c}^\dagger_{\lambda_2} - \tilde{c}^\dagger_{\lambda_2}, \tilde{c}_{\lambda_1} = \delta_{\lambda_1,\lambda_2}$$
$$[\tilde{c}^\dagger_{\lambda_1}, \tilde{c}^\dagger_{\lambda_2}] = [\tilde{c}_{\lambda_1}, \tilde{c}_{\lambda_2}] = 0$$

Any kind of operator like hopping, Coulomb repulsion or attractive interaction between two electrons can be represented in 2nd quantization by combining an interaction potential and the needed number of particle operators. That interaction potential can depend on all, some or no quantum numbers of the system. Depending on the number of particles such an operator acts on, it is called single-, two- , three-, ... particle operator. In this thesis, only operators acting on up to two particles are relevant.

One famous two-particle operator is the interaction between electrons, which can be repulsive as in the Coulomb interaction or attractive nature. The attractive interaction is the basis for a theory of superconductivity, which introduced in the next chapters.

2.3 Superconductivity

Superconductors are materials in their superconducting phase, which is reached upon cooling down the material. Typically, these materials show some kind of conductivity before the phase transition and change their behavior strongly under the transition. Zero electric resistivity and the Meissner effect characterize the superconducting phase [19, 20], which is entered when the critical temperature is crossed. The Meissner effect describes the magnetic behavior of superconductors, which most prominently features the expulsion of magnetic fields.
Superconductors offer promising possibilities for applications, especially because of their perfect conductance. But the required low temperatures constrain the applications so far, even though current superconductors in use have critical temperatures within the regime of liquid nitrogen [4, 21]. They are therefore mainly used to generate strong magnetic fields in for example particle accelerators [22] or magnetic resonance imaging (MRI) [23]. There also exist different smaller technical applications like magnetometers [24], but to make superconductors more accessible and more controllable, a deeper understanding of their properties is necessary.

2.3.1 Attractive Interaction

For superconductivity to arise, an attractive interaction between electrons is necessary. This can be a very weak interaction, as seen over the course of this section, but it has to overcome the Coulomb repulsion. There are several mechanisms leading to such an attractive interaction, but the phonon mediated electron-electron interaction is the basis for BCS theory. Therefore it is explained in more detail here.
A system with interacting electrons and phonons can be described by the Fröhlich Hamiltonian

$$\begin{aligned} H_F = &\sum_{\mathbf{k},\sigma} \epsilon_{\mathbf{k}} c^\dagger_{\mathbf{k},\sigma} c_{\mathbf{k},\sigma} + \sum_{\mathbf{q}} \hbar\omega_{\mathbf{q}} \left(\frac{1}{2} + a^\dagger_{\mathbf{q}} a_{\mathbf{q}} \right) \\ &+ \sum_{\mathbf{k},\mathbf{q}} g_{\mathbf{k},\mathbf{q}} c^\dagger_{\mathbf{k}+\mathbf{q},\sigma} c_{\mathbf{k},\sigma} \left(a_{\mathbf{q}} + a^\dagger_{-\mathbf{q}} \right) \end{aligned}$$

where $c^{[\dagger]}_{\mathbf{k},\sigma}$ annihilates [creates] an electron with momentum $\mathbf{k}$ and spin σ with the associated energy of $\epsilon_{\mathbf{k}}$. Phonons are annihilated [crated] by $a^{[\dagger]}_{\mathbf{q}}$ for momentum $\mathbf{q}$. The first term is the kinetic energy of electrons and the second term of phonons. The third term describes their interaction, which can be treated as a perturbation. Consequently, the effective interaction can be obtained using Schrieffer-Wolff transformation as explained in Sec. 3.2. The resulting effective electron-electron potential mediated by phonons is

$$V_{eff} = g_{\mathbf{k},\mathbf{q}} g_{\mathbf{k}',-\mathbf{q}} \frac{\omega_{\mathbf{q}}}{\left(\epsilon_{\mathbf{k}'} - \epsilon_{\mathbf{k}'-\mathbf{q}}\right)^2 - \left(\hbar\omega_{\mathbf{q}}\right)^2}$$

and becomes attractive i.e. negative for $\left(\epsilon_{\mathbf{k}'} - \epsilon_{\mathbf{k}'-\mathbf{q}}\right)^2 < \left(\hbar\omega_{\mathbf{q}}\right)^2$ and vanishes quickly for large energy differences $\epsilon_{\mathbf{k}'} - \epsilon_{\mathbf{k}'-\mathbf{q}}$. This leads to seeing the potential as constant within a thin shell of width q around the Fermi level and outside of this thin shell the potential is often neglected.

Electrons in crystals also experience the repulsive Coulomb interaction, which looks like

$$H_C = \sum_{\sigma,\sigma'} \sum_{\mathbf{k},\mathbf{k}',\mathbf{q}} V_C(\mathbf{q}) c^\dagger_{\mathbf{k}+\mathbf{q},\sigma} c^\dagger_{\mathbf{k}'-\mathbf{q},\sigma'} c_{\mathbf{k}',\sigma'} c_{\mathbf{k},\sigma}$$

in second quantization formalism. It describes a scattering process with momentum transfer $\mathbf{q}$. The Coulomb potential $V_C = \frac{4\pi e^2}{\mathbf{q}^2}$ is screened by the electrons in the system, whose density is $N(\epsilon)$. Since we are interested in the total interaction of electrons within a thin shell around the Fermi level, the renormalized Coulomb potential has the form

$$V_C = \frac{4\pi e^2}{\mathbf{q}^2 + 4\pi e^2 N(\epsilon_F)}$$

This potential weakens with increasing density of states at the Fermi level, which means it is relatively weak in good metals with a high density of states at the Fermi level.
Nevertheless, the repulsive Coulomb interaction counteracts the attractive phonon-mediated interaction. But while the phonon-mediated interaction is strongly localized in k-space around the Fermi surface, the Coulomb interaction is focused in time. Therefore the phonon-mediated interaction acts over larger time-scales than the Coulomb interaction, which allows it to overcome the repulsion when the electrons are separated by time.
A classic analog to this is depicted in Fig. 2. The attractive interaction can be understood by looking at two traveling electrons. Because of their charge they will deform the ion lattice in such way that they create an area with higher opposite charge. This higher charge density remains long after the electron left and is felt by the other electron, which means that it is attracted to the path of the first electron. Due to this retardation effect, the electrons are able to interact attractive despite of the present Coulomb interaction. The resulting electron pairs are called Cooper pairs and have integer spin (as opposed to half integer spin of single electrons). That integer spins makes them bosons and behave accordingly to the Bose-Einstein statistic, which in turn means that they are in a collective, macroscopic quantum state and do, for example, not experience resistance anymore.

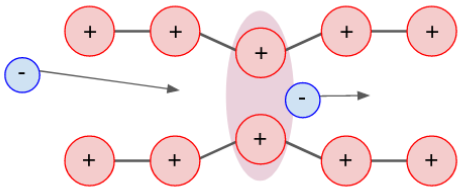

Figure 2: The deformation of the lattice and the resulting local charge distortion lead to an effective interaction between electrons despite their spatial separation.

Although all superconductors feature pairs of electrons, they show quite different properties originating from internal structures within the superconducting materials. That allows to classify superconductors in different ways.
One way is to look at the phase transition between superconducting and non-superconducting phase when a superconductor is exposed to a magnetic field [19]. All superconductors expel weak magnetic fields due to the Meissner effect after their specific London penetration depth, but when the magnetic field crosses a certain threshold, the superconducting phase is destroyed. In type-1 superconductors, the phase transition caused by an external magnetic field and out of supercon-

ductivity is discontinuous and therefore a phase transition of order one. In type-2 superconductors, this phase transition happens via an intermediate phase, which leads to a continuous phase transition and there a transition of order two. Before superconductivity is complete destroyed, there exists a phase where ordinary and superconducting properties are mixed and magnetic field vortices are formed. This intermediate phase is entered upon a first threshold in magnetic field strength. Increasing the magnetic field further leads to a higher density of magnetic field vortices and eventually to the complete loss of superconductivity. Therefore type-2 superconductors do not exhibit a complete Meissner effect.
Another way to categorize superconductors is by the total orbital angular momentum of the formed electron pairs [25]. Since the short-ranged Coulomb repulsion requires that no two identical electrons meet at the same point in space, the pair wave function has to vanish when two identical electrons meet. Their pair wave function is proportional to r^l (r is spatial coordinate, l is orbital angular momentum) for the spatial part and symmetric in its spin part. It has to be anti-symmetric under the exchange of the two electrons, because it is fermionic. Consequently, there are two cases: even and odd parity. Since parity can be written as $(-1)^l$ it corresponds to the orbital angular momentum and ultimately to only opposite spin pairing for even, and opposite as well as same spin pairing for odd l. Based on this a conventional superconductor is defined as the most symmetric $l = 0$ case, while all $l > 0$ cases are called unconventional superconductors [19, 25, 26].

2.3.2 BCS Theory for Conventional Superconductors

Most elemental superconductors like mercury, aluminum or molybdenum are conventional superconductors and they have critical temperatures of $T \leq 4.5K$. Mercury was actually the first superconductor to be discovered in 1911 by H. Kamerlingh Onnes [27], who experimented on the resistivity of different materials at temperatures of liquid helium. J. Bardeen, L. N. Cooper and J. R. Schrieffer developed in 1957 a formalism to describe the vanishing electrical resistivity of Mercury [28]. Their theory (BCS theory) is still the framework to describe conventional superconductors [29] and identifies attractive interaction between electrons as the reason for superconductivity. Unconventional superconductors can be explained in an extended BCS theory, which is introduced in Sec. 2.5.2.
Bardeen, Cooper and Schrieffer started the formulation of their formalism with the basic notion that the attractive interaction between electrons close to the Fermi surface leads to the formation of so-called Cooper pairs of electrons, which form a condensate [19]. They understood these pairs as made up of electrons with opposite spin and opposite momentum. In their presence a gap in the excitations spectrum forms around the Fermi surface as depicted in Fig. 3.

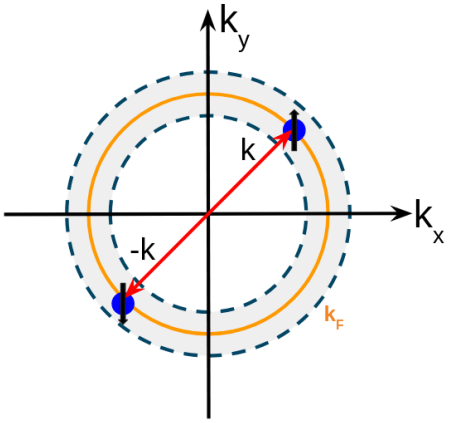

Figure 3: Electrons with opposite spin and from opposite sites of a thin shell around the Fermi surface (aka. opposite momentum) can pair into a Cooper pair.

Starting from the following Hamiltonian, a derivation of the BCS theory is presented,

$$H = -t \sum_{\langle i,j\rangle,\sigma} c^\dagger_{i,\sigma} c_{j,\sigma} - \sum_{i,\sigma} \mu_i c^\dagger_{i,\sigma} c_{i,\sigma} - \sum_i V_i c^\dagger_{i,\uparrow} c_{i,\uparrow} c^\dagger_{i,\downarrow} c_{i,\downarrow} \tag{2.5}$$

where $c^{[\dagger]}_{i,\sigma}$ annihilates [creates] an electron with spin σ at lattice site i, μ_i represents the local chemical potential and $V_i > 0$ is an attractive on-site interaction between electrons. The first term describes the hopping of electrons with amplitude t between nearest-neighbor sites as denoted by $\langle i, j\rangle$. The Hamiltonian describes exactly the previously discussed retardation effect, which leads to the possibility of attractive interaction between electrons.
Transforming Eq. (2.5) by Fourier transformation leads to

$$H = -\frac{1}{N} \sum_{\mathbf{k}_1 \ldots \mathbf{k}_4} V \delta_{\mathbf{k}_1 - \mathbf{k}_2 + \mathbf{k}_3 - \mathbf{k}_4} c^\dagger_{\mathbf{k}_1,\uparrow} c_{\mathbf{k}_2,\uparrow} c^\dagger_{\mathbf{k}_3,\downarrow} c_{\mathbf{k}_4,\downarrow} + \sum_{\mathbf{k},\sigma} \epsilon_{\mathbf{k},\sigma} c^\dagger_{\mathbf{k},\sigma} c_{\mathbf{k},\sigma}$$

where $\epsilon_{\mathbf{k},\sigma}$ is the electron dispersion including the chemical potential. Both potentials, μ and V, are assumed to be constant in space, although the attractive potential could have a momentum dependence, which we will keep explicitly. Additionally, the attractive interaction potential is assumed to be weak (weak-coupling approximation).
Following the BCS approach, only pairs between electrons with opposite momentum and spin are considered, which leads to the classical BCS Hamiltonian:

$$H_{BCS} = \sum_{\mathbf{k},\sigma} \epsilon_{\mathbf{k},\sigma} c^\dagger_{\mathbf{k},\sigma} c_{\mathbf{k},\sigma} - \frac{1}{N} \sum_{\mathbf{k}\mathbf{k}'} V_{\mathbf{k}\mathbf{k}'} c^\dagger_{\mathbf{k},\uparrow} c^\dagger_{-\mathbf{k},\downarrow} c_{-\mathbf{k}',\downarrow} c_{\mathbf{k}',\uparrow} \tag{2.6}$$

where $V_{\mathbf{k}\mathbf{k}'}$ is the attractive two-particle potential which is active if $\mathbf{k}$ and $\mathbf{k}'$ are both within a thin shell around the Fermi-surface. It therefore is the effective potential from the previous equation under all the assumptions made.
One way of solving the eigen-problem of Eq. (2.6) to determine its energy spectrum, is employing the so-called mean-field approximation. Any operator A can be expressed by its expectation value and its deviation from it: $A = \langle A\rangle + \delta A$. Taking the product of two operators A, B and assuming that their deviations from their expectation value is small, allows to write the product as

$$AB \approx A\langle B\rangle + B\langle A\rangle - \langle A\rangle\langle B\rangle$$

because we can neglect all terms of order δ^2. By defining $A = c^\dagger_{\mathbf{k},\uparrow} c^\dagger_{-\mathbf{k},\downarrow}$ and $B = c_{-\mathbf{k}',\downarrow} c_{\mathbf{k}',\uparrow}$, the mean-field BCS Hamiltonian can be formulated

$$\begin{aligned} H^{MF}_{BCS} =& \sum_{\mathbf{k},\sigma} \epsilon_{\mathbf{k},\sigma} c^\dagger_{\mathbf{k},\sigma} c_{\mathbf{k},\sigma} \\ & - \frac{1}{N} \sum_{\mathbf{k}\mathbf{k}'} V_{\mathbf{k}\mathbf{k}'} \left(c^\dagger_{\mathbf{k},\uparrow} c^\dagger_{-\mathbf{k},\downarrow} \langle c_{-\mathbf{k}',\downarrow} c_{\mathbf{k}',\uparrow} \rangle + \langle c^\dagger_{\mathbf{k},\uparrow} c^\dagger_{-\mathbf{k},\downarrow} \rangle c_{-\mathbf{k}',\downarrow} c_{\mathbf{k}',\uparrow} - \langle c^\dagger_{\mathbf{k},\uparrow} c^\dagger_{-\mathbf{k},\downarrow} \rangle \langle c_{-\mathbf{k}',\downarrow} c_{\mathbf{k}',\uparrow} \rangle \right) \end{aligned}$$

which can be further simplified by introducing the BCS gap function. The gap function is a gap in the energy spectrum, which will become clearer when looking at the resulting energies of the reformulated Hamiltonian. The self-consistent gap equation takes the form

$$\begin{aligned} \Delta_{\mathbf{k}} &= \frac{1}{N} \sum_{\mathbf{k}'} V_{\mathbf{k}\mathbf{k}'} \langle c_{-\mathbf{k}',\downarrow} c_{\mathbf{k}',\uparrow} \rangle \\ \Delta^*_{\mathbf{k}} &= \frac{1}{N} \sum_{\mathbf{k}'} V_{\mathbf{k}\mathbf{k}'} \langle c^\dagger_{\mathbf{k},\uparrow} c^\dagger_{-\mathbf{k},\downarrow} \rangle \end{aligned}$$

and therefore the mean-field BCS Hamiltonian can be expressed as

$$H^{MF}_{BCS} = \sum_{\mathbf{k},\sigma} \epsilon_{\mathbf{k},\sigma} c^\dagger_{\mathbf{k},\sigma} c_{\mathbf{k},\sigma} - \sum_{\mathbf{k}\mathbf{k}'} \left(\Delta_{\mathbf{k}} c^\dagger_{\mathbf{k},\uparrow} c^\dagger_{-\mathbf{k},\downarrow} + \Delta^*_{\mathbf{k}} c_{-\mathbf{k}',\downarrow} c_{\mathbf{k}',\uparrow} - \frac{1}{N} \Delta_{\mathbf{k}'} \Delta^*_{\mathbf{k}} \right)$$

This equation can be solved using the Bogoliubov transformation (BdG), which is explained more generally in Sec. 3.1. The main point here is that a transformation to new fermion operators allows to diagonalize the Hamiltonian, which yields an expression with the form of a Fermi gas

$$H_0 = \sum_{\mathbf{k},\sigma} E_{\mathbf{k}} (\gamma^\dagger_{\mathbf{k},\sigma} \gamma_{\mathbf{k},\sigma} + \eta^\dagger_{\mathbf{k},\sigma} \eta_{\mathbf{k},\sigma}) + \sum_{\mathbf{k}} \left(\epsilon_{\mathbf{k}} - E_{\mathbf{k}} + \frac{1}{V_{\mathbf{k},\mathbf{k}'}} \Delta_{\mathbf{k}'} \Delta^*_{\mathbf{k}} \right)$$

where $\gamma_{\mathbf{k},\sigma}$ ($\eta_{\mathbf{k},\sigma}$) are the quasi-particle operators corresponding to positive (negative) eigenvalues. The second sum is constant, while the first one describes the energy spectrum. The eigenvalues are $E_{\mathbf{k}} = \sqrt{\epsilon^2_{\mathbf{k}} + \Delta^2_{\mathbf{k}}}$ and they are two-fold degenerate in spin.
Based on this energy spectrum, the density of states can be calculated and its form is presented in Fig. 4. There the meaning of the gap becomes clearer, since it denotes half of the width of non-occupied states around zero energy. Regardless of the system parameters, this shape is expected for the local density of states of any conventional superconductor.

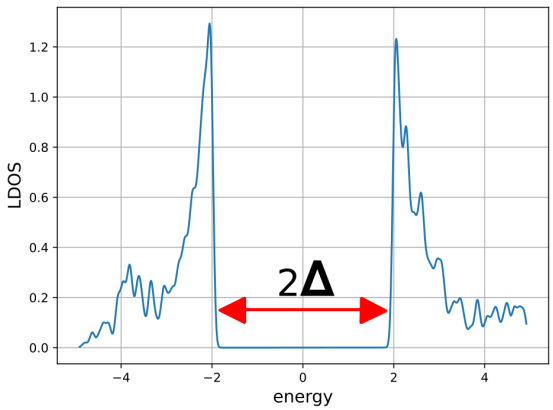

Figure 4: Local density of states (LDOS) for a conventional superconductor. The gap width is explicitly denoted by the red arrow.

One of the most prominent properties of superconductors is their critical temperature at which they become superconducting. This temperature can be calculated based on BCS theory and is therefore useful for the comparison between theory and experiment. The starting point for the explicit formulation of the critical temperature is the gap equation expressed via in the new quasi-particle basis

$$\Delta = -V \sum_{\mathbf{k}} \frac{\Delta}{2E_{\mathbf{k}}} \tanh\left(\frac{E_{\mathbf{k}}}{k_B T}\right) \tag{2.7}$$

which only depends on temperature now, since we approximated the potential as constant. The critical temperature T_c is now defined such that the gap Δ vanishes at that specific temperature. Eq. (2.7) linearizes for $\Delta \to 0$ to

$$\Delta = -V\Delta \sum_{\mathbf{k}} \frac{1}{2E_{\mathbf{k}}} \tanh\left(\frac{E_{\mathbf{k}}}{k_B T}\right) \quad \to \quad 1 = -V \int_{-\epsilon_c}^{\epsilon_c} dE \frac{N(E)}{2E} \tanh\left(\frac{E}{k_B T}\right)$$

where the sum over momentum is replaced with an integral over energy by using the density of states of electrons $N(E)$. The integral is taken only within the thin shell around the Fermi surface where the attractive interaction is present, which naturally introduces the energy cutoff ϵ_c. Additionally, the density of states can be assumed to be constant there, yielding

$$1 = -VN_0 \ln\left(\frac{1.14\epsilon_c}{k_B T_c}\right) \quad \Leftrightarrow \quad T_c = \frac{1}{k_B} 1.14\epsilon_c e^{-1/|V|N_0}$$

which is an expression for the critical temperature that only depends on material constants. Furthermore, solving the gap equation for $T = 0$ yields an expression for the gap at zero temperature

$$\Delta_{T=0} \approx 1.764 k_B T_c$$

which is a constant proportional to the critical temperature. This two results are central to the weak coupling approximation [19, 25].

2.4 Spin Orbit Coupling

Spin orbit coupling (SOC) is a relativistic effect in quantum mechanics, which stems from interaction between the spin and the effective magnetic field of an electron moving through it [30, 31]. Such a field can originate from a nucleus when the electron is moving on an orbit around it, or from an intrinsic electric field.

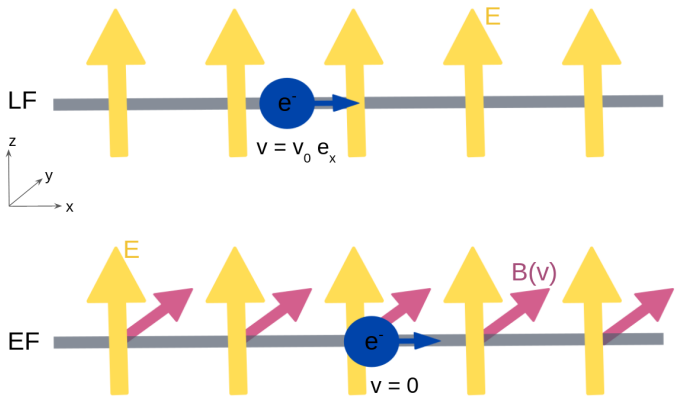

Figure 5: Spin orbit coupling describes the linear dependence between an electron's movement through an electric field with a material and the resulting lifting of spin degeneracy in the electron's energy caused by a Zeeman split. The upper graph shows the laboratory frame and the lower shows the electron frame. In the latter the spin splitting magnetic field becomes visible.

Fig. 5 shows an electrons movement through an electric field in the lab frame (LF) and in the electron frame (EF). In the lab frame only the electric field is present, but in the electron frame the Lorentz transformation of the electric field leads to a magnetic field, which in turn results into a Zeeman shift. Since the effective magnetic field is determined by the speed and direction of the moving charge its generated by, the spin of the electron has a preferred orientation depending on the orbital movement of the electron through the electric field of the surrounding nuclei or the band structure of a solid.

The resulting Zeeman shift splits energy levels that would otherwise be degenerate, although the splitting is of the same order as or slightly smaller than relativistic corrections to the kinetic energy when looking at the energy levels of atoms. The exact strength depends also on the electric field, which in turn depends on the atomic number of the considered material.

In addition to lifting energy degeneracy, SOC gives rise to a number of interesting phenomena, among them magnetic anisotropy [32], spin relaxation [33], magnetic damping [34], anisotropic magnetoresistance [35], and anomalous Hall effect [36]. On a more fundamental level, broken inversion symmetry in combination with the described atomic SOC leads to Rashba SOC which is the reason for its relevancy for this thesis. In such non-centrosymmetric systems exist two competing spin-spin interaction forms. As in the centrosymmetric case, there is Heisenberg type interaction giving rise to (anti-)ferromagnetic orientation. That implies a colinear orientation of the interacting spins and can be written as $J_{ij}^{H}\mathbf{S}_i \cdot \mathbf{S}_j$. The broken inversion symmetry additionally gives rise to the anti-symmetric Dzyaloshinskii-Moriya interaction of the form $\mathbf{D}_{ij} \cdot (\mathbf{S}_i \times \mathbf{S}_j)$ [37, 38]. Therefore the presence of Rashba SOC enables the formation of chiral magnetic objects.

Generally, Rashab SOC can be expressed as

$$H_\gamma = \sum_{\sigma,\sigma',\langle i,j\rangle} \gamma\, \mathbf{n}\,(\mathbf{d}_{i,j} \times \vec{\sigma}_{\sigma,\sigma'})\, c_{i,\sigma}^{\dagger} c_{j,\sigma'} \tag{2.8}$$

with σ, σ' being spin-indices and $\vec{\sigma}$ the Pauli-matrix vector. The SOC strength is denoted by γ. There are different types of Rashba SOC that have different origins and take slightly different forms. The different forms can be realized by choosing the interaction vector $\mathbf{d}_{i,j} = \hat{x}(\delta_{i+\hat{x},j} - \delta_{i-\hat{x},j}) + \hat{y}(\delta_{i+\hat{y},j} - \delta_{i-\hat{y},j}) + \hat{z}(\delta_{i+\hat{z},j} - \delta_{i-\hat{z},j})$, which connects the two sites i and j and therefore represents a kind of movement. The spin orbit field direction vector $\mathbf{n}$ is the symmetry breaking axis and chosen according to the type of SOC, too. Theoretically, it is possible to control the superconducting transition by the rotation of the symmetry breaking axis [39].
Motivated by the fact that p-wave superconductivity is predicted in $CePt_3Si$ [40], Rashba SOC is investigated in more detail. This type of SOC models the breaking of inversion symmetry in $CePt_3Si$ best.
The Rashba type of SOC was formulated in 1960 [41] and often arises due to symmetry breaking at the surface or at the interface in heterostructures. But it can also arise due to crystal structures that allow for an intrinsic electric field as it is the case in $CePt_3Si$, as illustrated in Fig. 6. To model such SOC correctly, the symmetry breaking axis $\mathbf{n}$ in Eq. (2.8) is chosen as out of plane $\mathbf{n} = \hat{z}$, while the thin film of the material is chosen to be in $x-y$ plane. Since all later calculations are going to be performed in k-space, the general expression is additionally Fourier transformed, which yields

$$H_\gamma = \sum_{\sigma,\sigma',k} \gamma(k_y\hat{x} - k_x\hat{y})c^\dagger_{k,\sigma}c_{k,\sigma'} \tag{2.9}$$

which clearly shows that Rashba SOC is linear in k. This symmetry can be concisely formulated as $H_\gamma(\mathbf{k}) = -H_\gamma(-\mathbf{k})$ and causes an energy difference between electrons moving in opposite directions. Therefore it breaks inversion symmetry.

2.5 Unconventional Superconductors

In unconventional superconductors, the angular momentum of the electron pair can be finite: $l = 1, 2, ...$ [3, 29]. This leads to different symmetry properties, since the Pauli exclusion principle is, for example, not broken anymore when the electrons have the same spin. Triplet pairing $(\uparrow\uparrow), (\downarrow\downarrow)$ and $(\uparrow\downarrow + \downarrow\uparrow)$ is therefore possible and different transport mechanisms can be expected. The different electron pairing channels are labeled analogous to atomic orbitals as s-wave superconductivity for angular momentum $l = 0$, p-wave superconductivity for angular momentum $l = 1$ and so on.
Experimentally it is difficult to determine the superconducting channel of a material, because the Meissner effect suppress the magnetic response of electron spins. Additionally, many p-wave states exhibit very similar thermodynamical characteristics as s-wave or d-wave states do [26]. That leads to many ongoing debates in the classification of superconductors regarding their symmetry.
Nevertheless, there is high evidence for triplet p-wave pairing in ^3He [19], recently discovered UTe_2 [42], under high pressure in UBe_{13} [43] and even in twisted graphene when an in-plane magnetic field is applied [44]. Sr_2RuO_4 used to be a strong candidate for p-wave superconductivity, too, but after nearly twenty years, recent experiments are considered to prove pure s-wave conductivity [45]. Some theories even suggest the presence of triplet superconductivity in doped semi-conductors [46]. In this thesis, the p-wave channel is of central interest and therefore the material $CePt_3Si$ is taken as reference.

2.5.1 CePt3Si

$CePt_3Si$ (Cerium - Platinum - Silicon) is a heavy fermion compound based on silicon and shows the tetragonal crystal structure P4mm. Fig. 6 depicts the structure of this compound, which is also called $CePt_3B$-type structure. The name originates from the fact that this crystal structure was first described for the compound $CePt_3B$, which also belongs to the $CePt_3X$ compound group. Because of this crystal structure, $CePt_3Si$ has no inversion symmetry and exhibits Rashba-like SOC effects without external forces. Experiments confirmed its superconductivity at $T_c = 0.75$ K in 2004 and with that $CePt_3Si$ was the first heavy fermion compound without inversion symmetry to have a confirmed superconducting phase [8]. Later similar materials and other heavy fermion compounds were also found to be superconducting.
There are ongoing experiments to determine the symmetry of the superconducting phase with certainty, but so far no experiments contradict the prediction of p-wave superconductivity [47–49]. Since $CePt_3Si$ conserves time reversal symmetry while breaking inversion symmetry, it is expected to have both s- and p-wave superconductivity [50]. Recent reviews of the current state of the art suggest that RKKY interaction might be enhanced in $CePt_3Si$ due to its crystal structure, which should also be visible in the superconducting phase [51]. Because of its gap symmetry and possible influence on RKKY interaction, $CePt_3Si$ is taken as a reference material in later calculations of this thesis. In order to do so, a new framework for describing $CePt_3Si$ is necessary, because the classic BCS theory does not account for the new Cooper pairing channels caused by the SOC. Therefore the extended BCS theory is introduced in the next section.

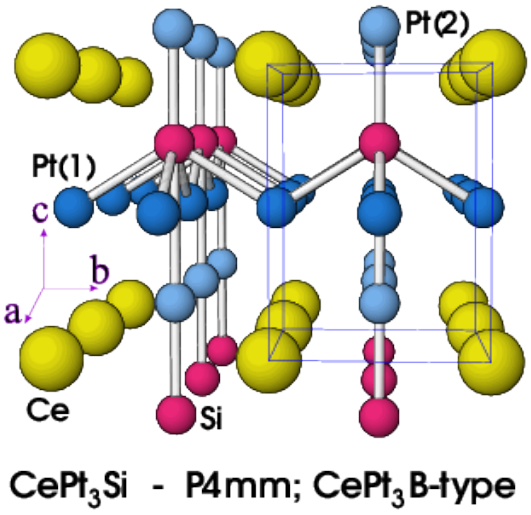

Figure 6: Atomic lattice structure of $CePt_3Si$. Copyright by the American Physical Society. [8]

2.5.2 Extended BCS Theory

The superconductivity explained so far is of isotropic s-wave type and arises from phonon mediated electron-electron interactions. In unconventional superconductors (angular momentum ≥ 1), the superconductivity can be of different origin and while the critical temperatures are relatively precisely measurable, the possible pairing symmetries are often strongly debated.
The classic BCS framework does not cover other than s-wave superconductors, but it can be extend

to describe those different pairing symmetries. Since the pairing symmetries are dictated by the symmetry of the corresponding interaction potential, it is possible to realize many different pairing symmetries by choosing different interaction potentials. An interaction potential can, for example, give rise to p-wave pairing, when it changes sign under $\mathbf{k} \to -\mathbf{k}$.
But although this is a possible description of unconventional superconductivity in the BCS framework, it does have different short-comings. Overcoming those short-comings mostly includes proposing a new pairing mechanism. Nevertheless, the extended BCS theory is introduced here to capture many aspects of unconventional superconductivity.
The classic BCS Hamiltonian in Eq. (2.5) is extended by adding the possibility of attractive interaction between electrons on nearest-neighbor lattice sites, which yields

$$H_{EBCS} = -t \sum_{\langle i,j\rangle,\sigma} c^\dagger_{i,\sigma} c_{j,\sigma} - \sum_{i,\sigma} \mu_i c^\dagger_{i,\sigma} c_{i,\sigma} - \sum_{\langle i,j\rangle,\sigma,\sigma'} V^{\sigma,\sigma'}_{ij} c^\dagger_{i,\sigma} c_{i,\sigma} c^\dagger_{j,\sigma'} c_{j,\sigma'} \tag{2.10}$$

The first two terms remain unchanged, while the third term allows for nearest-neighbor attraction now. That includes the possibility to form Cooper pairs from electrons with the same spin, which can give rise to spin-singlet and spin-triplet pairing. Anisotropic s-wave, d-wave and p-wave pairing are included in these possible pairing interactions that could be caused by e.g. long-range electron-phonon interactions [52]. Which pairing symmetry dominates, depends on the system's parameters, which includes the ratio between the pairing amplitudes from conventional and extended BCS theory.
Solving Eq. (2.10) involves the same steps as for the classic BCS Hamiltonian. Performing the Fourier transformation, assuming a spatially uniform interaction potential and focusing on the pairing between electrons with opposite momenta, the extended BCS Hamiltonian can be rewritten as

$$\begin{aligned} H_{EBCS} = &\sum_{\mathbf{k},\sigma} \epsilon_{\mathbf{k},\sigma} c^\dagger_{\mathbf{k},\sigma} c_{\mathbf{k},\sigma} \\ &+ \frac{1}{2N} \sum_{\mathbf{k},\mathbf{k}',\sigma,\sigma'} V^{\sigma,\sigma'} \left(e^{-i(\mathbf{k}-\mathbf{k}')\hat{x}} + e^{i(\mathbf{k}-\mathbf{k}')\hat{x}} + e^{-i(\mathbf{k}-\mathbf{k}')\hat{y}} + e^{i(\mathbf{k}-\mathbf{k}')\hat{y}} \right) c^\dagger_{\mathbf{k},\sigma} c^\dagger_{-\mathbf{k},\sigma'} c_{-\mathbf{k}',\sigma'} c_{\mathbf{k}',\sigma} \end{aligned}$$

Introducing a similar mean-field approximation as before and defining the pairing amplitudes

$$\begin{aligned} F^{x\pm}_{\sigma,\sigma'}(\mathbf{k}) &= -\frac{1}{N} \sum_{\mathbf{k}'} e^{\mp i\mathbf{k}'\cdot\hat{x}} \langle c_{-\mathbf{k}',\sigma'} c_{\mathbf{k}',\sigma} \rangle \\ F^{y\pm}_{\sigma,\sigma'}(\mathbf{k}) &= -\frac{1}{N} \sum_{\mathbf{k}'} e^{\mp i\mathbf{k}'\cdot\hat{y}} \langle c_{-\mathbf{k}',\sigma'} c_{\mathbf{k}',\sigma} \rangle \\ A_{\sigma,\sigma'}(\mathbf{k}) &= V^{\sigma,\sigma'} \left(e^{i\mathbf{k}\cdot\hat{x}} F^{x+}_{\sigma,\sigma'}(\mathbf{k}) + e^{-i\mathbf{k}\cdot\hat{x}} F^{x-}_{\sigma,\sigma'}(\mathbf{k}) + e^{i\mathbf{k}\cdot\hat{y}} F^{y+}_{\sigma,\sigma'}(\mathbf{k}) + e^{-i\mathbf{k}\cdot\hat{y}} F^{y-}_{\sigma,\sigma'}(\mathbf{k}) \right) \end{aligned}$$

yields the final form of Eq. (2.10):

$$H^{MF}_{BCS} = \frac{1}{2} \sum_{\mathbf{k},\sigma,\sigma'} \left(A^*_{\sigma,\sigma'} c_{-\mathbf{k},\sigma'} c_{\mathbf{k},\sigma} + A_{\sigma,\sigma'} c^\dagger_{\mathbf{k},\sigma} c^\dagger_{-\mathbf{k},\sigma'} \right) + \sum_{\mathbf{k},\sigma} \epsilon_{\mathbf{k},\sigma} c^\dagger_{\mathbf{k},\sigma} c_{\mathbf{k},\sigma} + H^0_{EBCS} \tag{2.11}$$

where

$$\begin{aligned} H^0_{EBCS} = \frac{1}{N} \sum_{\mathbf{k},\mathbf{k}',\sigma,\sigma'} &V^{\sigma,\sigma'} \left(e^{-i\mathbf{k}\cdot\hat{x}} e^{i\mathbf{k}'\cdot\hat{x}} + e^{i\mathbf{k}\cdot\hat{x}} e^{-i\mathbf{k}'\cdot\hat{x}} + e^{-i\mathbf{k}\cdot\hat{y}} e^{i\mathbf{k}'\cdot\hat{y}} + e^{i\mathbf{k}\cdot\hat{y}} e^{-i\mathbf{k}'\cdot\hat{y}} \right) \\ &\times \langle c^\dagger_{\mathbf{k},\sigma} c^\dagger_{-\mathbf{k},\sigma'} \rangle \langle c_{-\mathbf{k},\sigma'} c_{\mathbf{k},\sigma} \rangle \end{aligned}$$

The expression can be shorted by defining the spin and momentum dependent potential

$$V_{\mathbf{k},\mathbf{k}'}^{\sigma,\sigma'} = V^{\sigma,\sigma'}\left(e^{-i\mathbf{k}\cdot\hat{x}}e^{i\mathbf{k}'\cdot\hat{x}} + e^{i\mathbf{k}\cdot\hat{x}}e^{-i\mathbf{k}'\cdot\hat{x}} + e^{-i\mathbf{k}\cdot\hat{y}}e^{i\mathbf{k}'\cdot\hat{y}} + e^{i\mathbf{k}\cdot\hat{y}}e^{-i\mathbf{k}'\cdot\hat{y}}\right)$$
$$\Rightarrow A_{\sigma,\sigma'}(\mathbf{k}) = -\frac{1}{N}\sum_{\mathbf{k}'} V_{\mathbf{k},\mathbf{k}'}^{\sigma,\sigma'}\langle c_{-\mathbf{k}',\sigma'}c_{\mathbf{k}',\sigma}\rangle$$

The pairing amplitude $A_{\sigma,\sigma'}(\mathbf{k})$ allows for different spin and momentum symmetries, depending on the system's parameters. Since the interaction potential $V_{\mathbf{k},\mathbf{k}'}^{\sigma,\sigma'}$ has to follow the fermionic anti-commutation relations, it has to be even under inversion of momentum and exchange of spin. Writing the pairing amplitude as a matrix $A(\mathbf{k})$, the symmetry of the interaction potential translates into $A(\mathbf{k}) = -A(-\mathbf{k})^T$, where T is the matrix transpose. Consequently, the matrix $A(\mathbf{k})$ has even parity for spin-singlet and odd parity for spin-triplet Cooper pairs.
For later convenience, one can rewrite the matrix $A(\mathbf{k})$ in terms of a three dimensional vector $\mathbf{d}(\mathbf{k})$ representing spin-triplet Cooper pairs and a scalar $\Delta_s(\mathbf{k})$ representing spin-singlet Cooper pairs. That takes the form

$$A(\mathbf{k}) = \begin{pmatrix} -d_x(\mathbf{k}) + id_y(\mathbf{k}) & d_z(\mathbf{k}) + \Delta_s(\mathbf{k}) \\ d_z(\mathbf{k}) - \Delta_s(\mathbf{k}) & d_x(\mathbf{k}) + id_y(\mathbf{k}) \end{pmatrix} \tag{2.12}$$

where the components of the spin-triplet Cooper pair vector are defined as

$$d_x(\mathbf{k}) = \frac{1}{2}\left(-A_{\uparrow,\uparrow}(\mathbf{k}) + A_{\downarrow,\downarrow}(\mathbf{k})\right)$$
$$d_y(\mathbf{k}) = \frac{1}{2i}\left(A_{\uparrow,\uparrow}(\mathbf{k}) + A_{\downarrow,\downarrow}(\mathbf{k})\right)$$
$$d_z(\mathbf{k}) = -A_{\uparrow,\downarrow}(\mathbf{k}) - \Delta_s(\mathbf{k})$$

This is a general expression for triplet gap equations and the exact form is determined by the symmetry breaking that leads to the triplet pairing in the first place. In this thesis, inversion symmetry is chosen to be broken and the resulting Rashba SOC determines the preferred triplet gap vector $\mathbf{d}$ as is discussed in the next section. That allows to study an unconventional superconductor and therefore the influence of triplet Cooper pairs on RKKY interaction on a system that corresponds to a material with confirmed p-wave gap symmetry, namely $CePt_3Si$.

2.5.3 Preferred Triplet Pairing Vector

Triplet pairing occurs among others in superconductors with broken inversion symmetry, which can be achieved by introducing SOC. Since electron movements within a non-centrosymmetric superconductor are strongly influenced by the SOC, the preferred symmetry of the triplet gap can be explained with the direction of the SOC as done by Frigeri et al. [40].
In their work, the SOC is defined as $H_{SOC}^{\text{Frigeri}} = \gamma\sum_{k,s,s'}\mathbf{g}_{\mathbf{k}}\sigma_{s,s'}c_{k,s}^{\dagger}c_{k,s'}$, where σ is the Pauli matrix vector, s, s' are spin indices, γ the SOC strength, and $\mathbf{g}_k = -\mathbf{g}_{-k}$ is the three dimensional SOC vector. This term is embedded into a superconductor that consequently exhibits singlet and triplet pairing. The coupling depends on the difference of the density of states on the two separated Fermi surfaces and therefore is of order $\gamma/\epsilon_F << 1$, where ϵ_F is the Fermi energy of the higher Fermi surface. That allows to decouple the singlet and triplet gap equations and to find the critical temperature T_c for singlet and triplet pairing separately. For the singlet pairing the

critical temperature T_c is found to obey the relation

$$\ln\left(\frac{T_c}{T_{cs}}\right) = O\left(\frac{\gamma^2}{\epsilon_F^2}\right)$$

which means that the critical temperature essentially is the same with and without SOC. It is expressed relative to the critical temperature of the system without SOC T_{cs}, which is a pure s-wave superconductor.
For the triplet pairing the critical temperature obeys

$$\ln\left(\frac{T_c}{T_{ct}}\right) = 2\langle\left(|\mathbf{d}(\mathbf{k})|^2 - |\mathbf{g}(\mathbf{k})\cdot\mathbf{d}(\mathbf{k})|^2\right) f(\rho_k)\rangle_k + O\left(\frac{\gamma^2}{\epsilon_F^2}\right) \tag{2.13}$$

where $\mathbf{d}(\mathbf{k})$ is the normalized triplet gap function and the function $f(\rho)$ is dependent on the SOC, but not relevant for the further argumentation and therefore not specified here. This critical temperature is express relative to T_{ct}, which is the critical temperature of the pure p-wave superconductor. The highest possible critical temperature is according to Eq. (2.13) reached at $T_c = T_{ct}$, which is the case for $\mathbf{d}(\mathbf{k})||\mathbf{g}_\mathbf{k}$. This suggests a preferred spin alignment parallel to the SOC and that there might be triplet states, which are unaffected by the lack of inversion symmetry. That means that triplet state with a certain alignment to the SOC are not split by it.

3 Methods

The subject of RKKY interaction in non-centrosymmetric superconductors is approached analytically as well as numerically. Both approaches have the goal of determining the energy spectrum of the system in dependency on the orientation and separation of the impurity spins, as well as on the present SOC and superconducting parameters.

3.1 Bogoliubov-de Gennes Transformation

The Bogoliubov-de Gennes method (BdG) was developed by Pierre-Gilles de Gennes [53, 54] and is applicable on the BCS theory. It is based on a set of coupled Schrödinger equations and enables to solve those, which allows to study more detailed and complicated (superconducting) systems. The main idea is that the coupled equations can be solved by introducing effective new quasi-particles, which contain all information about the system. Therefore the BdG is a complementary approach to the Ginzburg-Landau theory [55].
As first step, the system of coupled Schrödinger equations is formulated in matrix form. The focus is set onto a 4x4 matrix here, which allows to demonstrate the formalism for a quite general system. It can be reduced to less dimensions in order to describe easier systems. The eigenvalue problem can be formulated as

$$\begin{bmatrix} \epsilon_k\sigma_0 & \mathbf{A}(k) \\ \mathbf{A}^\dagger(k) & -\epsilon_k\sigma_0 \end{bmatrix} \begin{pmatrix} \mathbf{a} \\ \mathbf{b} \end{pmatrix} = E_k \begin{pmatrix} \mathbf{a} \\ \mathbf{b} \end{pmatrix} \tag{3.1}$$

where $\mathbf{A}(k)$ is a 2x2 matrix with $\mathbf{A}(k)\mathbf{A}^\dagger(k) = |\mathbf{A}(k)|^2\sigma_0$, k momentum index, σ_0 the unit matrix in Pauli matrix formulation and E_k are the eigenvalues of the matrix. The eigenvector's two dimensional components $\mathbf{a}$ and $\mathbf{b}$ have to be determined.
The notation in the following is close to the notation of Ghanbari [5].
Based on Eq. 3.1, the two components of the eigenvectors can be related via

$$\mathbf{b} = \frac{\mathbf{A}^\dagger(k)}{|\mathbf{A}(k)|^2}(E_k - \epsilon_k)\mathbf{a}$$

and therefore the first two eigenvectors can be written as

$$\Psi_1 = \begin{pmatrix} \mathbf{a}_1 \\ \frac{\mathbf{A}^\dagger(k)}{|\mathbf{A}(k)|^2}(E_k - \epsilon_k)\mathbf{a}_1 \end{pmatrix}, \quad \Psi_2 = \begin{pmatrix} \mathbf{a}_2 \\ \frac{\mathbf{A}^\dagger(k)}{|\mathbf{A}(k)|^2}(E_k - \epsilon_k)\mathbf{a}_2 \end{pmatrix}$$

The remaining two eigenvectors for the four dimensional matrix can be obtained in the same way from

$$\mathbf{a} = -\frac{\mathbf{A}(k)}{(E_k + \epsilon_k)}\mathbf{b}$$

and consequently read

$$\Psi_3 = \begin{pmatrix} -\frac{\mathbf{A}(k)}{(E_k+\epsilon_k)}\mathbf{b}_3 \\ \mathbf{b}_3 \end{pmatrix}, \quad \Psi_2 = \begin{pmatrix} -\frac{\mathbf{A}(k)}{(E_k+\epsilon_k)}\mathbf{b}_4 \\ \mathbf{b}_4 \end{pmatrix}$$

These eigenvectors have to be orthonormal in order to form a unitary transformation, which is

needed to transform the operators without loss of information about the system. The condition for orthonormality reads $\langle \Psi_i | \Psi_j \rangle = \delta_{ij}$, where δ is the Dirac-Delta function, and takes the following form for the proposed eigenvectors

$$|\mathbf{a}_1|^2 = |\mathbf{a}_2|^2 = \frac{|\mathbf{A}(k)|^2}{|\mathbf{A}(k)|^2 + (E_k - \epsilon_k)^2}$$
$$|\mathbf{b}_3|^2 = |\mathbf{b}_4|^2 = \frac{(E_k + \epsilon_k)^2}{|\mathbf{A}(k)|^2 + (E_k + \epsilon_k)^2}$$

These factors are used as normalization for the components of the eigenvectors.
The transformation matrix P is comprised of the four eigenvectors as columns and transforms between the original particle and new quasi-particle basis. The vector part of the components is chosen in accordance with the requirement that P is unitary and is therefore

$$\mathbf{a}_1 = \begin{pmatrix} 1 \\ 0 \end{pmatrix}, \quad \mathbf{a}_2 = \begin{pmatrix} 0 \\ 1 \end{pmatrix}, \quad \mathbf{b}_3 = \begin{pmatrix} 1 \\ 0 \end{pmatrix}, \quad \mathbf{b}_4 = \begin{pmatrix} 0 \\ 1 \end{pmatrix}$$

With this, the P can be written as

$$\mathbf{P} = \begin{bmatrix} \mathbf{u}_k & \mathbf{v}_k \\ -\mathbf{v}_k^\dagger & \mathbf{u}_k \end{bmatrix}$$

with the components

$$\mathbf{u}_k = \frac{E_K + \epsilon_k}{\sqrt{(e_k + \epsilon_k)^2 + |\mathbf{A}(k)|^2}} \sigma_0 \,, \quad \mathbf{v}_k = \frac{-\mathbf{A}(k)}{\sqrt{(e_k + \epsilon_k)^2 + |\mathbf{A}(k)|^2}} \tag{3.2}$$

The new quasi-particle operators that diagonalize the originally coupled set of Schrödinger equations are defined as $c' = \mathbf{P}c$.

3.2 Schrieffer-Wolff Transformation

The RKKY-interaction is a second-order in perturbation phenomenon. In order to calculate analytically the correction to the energy spectrum of the unperturbed system, the so-called Schrieffer-Wolff transformation (SWT) is going to be used [56, 57]. This method is based on a unitary transformation from the eigenbasis of the unperturbed system H_0 towards the basis of the effective Hamiltonian $\tilde{H} = H_0 + H_{RKKY}$. This effective Hamiltonian is valid in the low-energy regime, because the transformation decoupled the low- and high-energy subspaces, which makes this method very suitable to study superconductors.
The interaction strength of the perturbation is denoted by J and the unitary matrix U is defined as $U = e^{iS}$. This leads to a unitary transformation of the total Hamiltonian of

$$\begin{aligned} \tilde{H} &= UHU^\dagger = e^{iS} H e^{-iS} \\ &= H_0 + H_{RKKY} + i[S, H_0] + i[S, H_{RKKY}] + O(J^3) \end{aligned} \tag{3.3}$$

The expansion in the second line is going to be cut at $O(J^3)$, so that the effective Hamiltonian is determined up to $O(J^2)$. Choosing the unitary matrix such that $H_{RKKY} + i[S, H_0] = 0$ leads to an effective Hamiltonian of $\tilde{H} = H_0 + i[S, H_{RKKY}]$.
In order to get an explicit expression for $\tilde{H}$, an ansatz has to be made that has the same structure

as the RKKY interaction term. This structure depends on the basis in which the unperturbed system is diagonalized, since the RKKY term is transformed into the same basis. Additionally, all coefficients in front of the single terms within the RKKY are formulated as general as necessary. The coefficients are then explicitly determined by the requirement $H_{RKKY} + i[S, H_0] = 0$, which enables to calculate the missing commutator in Eq. (3.3).

3.3 Numerical Approach

In addition to the analytical approach, the Hamiltonian of the two dimensional system is exactly diagonalized numerically in *python*. The formulation of the Hamiltonian is done in a spin basis with Nambu basis structure and the BdG formalism is used for the exact diagonalization. The system is a superconductor with SOC and RKKY interaction and the boundary conditions are chosen to be hard-wall for the x-direction and periodic for the y-direction. Such boundary conditions are reasonable for thin film superconductors. With this choice of boundary conditions, the real-space Hamiltonian has to be partially Fourier-transformed by

$$c_{\vec{i},\sigma} = \frac{1}{N_y} \sum_{k_y} c_{i_x,k_y,\sigma} e^{i(k_y i_y)} \tag{3.4}$$

where the indices of the operator c change from the two dimensional position $\vec{i}$ in real space and spin σ to partially Fourier transformed coordinates. The position in x-direction i_x is still in real space, while the y-direction k_y is transformed into k-space. The spin σ stays the same under this fourier transformation.
Such partially Fourier transformed operators allow to express the Hamilton operator of the system as

$$H = H_0 + \frac{1}{2} \sum_{k_y} W_{k_y}^\dagger H_{k_y} W_{k_y} \tag{3.5}$$

where W_{k_y} is the vector containing Ψ_{i_x,k_y} for all positions in x-direction i_x of the system. Ψ_{i_x,k_y} contains the Nambu-basis [58] for one position i_x, which has the form

$$\Psi_{i_x}^\dagger = \left(c_{i_x,\uparrow}^\dagger, c_{i_x,\downarrow}^\dagger, c_{i_x,\uparrow}, c_{i_x,\downarrow} \right)$$

The matrix H_{k_y} is of dimension $4N_x \times 4N_x$, where N_x is the number of lattice sites in x-direction. This Hamiltonian fulfills the relation $H_{i_x,j_x,k_y} = H_{j_x,i_x,k_y}^\dagger$, which is imposed by complex conjugating Eq. (3.5).
Later in this thesis, the Hamiltonian is going to consist of terms for a tight-binding model, SOC of Rashba-type and superconducting terms in BCS formulation. All of these terms have to be partially Fourier transformed with Eq. 3.4. As it is one of the more complicated terms to transform, the transformation of the SOC term is done explicitly here. The general expression in real space

is taken from Sec. 2.4 and serves as the starting point:

$$
\begin{aligned}
H_{SOC} &= i\gamma \sum_{\langle i,j\rangle,\alpha,\beta} c^{\dagger}_{i,\alpha}\mathbf{n}\cdot(\mathbf{d}_{i,j}\times\vec{\sigma})\,c_{j,\beta} \\
&= \frac{i\gamma}{N} \sum_{\substack{i_x,\vec{\delta} \\ k_y,k_y',\alpha,\beta}} c^{\dagger}_{i_x,k_y,\alpha}\left(\vec{\delta}\cdot\mathbf{y}\sigma_x - \vec{\delta}\cdot\mathbf{x}\sigma_y\right) c_{i_x+\vec{\delta}\cdot\mathbf{x},k_y',\beta}\, e^{-ik_y i_y}\, e^{ik_y'(i_y+\vec{\delta}\cdot\mathbf{y})} \\
&= i\gamma \sum_{i_x\vec{\delta},k_y,\alpha,\beta} c^{\dagger}_{i_x,k_y,\alpha}\left(\vec{\delta}\cdot\mathbf{y}\sigma_x - \vec{\delta}\cdot\mathbf{x}\sigma_y\right) c_{i_x+\vec{\delta}\cdot\mathbf{x},k_y,\beta}\, e^{ik_y\vec{\delta}\cdot\mathbf{y}} \\
&= \gamma \sum_{i_x,k_y,\alpha,\beta} \Big[c^{\dagger}_{i_x,k_y,\alpha}(i\sigma_y)_{\alpha\beta}c_{j_x,k_y,\beta}(\delta_{j_x,i_x+1}-\delta_{j_x,i_x-1}) - c_{i_x,k_y,\alpha}(\sigma_x)_{\alpha\beta}c_{j_x,k_y,\beta}\delta_{i_x j_x}2\sin(k_y a)\Big]
\end{aligned}
$$

where $\vec{\delta}$ is the distance between two nearest-neighbors on a square lattice with lattice constant a. Therefore, there are local and nearest-neighbor terms in the SOC, although the original term contained only nearest neighbor terms. Terms local in x-direction arise due to the transformation because the nearest-neighbor in y-direction has a different k_y-value, but the same i_x-value.
After partially Fourier transforming all terms of the Hamiltonian in Eq. 7.5, the local components of H_{k_y} can be expressed by the following $4x4$ matrix

$$
H_{i_x=j_x,k_y} =
\begin{bmatrix}
-\mu+J\vec{S}_{i_x}\vec{\sigma}_{\uparrow\uparrow}\delta_{i_x,i} & -2\gamma\sin(k_y a)+J\vec{S}_{i_x}\vec{\sigma}_{\uparrow\downarrow}\delta_{i_x,i} & 0 & U^{*}_{i_x,k_y} \\
-2\gamma\sin(k_y a)+J\vec{S}_{i_x}\vec{\sigma}_{\downarrow\uparrow}\delta_{i_x,i} & -\mu+J\vec{S}_{i_x}\vec{\sigma}_{\downarrow\downarrow}\delta_{i_x,i} & -U^{*}_{i_x,k_y} & 0 \\
0 & -U_{i_x,k_y} & \mu-J\vec{S}_{i_x}\vec{\sigma}_{\uparrow\uparrow}\delta_{i_x,i} & 2\gamma\sin(k_y a)-J\vec{S}_{i_x}\vec{\sigma}_{\uparrow\downarrow}\delta_{i_x,i} \\
U_{i_x,k_y} & 0 & 2\gamma\sin(k_y a)-J\vec{S}_{i_x}\vec{\sigma}_{\downarrow\uparrow}\delta_{i_x,i} & \mu-J\vec{S}_{i_x}\vec{\sigma}_{\downarrow\downarrow}\delta_{i_x,i}
\end{bmatrix}
\tag{3.6}
$$

where all sites i_x containing an impurity spin are selected by $\delta_{i_x,i}$. In order to see the symmetry of the Hamiltonian more clearly, it can be simplified by expressing each of the four 2x2 blocks by a 2x2 matrix. The resulting symmetry structure of the local interaction Hamiltonian therefore takes the form

$$
\begin{bmatrix}
\mathbf{A} & \mathbf{B} \\
\mathbf{B}^{*} & -\mathbf{A}
\end{bmatrix}
$$

which is the structure of a Hermitian matrix as expected.
The nearest-neighbor terms have the structure

$$
\begin{bmatrix}
\mathbf{C} & \mathbf{D} \\
\mathbf{E}^{\dagger} & -\mathbf{C}
\end{bmatrix}
$$

where $\mathbf{C},\mathbf{D},\mathbf{E}$ are 2x2 matrices, and the terms get complex conjugated and transposed (†) for the nearest neighbor in the other direction. Triplet pairing interaction is taken into account here.

Similar to the SOC term, the partial Fourier transformation of the triplet pairing term looks like

$$\begin{aligned}
H_{tri} &= \sum_{i,j,\alpha,\beta} \Delta^{i,j}_{\alpha,\beta} c^\dagger_{i,\alpha} c^\dagger_{j,\beta} + \text{h.c.} \\
&= \sum_{i_x,j_x,\alpha,\beta} \sum_{k_y,k'_y} \Delta^{i_x,j_x}_{\alpha,\beta} c^\dagger_{i_x,k_y,\alpha} c^\dagger_{j_x,k'_y,\beta} e^{-i(k_y i_y)} e^{-i(k'_y j_y)} + \text{h.c.} \\
&= \sum_{i_x,\delta,\alpha,\beta} \sum_{k_y,k'_y} \Delta^{i_x,j_x}_{\alpha,\beta} c^\dagger_{i_x,k_y,\alpha} c^\dagger_{i_x+\delta_x,k'_y,\beta} e^{-i(k_y i_y + k'_y i_y)} e^{-i(k'_y \delta_y)} + \text{h.c.} \\
&= \sum_{i_x,k_y,\alpha,\beta} (\Delta^{i_x,j_x}_{\alpha,\beta} c^\dagger_{i_x,k_y,\alpha} c^\dagger_{j_x,-k_y,\beta})(\delta_{j_x,i_x+1} + \delta_{j_x,i_x-1}) 2\cos(k_y a) + \text{h.c.}
\end{aligned}$$

where only nearest neighbor interaction is considered. Since Rashba SOC is considered, triplet pairing is only considered for the case of equal spins [40]. Together with the remaining part of the SOC term, the hopping term and the symmetry, this imposes the following formulation in order to fulfill the requirement of a Hermitian matrix

$$H_{i_x<j_x,k_y} = \begin{bmatrix} -2t\cos(k_y) & -\gamma & 2\cos(k_y)V^{\uparrow}_{i_x,k_y} & 0 \\ \gamma & -2t\cos(k_y) & 0 & 2\cos(k_y)(V^{\downarrow}_{i_x,k_y})^* \\ -2\cos(k_y)(V^{\uparrow}_{i_x,k_y})^* & 0 & 2t\cos(k_y) & \gamma \\ 0 & -2\cos(k_y)V^{\downarrow}_{i_x,k_y} & -\gamma & 2t\cos(k_y) \end{bmatrix} \tag{3.7}$$

were $V^{\sigma}_{i_x,k_y}$ represents the pairing potential for same spin Cooper pairs with spin σ at site i_x for momentum k_y and the lattice constant $a = 1$. The combination of matrix 3.6 and 3.7 describes the on-site as well as nearest-neighbor interaction of the system. It takes the form

$$\left[\begin{array}{cc|cc} \mathbf{A} & \mathbf{B} & \mathbf{C} & \mathbf{D} \\ \mathbf{B}^* & -\mathbf{A} & \mathbf{E}^\dagger & -\mathbf{C} \\ \hline \mathbf{C} & \mathbf{E} & \mathbf{A} & \mathbf{B} \\ \mathbf{D}^\dagger & -\mathbf{C} & \mathbf{B}^* & -\mathbf{A} \end{array}\right]$$

When looking at the eigenvalue equations of the full H_{k_y}, one finds that if E_{n,k_y} is an eigenvalue of H_{k_y} then $-E_{n,-k_y}$ is also an eigenvalue of H_{k_y}. The eigenvector of $-E_{n,-k_y}$ is found to be the complex conjugate of the eigenvector of E_{n,k_y}, when additionally the momentum is reversed. This symmetry can be exploited when diagonalizing the Hamiltonian numerically.
The diagonalized Hamiltonian can be expressed by the diagonal matrix D, which contains all eigenvalues on its diagonal, when the original basis W is transformed into a new basis Γ. This new basis is the eigenbasis of the Hamiltonian and defined by the relation

$$\Gamma^\dagger_{k_y} = W^\dagger_{k_y} P_{k_y} = \left(\gamma_{k_y,1}, \gamma_{k_y,2}, \ldots \gamma_{k_y,4N_x}\right)$$

to the old, Nambu basis W_{k_y}, where P_{k_y} contains all eigenvectors as columns.
The components of these eigenvectors can be labeled as

$$P^T_{k_y} = \begin{bmatrix} u_{1,1,k_y} & v_{1,1,k_y} & w_{1,1,k_y} & x_{1,1,k_y} & u_{2,1,k_y} & \ldots & x_{N_x,1,k_y} \\ \vdots & & & & & \vdots & \\ u_{1,N_x,k_y} & v_{1,N_x,k_y} & w_{1,N_x,k_y} & x_{1,N_x,k_y} & u_{2,N_x,k_y} & \ldots & x_{N_x,N_x,k_y} \end{bmatrix}$$

which leads to the definition of each single entry of the eigenbasis-vector as

$$\gamma^\dagger_{k_y,n} = \sum_{i_x} \left(c^\dagger_{i_x,k_y,\uparrow} u_{i_x,n,k_y} + c^\dagger_{i_x,k_y,\downarrow} v_{i_x,n,k_y} + c_{i_x,-k_y,\uparrow} w_{i_x,n,k_y} + c^\dagger_{i_x,-k_y,\downarrow} x_{i_x,n,k_y} \right)$$

Using the symmetry of the eigenvectors under complex conjugation, which can be written as

$$P^T_{k_y,n} = P^\dagger_{k_y,n} = w^*_{1,n,k_y}, x^*_{1,n,k_y}, u^*_{1,n,k_y}, v^*_{1,n,k_y}, w^*_{2,n,k_y}, \dots v^*_{N_x,n,k_y}$$

and using the symmetry under reversing momentum, the eigenbasis-vector components can also be defined as

$$\gamma^\dagger_{-k_y,n} = \sum_{i_x} \left(c^\dagger_{i_x,-k_y,\uparrow} w^*_{i_x,n,k_y} + c^\dagger_{i_x,-k_y,\downarrow} x^*_{i_x,n,k_y} + c_{i_x,k_y,\uparrow} u^*_{i_x,n,k_y} + c_{i_x,k_y,\downarrow} v^*_{i_x,n,k_y} \right)$$

which also follows from the relation $W_{-k_y} = P_{-k_y} \Gamma_{-k_y}$. It follows directly, that $\gamma^\dagger_{-k_y,n} = \gamma_{k_y,n}$, which implies that not all $\gamma_{k_y,n}$ operators are independent of each other for all k_y-values what restores the correct amount of degrees of freedom.
The diagonal Hamiltonian can now be written in terms of the new basis, which consist of the new operators as suggested in BdG formalism, and reads

$$H = H_0 + \frac{1}{2} \sum_{n,k_y>0} E_{n,k_y} \gamma^\dagger_{n,k_y} \gamma_{n,k_y} + \frac{1}{2} \sum_{n,k_y<0} E_{n,k_y} \gamma^\dagger_{n,k_y} \gamma_{n,k_y} + K$$

where the sum was split into a $k_y < 0$, $k_y > 0$ and $k_y = 0$ part. The latter is simply denoted by K for now.
Substituting $E_{n,k_y} \to -E_{n,k_y}$ in the sum over $k < 0$ allows to use the relation $\gamma^\dagger_{-k_y,n} = \gamma_{k_y,n}$ in the $k < 0$ term. After renaming $k_y \to -k_y$ and applying the relation $\gamma^\dagger_{-k_y,n} = \gamma_{k_y,n}$ a second time, the Hamiltonian reads

$$H = H_0 - \frac{1}{2} \sum_{n,k_y>0} E_{n,k_y} + \sum_{n,k_y>0} E_{n,k_y} \gamma^\dagger_{k_y,n} \gamma_{k_y,n} + K$$

In order to evaluate the $k_y = 0$ term, the problem that this mode does not have a negative partner has to be resolved. That is done by applying the relation $\gamma^\dagger_{-k_y,n} = \gamma_{k_y,n}$ and using that the eigenvalues of H_{-k_y} are $-E_{n,k_y}$, since the Hamiltonian then is

$$H = H_0 - \frac{1}{2} \sum_{n,k_y>0} E_{n,k_y} + \frac{1}{2} \sum_{n,k_y>0} E_{n,k_y} \gamma^\dagger_{n,k_y} \gamma_{n,k_y} + \frac{1}{2} \sum_{n} E_{n,0} \gamma^\dagger_{n,0} \gamma_{n,0}$$

Here, the Fermi-Dirac distribution may be used, since all γ-operators in $\sum_{n,k_y>0}$ are independent in this formulation of the Hamiltonian.
It is possible that for the $k_y = 0$ mode, $H_{k_y} = H_{-k_y}$ holds true. In that case, it also holds that if $E_{n,0}$ is an eigenvalue then so is $-E_{n,0}$. Consequently, the eigenvalues can be sorted such that the first $2N_x$ ones are negative and the last $2N_x$ ones are positive. If one of the eigenvalues is zero, then there is a pair of eigenvalues equaling zero and the first and second half of the eigenvalues is going to contain one of them each. The final expression for the Hamiltonian is therefore

$$H = H_0 - \frac{1}{2} \sum_{n,k_y>0} E_{n,k_y} - \frac{1}{2} \sum_{E_{n,0} \geq 0} E_{n,0} + \sum_{n,k_y>0} E_{n,k_y} \gamma^\dagger_{n,k_y} \gamma_{n,k_y} + \sum_{E_{n,0} \geq 0} E_{n,0} \gamma^\dagger_{n,0} \gamma_{n,0}$$

where all operators are independent of each other.

3.3.1 Local Density of States

Since spin-impurities are introduced into the non-centrosymmetric superconductor and they are expected to interact and interfere with its behavior due to the local RKKY-interaction, it makes sense to study the local density of states (LDOS). It allows to study the local symmetry characteristics and their dependencies.
The starting point to derive the LDOS is the local charge in spin-basis ρ_i, which can be expressed with the LDOS $D_i(E)$ and the occupation probability $f(E)$, which is the Fermi-Dirac distribution. That can be rewritten with the coefficients of the eigenbasis

$$\begin{aligned}\rho_i &= \int_{-\infty}^{\infty} D_i(E) f(E) dE = \sum_{\sigma} \langle c_{i,\sigma}^{\dagger} c_{i,\sigma} \rangle \\ &= \sum_n \left[\left(|u_{i,n}|^2 + |v_{i,n}|^2 \right) (1 - f(E_n)) + \left(|w_{i,n}|^2 + |x_{i,n}|^2 \right) f(E_n) \right]\end{aligned}$$

For a superconducting system, low temperatures can be assumed and therefore the Fermi-Dirac distribution can be approximated as Heaveside step-function $\Theta(x)$. That changes the upper limit of the integral $\infty \to 0$ and replaces the $f(E) \to 1$, which in turn allows the formulate the charge density as

$$\begin{aligned}\rho_i &= \int_{-\infty}^{0} D_i(E) dE \\ &= \sum_n \left[\left(|u_{i,n}|^2 + |v_{i,n}|^2 \right) \Theta(E_n) + \left(|w_{i,n}|^2 + |x_{i,n}|^2 \right) \Theta(-E_n) \right]\end{aligned}$$

The LDOS can therefore be obtained by calculating

$$D_i(E) = \sum_n \left[\left(|u_{i,n}|^2 + |v_{i,n}|^2 \right) \delta(E + E_n) + \left(|w_{i,n}|^2 + |x_{i,n}|^2 \right) \delta(E - E_n) \right]$$

In the implementation, the Dirac-delta function $\delta(E)$ is approximated by a Gaussian distribution with standard derivation of 0.05.

3.3.2 Groundstate Orientation of Impurity Spins

The orientation of the impurity spins is discussed analytically in Section 7.6 and leads to a combination of Heisenberg, Ising and Dzyaloshinskii-Moriya terms.
For the numerical approach the impurity spin-1/2 orientations are parameterized and their respective free energies calculated. All possible spin configurations have to be considered, since the numerical system has hard wall boundary conditions in x-, and periodic boundary conditions in y-direction. Additionally, the symmetry in z-direction is broken by the SOC, which leaves each direction unique. If the system had either only hard wall or only periodic boundary conditions, then the xy-plane would be rotationally invariant and only the relative position of the spins would matter.
Therefore, all possible spin configurations are parameterized in spherical coordinates and the discretization is chosen such that colinear and non-colinear alignments in all three directions are included yielding 625 different spin configurations.

For each of the spin configurations the Hamiltonian is diagonalized and the free energy of the system is calculated based on

$$F = \sum_{n,k>0} \left[-\frac{E_{n,k}}{2} - \frac{1}{\beta} \ln\left(1 + e^{-\beta E_{n,k}}\right) \right] - \sum_{E_n \geq 0} \frac{E_{n,k=0}}{2} - \sum_{E_{n,k=0} \geq 0} \frac{1}{\beta} \ln\left(1 + e^{-\beta E_{n,k=0}}\right)$$

The groundstate than is determined by comparing the free energies of all spin configurations and identifying the minimum.

4 Normal Metal with RKKY interaction

A normal metal can be described by a tight-binding model for fermions, which has the Hamiltonian

$$H_{nm} = H_{kin} + H_{pot} = -t \sum_{\langle i,j\rangle,\sigma} c^{\dagger}_{i,\sigma} c_{j,\sigma} - \mu \sum_{i,\sigma} c^{\dagger}_{i,\sigma} c_{i,\sigma}$$

with the annihilation [creation] operators $c^{[\dagger]}_{i,\sigma}$ for fermions with spin σ at lattice site i, and the hopping amplitude t. Only nearest neighbor-hopping is included as indicated by $\langle i,j\rangle$ and the hopping amplitude is used to shift all interaction potentials to a unitless expression That also leaves the expectation value of the Hamiltonian unitless, when divided by t. The lattice can be chosen freely and such that comparisons to possible experimental data become more easy. The last term describes the potential energy of the system and is proportional to the chemical potential $\mu = \tilde{\mu}/t$, which is unitless.
The Hamiltonian can be diagonalized by transforming the fermion operators from real space to k-space via a Fourier-transformation of the form

$$c_{i,\sigma} = \frac{1}{\sqrt{N}} \sum_{\mathbf{k}} e^{i\mathbf{k}\mathbf{r_i}} c_{k,\sigma}$$

and its hermitian conjugate. For brevity, the vector $\mathbf{k} \in \mathbb{R}^2$ is going to be written as k only. Furthermore, the lattice constant a and any further lattice constant is set to one.
By defining the energy $\epsilon_k = -t \sum_{\langle i,j\rangle} \exp(-ik\delta_{ij})$, the Hamiltonian can be expressed as

$$H_{nm} = \sum_{k,\sigma,\sigma'} (\epsilon_k - \mu) c^{\dagger}_{k,\sigma} c_{k,\sigma'} \tag{4.1}$$

The RKKY interaction as defined in Eq. (2.1) can also be Fourier transformed and then added to H_{nm}. Note that the energy ϵ_k in Eq. 4.1 is not specified for any lattice. In the numerical calculations, however, the lattice is chosen to be a square lattice and the energy takes the form $\epsilon_k = -2t(\cos(k_x) + \cos(k_y))$, which will be used in all following calculations.
The total system including the RKKY interaction can consequently be expressed as

$$H^{RKKY}_{nm} = \sum_{k,\sigma,\sigma'} (\epsilon_k - \mu) c^{\dagger}_{k,\sigma} c_{k,\sigma'} + \sum_{k,k',\sigma,\sigma'} \sum_{i} \frac{J}{N} e^{i(k-k')r_i} (\mathbf{S}_i \cdot \vec{\sigma}_{\sigma,\sigma'}) c^{\dagger}_{k,\sigma} c_{k',\sigma'}$$

where r_i denotes the position of the impurity spin $\mathbf{S}_i$. The added term containing the RKKY-interaction can be treated as a perturbation to the normal metal, which allows to use the Schrieffer-Wolff transformation (SWT) to obtain the effective interaction.
After calculating the necessary commutators and taking the expectation value of the effective Hamiltonian, the spin structure can be identified as

$$\langle H^{RKKY}_{nm} \rangle = \langle H_{nm} \rangle - \sum_{i,j,k,k'} \left(\frac{J}{N}\right)^2 e^{i(k-k')(r_i - r_j)} \, 2\, \mathbf{S}_i \mathbf{S}_j \, (f(E_k) - f(E_{k'})) \tag{4.2}$$

where $f(E_{k,\sigma}) = \langle c^{\dagger}_{k,\sigma} c_{k,\sigma} \rangle$ denotes the Fermi-Dirac distribution and $\langle H_{nm} \rangle$ is the expectation value for the unperturbed system. This spin structure is of Heisenberg form with a coupling constant oscillating between positive and negative and, consequently, the preferred orientation of the impurity spins is either parallel or anti-parallel without any preference regarding the axis, meaning

that the system is isotropic in spin.
The changes within the normal metal because of the impurities are neglected and only the influence of the normal metal environment onto the configuration of the impurity spins is investigated. This simplification can be justified by the low density of impurity spins in the system and is applied to all systems studied in this thesis.

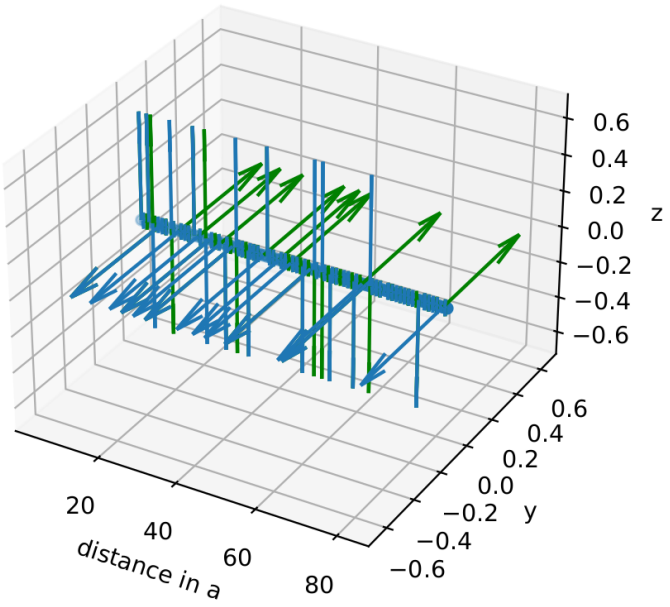

(a)

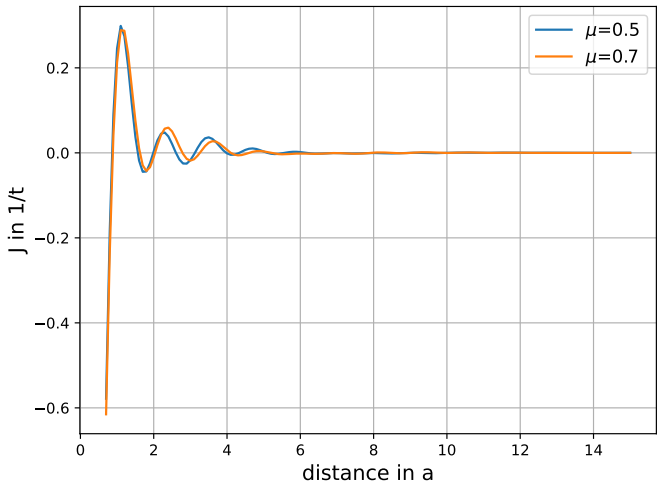

(b)

Figure 7: Figure (a) displays the orientation of the two impurity spins in the groundstate determined numerically for a system size of 240x20, $\mu = 0.5$ and $J = 2$. This orientation is Heisenberg-like and oscillates over distance. Figure (b) shows the oscillation in more detail for two different chemical potentials μ calculate with the numerical approach. A stronger chemical potential leads to a slightly longer oscillation period, but also to an earlier decay. It is a system with size 100x100 and $J = 2$.

The numerical solution presented in Fig. 7 displays a Heisenberg-type spin-spin interaction. The impurity spins align only parallel and anti-parallel, and the axis to which the spins are aligned is

to a certain degree arbitrary and seems to oscillate with distance, too. Such a change in preferred axis is in accordance the analytical theory, just as the Heisenberg interaction, as can be seen in Fig. 7(b) Fig. 7(b) displays the oscillation of the RKKY interaction strength as calculated in Eq. (4.2) over distance. A positive interaction strength corresponds to ferromagnetic (FM) ordering, while a negative interaction strength corresponds to anti-ferromagnetic (AFM) ordering of the impurity spins. The expected decay in interaction strength is clearly visible. It can be explained by the fact, that the electrons can not travel entirely free within the metal and therefore loose information about the spin while moving from one to the other impurity spin. The change in total orientation of the impurity strength is due to the degeneracy of the system and is clearly reflected in the numerical results, too.

Additionally, the influence of the chemical potential μ is visible in Fig. 7(b). The chemical potential affects the RKKY interaction by altering the density of states of the conduction electrons that mediate the interaction, since it affects the density of states by modifying the energy levels available to the electrons. At higher chemical potential, the density of states is increased and the RKKY interaction is strengthened, which can be seen by the longer periodicity of the oscillation. At lower chemical potential, the density of states is decreased and the RKKY interaction is weakened. The discrepancies between theoretical and numerical results stems from the limited numerical accuracy. Since the energy levels of the lowest lying states only show differences of order 10^{-13}, they are numerically equivalent, which means that the actual groundstate is chosen somewhat random. Nevertheless, the difference between the energy levels corresponding to non-colinear alignments are of numerical significance. This form of degeneracy is also expected because of the symmetry of the system.

Note that the RKKY interaction constant is kept within the interval $[0, 3.5t]$, because a higher interaction constant would lead a swap between FM and AFM ordering. The explanation lies in the spin splitting of the metal's bands that due to the RKKY interaction takes the form $J\vec{\sigma} \cdot \mathbf{S}$. With increasing interaction strength J, the splitting becomes stronger and pushes the bands away from the Fermi-energy level as illustrated in Fig. 8.

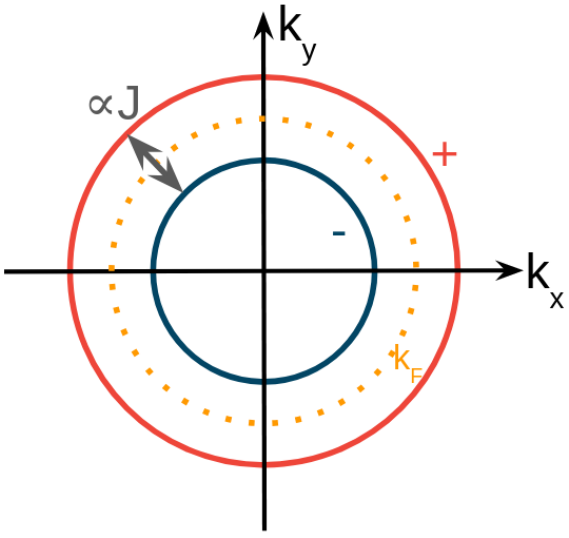

Figure 8: Splitting of positive and negative spin bands away from Fermi surface k_F is proportional to the RKKY interaction strength J for sites with impurities.

The two emerging separated bands correspond each to one spin orientation and they are filled up

to the Fermi-energy.
These changes in the LDOS happen only at the sites of impurity spins, but the LDOS of sites in between impurities are also influenced by the changes, because of the interaction between impurity spins. As soon as the overlap of the two spin-bands vanishes and the LDOS at impurity sites shows a gap, the LDOS of sites in between will also show a gap, if the impurity spins are aligned parallel. That can be understood by looking at Fig. 9, which shows the LDOS of the two impurity sites as well as one site in between. These changes in LDOS in the entire system influences the free energy in such way that an AFM impurity spin orientation is preferred for short distances. For long distances, on the other hand, the influences on the LDOS on sites between impurities is too short ranged to have an effect on the free energy, since they neutralize over distance due to the imperfect conductance of electrons.
Therefore the RKKY interaction strength is kept within $J \in [0, 3.5t]$ to avoid such effects.

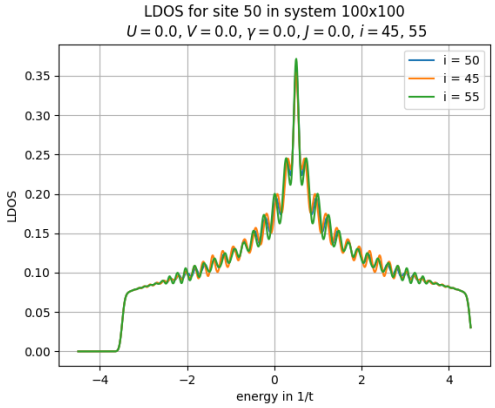

(a) RKKY $J = 0$

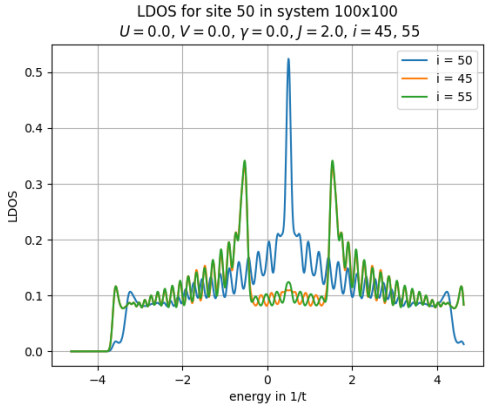

(b) RKKY $J = 2$

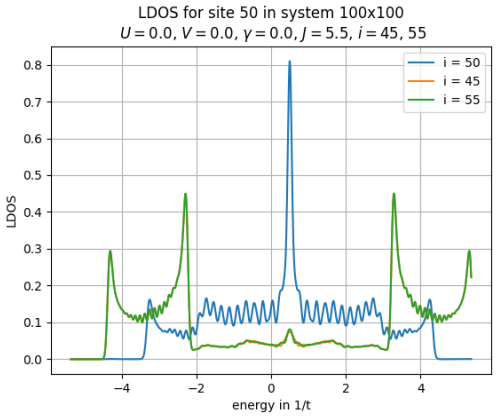

(c) RKKY $J = 5$

Figure 9: LDOS for a normal metal with two impurities at three different sites. For $J = 0$ in (a) all LDOS are nearly identical, for weak $J = 2$ in (b) the development of two bands because of spin orientation is visible, and for strong $J = 5$ in (c) the bands do not overlap any longer. The bands form on the sites of the impurities at $i = 45, 55$, while the site $i = 50$ between them is influenced by the changes of LDOS on the impurity sites. Depending on the impurity spin orientation, the changes in LDOS on $i = 50$ differ.

5 Superconductor with RKKY

RKKY interaction in both s- and d-wave superconductors has been the subject of extensive research, as demonstrated by Ghanbari [5] and others. However, a brief examination of the system is conducted in this study to assess the efficacy of the applied method and obtain results that can be compared with previous findings.
The Hamiltonian of the system without impurity spins has the form

$$H_{SC} = H_{nm} + \sum_i U c^\dagger_{i,\uparrow} c^\dagger_{i,\downarrow} c_{i,\downarrow} c_{i,\uparrow}$$

where $U = \tilde{U}/t$ denotes the strength of the attractive potential, which is a BCS on-site attractive interaction. Therefore the system can be treated with the BCS formalism.
As the first step to diagonalize H_{SC}, the attractive interaction term is transformed into k-space and a mean-field treatment is performed as introduced in Sec. 2.3.2. H_{SC} reads afterwards

$$H_{SC} = \sum_{k,\sigma} (\epsilon_k - \mu) c^\dagger_{k,\sigma} c_{k,\sigma} - \sum_{k,\sigma} \left[\Delta c^\dagger_{k,\uparrow} c^\dagger_{-k,\downarrow} + \Delta^* c_{-k,\downarrow} c_{k,\uparrow} \right] - \frac{|\Delta|^2}{V}$$

The attractive interaction leads to an s-wave superconductor with $\Delta \in \mathrm{R}$, which follows from the definition of the superconducting gap and the fact that all involved quantities are real for singlet s-wave pairing.
Secondly, a BdG transformation as described in Sec. 3.1 is applied which defines new fermion operators as

$$\begin{aligned} c_{k,\sigma} &= \eta_k \, \gamma_{k,\sigma} + \sigma \, \nu_k \, \gamma^\dagger_{-k,-\sigma} \\ c^\dagger_{-k,-\sigma} &= -\sigma \, \nu_k \, \gamma_{k,\sigma} + \eta_k \, \gamma^\dagger_{-k,-\sigma} \end{aligned}$$

where

$$\begin{aligned} \eta_k &= \frac{(\sqrt{(\epsilon_k - \mu)^2 + \Delta^2} + \epsilon_k - \mu)}{\sqrt{(\sqrt{(\epsilon_k - \mu)^2 + \Delta^2} + \epsilon_k - \mu)^2 + \Delta^2}} \\ \nu_k &= \frac{\Delta}{\sqrt{(\sqrt{(\epsilon_k - \mu)^2 + \Delta^2} + \epsilon_k - \mu)^2 + \Delta^2}} \end{aligned}$$

and the notation is adapted from Ghanbari [59].
Ultimately, the diagonalized H_{SC} takes the form

$$\begin{aligned} H_{SC} &= -\frac{|\Delta|^2}{V} + \sum_k (\epsilon_k - \mu) + \sum_{k,\sigma} \sqrt{(\epsilon_k - \mu)^2 + \Delta^2} \left(\gamma^\dagger_{k,\sigma} \gamma_{k,\sigma} - \frac{1}{2} \right) \\ &= -\frac{|\Delta|^2}{V} + \sum_k (\epsilon_k - \mu) + \sum_{k,\sigma} E^{SC}_k \left(\gamma^\dagger_{k,\sigma} \gamma_{k,\sigma} - \frac{1}{2} \right) \end{aligned}$$

This energy spectrum allows to investigate different properties of the superconductor, before the RKKY interaction is added and studied.

5.1 Bound States

Although the density of impurities in the system is chosen so small that their effects on the overall superconducting gap can be neglected, the impurities still have an influence on the LDOS in their close environment.
The impurity spins are chosen classical, which allows to treat them as magnetic impurities. Previous work on their influence on the energy spectrum of the neighboring sites has shown that states within the superconducting gap are occupied [3, 60], which in turn influences the phase transition and gap itself [61].
The states that emerge are due to the Kondo effect. As derived by Shiba for the classical limit, the presence of an impurity shifts the poles of the Green function of the system towards a Green function with poles at

$$E_{\text{bound}} = \pm\Delta_0 \frac{1 - \left(\frac{1}{2}JS\rho\pi\right)^2}{1 + \left(\frac{1}{2}JS\rho\pi\right)^2}$$

relative to the initial gap Δ_0, where the RKKY interaction strength is J, the spin S and the density of states ρ at the Fermi level in the normal state.
Spin, density of states and π are constants and therefore they are set to one for the numerical calculations and the factor $1/2$ is absorbed into J. Since the energy depends only on the oscillating RKKY interaction strength, the energy of the electrons localized around the impurity depends only on the distance to the impurity. Those electrons are localized around the impurities in the first place, because the presence of the impurities lowers their energy. The oscillating nature of the RKKY interaction is reflected in the position of the bound states. Generally, the LDOS shows a strong superconducting gap, which closes with increasing RKKY interaction at the impurity site, because it breaks the Cooper pairs [3].
On the sites next to the impurity, the bound states form as can be seen in Fig. 10. The different colored lines there represent LDOS on different sites in the system and the dotted line is the impurity site. An increasing RKKY interaction strength gives rise to clear in-gap peaks for negative energies and only very small alternations for positive in-gap states. This relation changes to a nearly equal distribution for the next-nearest neighbor site. Although not depicted here, with increasing distance from the impurity the relation between positive and negative energy in-gap states oscillates in the qualitatively same behavior as the RKKY interaction strength itself does. Therefore the numerical results match the expected behavior for bound states.

Bound states do also exist in unconventional superconductors, but are more difficult to find and exhibit more complex behavior, due to the presence of triplet Cooper pairs. In Sec. 7.4, an attempt to study these bound states is made despite that difficulty.

5.2 Spin Structure of Superconductor with RKKY

The RKKY interaction is treated perturbatively again and therefore a SWT is applied. The ansatz

$$S = \sum_{k,k',\alpha,\beta} (A_{k,k',\alpha,\beta}\gamma^\dagger_{k,\alpha}\gamma_{k',\beta} + B_{k,k',\alpha,\beta}\gamma^\dagger_{k,\alpha}\gamma^\dagger_{-k',-\beta} + C_{k,k',\alpha,\beta}\gamma_{-k,-\alpha}\gamma_{k',\beta} + D_{k,k',\alpha,\beta}\gamma_{-k,-\alpha}\gamma^\dagger_{-k',\beta})$$

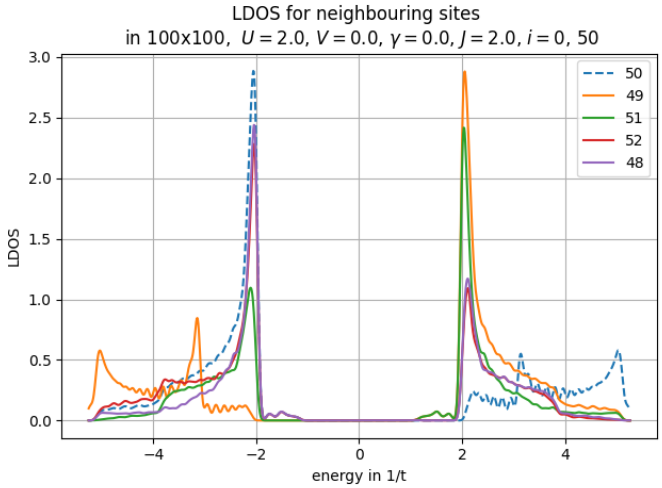

Figure 10: Bound states at impurity spin in a s-wave superconductor.

is used in the SWT and yields the four coefficients

$$A_{k,k',\alpha,\beta} = i\sum_i \frac{J}{N} e^{i(k-k')r_i} \left(\mathbf{S}_i \cdot \vec{\sigma}_{\alpha,\beta}\right) \frac{\eta_k^* \eta_{k'}}{E_{k'} - E_k}$$

$$B_{k,k',\alpha,\beta} = -\beta i\sum_i \frac{J}{N} e^{i(k-k')r_i} \left(\mathbf{S}_i \cdot \vec{\sigma}_{\alpha,\beta}\right) \frac{\eta_k^* \nu_{k'}}{E_{-k'} + E_k}$$

$$C_{k,k',\alpha,\beta} = \alpha i\sum_i \frac{J}{N} e^{i(k-k')r_i} \left(\mathbf{S}_i \cdot \vec{\sigma}_{\alpha,\beta}\right) \frac{\nu_k^* \eta_{k'}}{E_{k'} + E_{-k}}$$

$$D_{k,k',\alpha,\beta} = \alpha\beta i\sum_i \frac{J}{N} e^{i(k-k')r_i} \left(\mathbf{S}_i \cdot \vec{\sigma}_{\alpha,\beta}\right) \frac{\nu_k^* \nu_{k'}}{-E_{-k'} + E_{-k}}$$

Based on these coefficients, the effective interaction H_{SC}^{RKKY} can be calculated. After computing the missing commutator and evaluating the Hamiltonian in the groundstate of the unperturbed system, $\langle H_{SC}^{RKKY} \rangle$ is determined and the spin structure can be written in form of Heisenberg interaction:

$$\langle H_{SC}^{RKKY} \rangle = \langle H_{SC} \rangle - \sum_{i,j,k,k'} J_{k,k'}^{SC} \mathbf{S}_i \mathbf{S}_j$$

where $J_{k,k'}^{SC}$ is defined as

$$J_{k,k'}^{SC} = \sum_{k,k'} \left(\frac{J}{N}\right)^2 e^{i(k-k')(r_1-r_2)} \left(|\eta_k \eta_{k'}|^2 + |\nu_k \nu_{k'}|^2 + 2\eta_k^* \eta_{k'} \nu_k^* \nu_{k'}\right) \frac{f(E_k) - f(E_{k'})}{E_{k'} - E_k}$$

This interaction strength oscillates with the separation distance between the impurities with a similar behavior as a normal metal. The main difference is how strongly the oscillation is damped, which can be seen in Fig. 11. There the oscillation between ferromagnetic and anti-ferromagnetic ordering is depicted for different Cooper pairing potentials based on the numerical approach. Here, the oscillation can be calculated as the difference between the free energy for ferromagnetic and anti-ferromagnetic ordering, because those two are the only possible groundstates of the system. A positive difference means that anti-ferromagnetic ordering is favored and for a negative difference ferromagnetic ordering.
It can be seen that the RKKY interaction strength decreases significantly faster in a superconductor

than in a normal metal. That originates from the behavior of the electrons, which ultimately lead to the RKKY interaction. In a superconductor, the electrons close to the Fermi surface pair into Cooper pairs, which leaves only the electrons in the lower energy states as available information carriers of the RKKY interaction. The longer the distance between the impurity spins is, the more likely it is that those previously single electrons also pair up into Cooper pairs and loose the spin information in this process. Consequently, the range of interaction between impurity spins in superconductors decreases with increasing attractive electron potential aka. increasing superconducting gap.

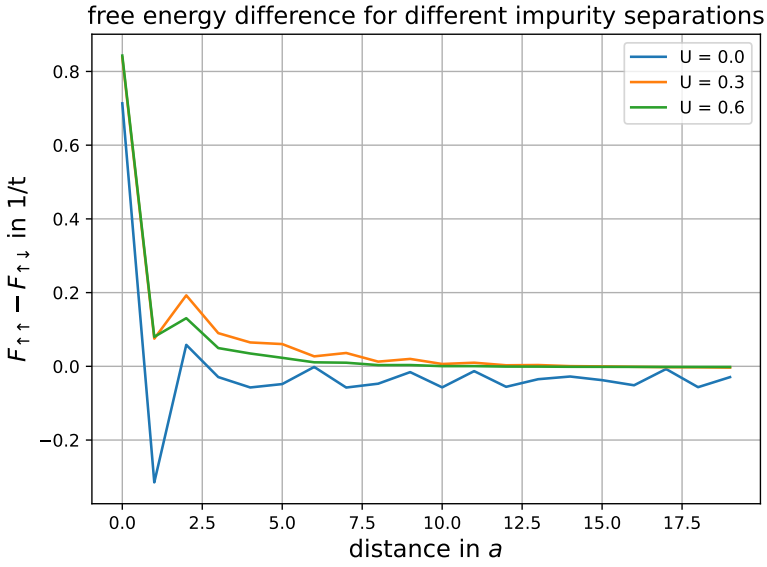

Figure 11: Oscillation of numerical RKKY interaction strength between ferromagnetic and antiferromagnetic, which is stronger damped with higher Cooper pairing potential. The system has size 50x50, $\mu = 0.5$, $J = 2$.

For the same reason as in normal metals, the ordering will switch between FM and AFM for $J > 3.8t$ (see App. A). Therefore the RKKY interaction strength is kept within $J \in [0, 3.5t]$ to avoid such effects for superconducting systems, too.
The numerical results agree with the analytical results as can be seen by comparing Fig. 11 and Fig. 12. In the latter, the RKKY interaction strength J^{SC} is presented for increasing distance between the impurity spins, and for two different Cooper pairing potentials. The stronger potential leads to a stronger damping of the oscillation just as in the numerical case. Nevertheless, there are some differences visible for the smaller distances. While there are two clear peaks in the analytically determined oscillation, there is only one distinct peak visible in the numerical result. This difference might be caused by the fact that the numerical solution takes bound states in account, while the analytical does not do so. Therefore the in-gap states influence the availability of electrons for information transfer in such way, that the information loss is slightly slower in the numerical result. That means in turn that the ferromagnetic ordering is favorable over longer distances and slightly more comparable to the behavior in a normal metal than the results from the analytical approach. But note that the RKKY interaction strength stays completely positive for the superconducting case due to the modified density of states of the conduction electrons that mediate the interaction.

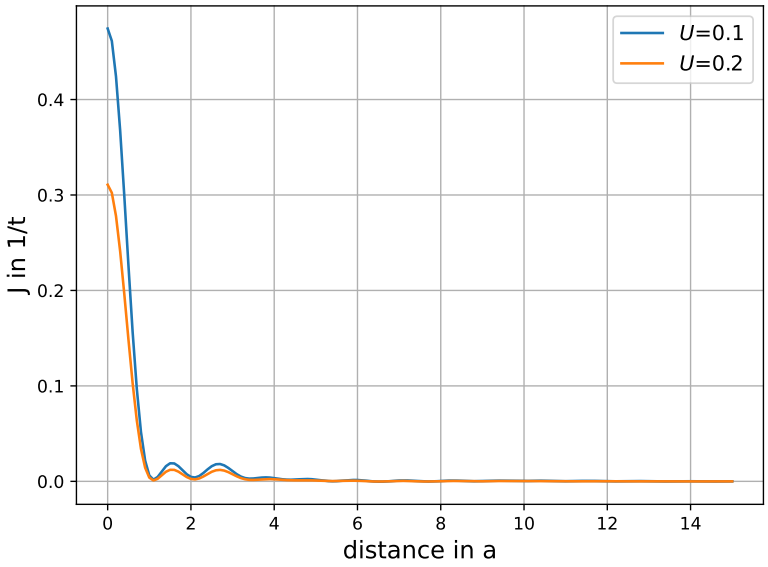

Figure 12: Oscillation of analytical RKKY interaction strength between ferromagnetic (positive) and anti-ferromagnetic (negative), which is stronger damped with higher Cooper pairing potential. The system is of size 100x100 and has $\mu = 0.5$, $J = 2$.

6 Normal Metal with Spin Orbit Coupling and RKKY

A normal metal with Rashba SOC with coupling strength $\gamma = \tilde{\gamma}/(at)$ is studied now. This type of SOC is a consequence of the broken inversion symmetry of the metal, since it is non-centrosymmetric. The SOC strength is assumed to be the same in the entire system, which is reasonable since only the bulk properties are of interest here.
Employing the Fourier transformation of the fermion operators, leads to the following formulation of the system's Hamiltonian

$$H_{SOC} = \sum_{k,\sigma,\sigma'} [(\epsilon_k - \mu)\delta_{\sigma\sigma'} + \gamma\, \mathbf{n}\,(\mathbf{d}_k \times \vec{\sigma}_{\sigma,\sigma'})] c^\dagger_{k,\sigma} c_{k,\sigma'} \tag{6.1}$$

The Hamiltonian is therefore diagonal in momentum k, but not in spin σ.
Since the SOC couples spin and momentum, this is to be expected and leads to the definition of helicity λ, which expresses exactly this dependency. The fermion operators are therefore transformed from spin-space to helicity-space [62, 63] by the transformation

$$b_{k,\lambda} = \frac{1}{\sqrt{2|\gamma_k|}} \left(\sqrt{(|\gamma_k| + \lambda\gamma_{k,z})} c_{k,\uparrow} + \lambda \frac{\gamma k, x + i\gamma_{k,y}}{\sqrt{|\gamma_k| + \lambda\gamma_{k,z}}} c_{k,\downarrow} \right) \tag{6.2}$$

$$c_{k,\sigma} = \frac{1}{\sqrt{2|\gamma_k|}} \frac{(\gamma_{k,x} + i\gamma_{k,y})(1 - \delta_{\sigma=\uparrow})}{|\gamma_k|} \left(\sqrt{|\gamma_k| + \sigma\gamma_{k,z}} b_{k,+} + \sigma \sqrt{|\gamma_k| - \sigma\gamma_{k,z}} b_{k,-} \right) \tag{6.3}$$

where $\lambda = \pm 1$ is the helicity index and $\gamma(k) = \gamma \mathbf{n} \mathbf{d}_k = \gamma_k$. This transformation is unitary and therefore preserves the fermionic anti-commutation relations of the particle operators c.
Inserting this into the Hamiltonian in Eq. (6.1) leads to the diagonalized expression for the non-centrosymmetric metal

$$H_{SOC} = \sum_{k,\lambda} ((\epsilon_k - \mu) + \lambda|\gamma_k|)\, b^\dagger_{k,\lambda} b_{k,\lambda} = \sum_{k,\lambda} \xi_{k,\lambda} b^\dagger_{k,\lambda} b_{k,\lambda} \tag{6.4}$$

Therefore the system's energy spectrum in helicity basis is

$$\xi_{k,\lambda} = (\epsilon_k - \mu) + \lambda|\gamma_k|$$

which describes the lifting of the spin-degeneracy, because although each helicity-basis operator $b_{k,\lambda}$ contains both $c_{k,\uparrow}$ and $c_{k,\downarrow}$, they are weighted differently. That leads to different energies associated with the different spin-orientations.
The RKKY interaction is also transformed into helicity basis by means of Eq. (6.2):

$$H_{RKKY} = \sum_{k,k',i,\lambda,\lambda'} T^{\gamma}_{i,k,k',\lambda,\lambda'} b^\dagger_{k,\lambda} b_{k',\lambda'}$$

where $T_{\gamma,k,k',i,\lambda,\lambda'}$ contains all pre-factors. The exact expression for T for a general SOC can be found in App. B. For the case of Rashba-SOC, the entire transformation factor takes the form

$$\begin{aligned}
H_{RKKY} = & \sum_{\substack{i,k,k' \\ \lambda,\lambda',\sigma,\sigma'}} \frac{J}{N} \frac{e^{i(k-k')r_i}}{2\sqrt{|\gamma_k||\gamma_{k'}|}} \begin{bmatrix} S_z & (S_x - iS_y)\frac{\gamma_{k',x}+i\gamma_{k',y}}{|\gamma_{k'}|} \\ (S_x+iS_y)\frac{\gamma_{k,x}-i\gamma_{k,y}}{|\gamma_k|} & -S_z \frac{(\gamma_{k',x}+i\gamma_{k',y})(\gamma_{k,x}-i\gamma_{k,y})}{|\gamma_k||\gamma_{k'}|} \end{bmatrix}_{\sigma,\sigma'} \\
& \times \sqrt{|\gamma_k||\gamma_{k'}|} \begin{bmatrix} 1 & \sigma' \\ \sigma & \sigma\sigma' \end{bmatrix}_{\lambda,\lambda'} b^\dagger_{k,\lambda} b_{k',\lambda'} \\
= & \sum_{\substack{i,k,k' \\ \lambda,\lambda',\sigma,\sigma'}} \frac{J}{N} \frac{e^{i(k-k')r_i}}{2} \Bigg[S_z - \lambda\lambda' S_z \frac{(\gamma_{k',x}+i\gamma_{k',y})(\gamma_{k,x}-i\gamma_{k,y})}{|\gamma_k||\gamma_{k'}|} \\
& + \lambda'(S_x - iS_y)\frac{\gamma_{k',x}+i\gamma_{k',y}}{|\gamma_{k'}|} + \lambda(S_x+iS_y)\frac{\gamma_{k,x}-i\gamma_{k,y}}{|\gamma_k|} \Bigg]
\end{aligned}$$

For employing the SWT (see Sec. 3.2) again, a fitting ansatz has to be made based on the structure of RKKY in helicity basis. This ansatz takes the form

$$S = \sum_{i,k,k',\lambda,\lambda'} A_{i,k,k',\lambda,\lambda'} b^\dagger_{k,\lambda} b_{k',\lambda'}$$

and after calculating the two necessary commutators, the spin structure of two impurity spins interacting via RKKY-interaction is found to be

$$\begin{aligned}
\langle H^{RKKY}_{SOC} \rangle = & \langle H_{SOC} \rangle \\
& + \sum_{k,k'} (J_{i,j,k,k'} + \mathbf{I}_{i,j,k,k'}) \mathbf{S}_i \mathbf{S}_j + D_{i,j,k,k'} (\mathbf{S}_i \times \mathbf{S}_j) + \mathbf{S}_i \cdot \overleftrightarrow{\Gamma}_{i,j,k,k'} \cdot \mathbf{S}_j
\end{aligned}$$

where the coefficients $J, \mathbf{I}, D$ and $\overleftrightarrow{\Gamma}$ are defined as

$$J_{i,j,k,k'} = -2 \left(\frac{J}{2N}\right)^2 e^{i(k-k')(r_1-r_2)} F^{+++}_{k,k'} \tag{6.5}$$

$$\mathbf{I}_{i,j,k,k'} = \begin{pmatrix} m+m^* \\ -(m+m^*) \\ i(m-m^*) \end{pmatrix} \left(\frac{J}{2N}\right)^2 e^{i(k-k')(r_1-r_2)} F^{+--}_{k,k'} \tag{6.6}$$

$$\mathbf{D}_{i,j,k,k'} = \left(\frac{J}{2N}\right)^2 e^{i(k-k')(r_1-r_2)} \begin{pmatrix} i\left(\Phi_1^* + \Phi_1\right) F^{++-}_{k,k'} - i\left(\Phi_1' + (\Phi_1')^*\right) F^{+-+}_{k,k'} \\ \left(\Phi_1^* - \Phi_1\right) F^{++-}_{k,k'} + \left(\Phi_1' - (\Phi_1')^*\right) F^{+-+}_{k,k'} \\ 0 \end{pmatrix} \tag{6.7}$$

$$\overleftrightarrow{\Gamma}_{i,j,k,k'} = \begin{pmatrix} 0 & i(m^*-m) & 0 \\ i(m^*-m) & 0 & 0 \\ 0 & 0 & 0 \end{pmatrix} \left(\frac{J}{2N}\right)^2 e^{i(k-k')(r_1-r_2)} F^{+--}_{k,k'} \tag{6.8}$$

where the following short-hand notation is used for the energy dependence

$$\begin{aligned}
F^{\pm\pm\pm}_{k,k'} &= K^{k,k'}_{+,+} \pm K^{k,k'}_{-,-} \pm K^{k,k'}_{+,-} \pm K^{k,k'}_{-,+} \\
K^{k,k'}_{\lambda,\lambda'} &= \frac{f(\xi_{k,\lambda}) - f(\xi_{k',\lambda'})}{\xi_{k',\lambda'} - \xi_{k,\lambda}}
\end{aligned}$$

In addition, the phase factors stemming from SOC are defined as

$$m = \frac{1}{|\gamma_k|\,|\gamma_{k'}|}(\gamma_{k,x}\gamma_{k',x} - \gamma_{k,y}\gamma_{k',y} + i\gamma_{k,x}\gamma_{k',y} + i\gamma_{k,y}\gamma_{k',x})$$

RKKY interaction has already been investigated in normal metals with SOC [15, 64, 65], and therefore the found spin structure can be compared to existing solutions.
The general spin structure for a two dimensional electron gas (2DEG) with SOC and RKKY was calculated with the Green's functions approach by Mohammad [15]. The notation used in that thesis leads to a spin structure with three terms

$$H_{eff} = J\,\mathbf{S}_i \cdot \mathbf{S}_j + \mathbf{D}\,(\mathbf{S}_i \times \mathbf{S}_j) + \mathbf{S}_i \cdot \overleftrightarrow{\Gamma} \cdot \mathbf{S}_j \tag{6.9}$$

This is for a general SOC, while in the case of Rashba-SOC the $\overleftrightarrow{\Gamma}$ becomes zero.
The spin structure in Eq. (6.5) - (6.8) matches with the findings of Mohammad, because there is a non-zero Heisenberg interaction as well as a Dzyaloshinskii–Moriya (DM) interaction. The exact form differs from Mohammad's, because the odd/even parts in the Green function formalism are defined in a way that does not match with the approach presented in this work. But the crucial part of DM interaction is similar and shows a similar structure, and therefore these two results are considered to be physically equivalent.
The additional DM term in a 2DEG with SOC allows to interpret the spin interaction as a twisted RKKY-interaction as shown by Imamura et al. [64]. They investigate a 2DEG with Rashba-SOC and comparing the results for the spin-structure obtained with the Green's function formalism to the inner product of the untwisted spin space of the first spin and the twisted spin space of the second spin. Namely, the spin space of the second impurity spin is twisted as

$$\begin{aligned} S_2^x(\theta_{12}) &= \cos\theta_{12} S_2^x + \sin\theta_{12} S_2^z \\ S_2^y &= S_2^y \\ S_2^z &= \cos\theta_{12} S_2^z - \sin\theta_{12} S_2^x \end{aligned}$$

where the angle $\theta = 2m\alpha|\mathbf{R}_1 - \mathbf{R}_2|$ with the SOC strength α.
The inner product with the untwisted spin space of the first impurity spin is consequently

$$\mathbf{S}_1 \cdot \mathbf{S}_2(\theta_{12}) = \cos\theta_{12}\mathbf{S}_1\mathbf{S}_2 + \sin\theta_{12}\,(\mathbf{S}_1 \times \mathbf{S}_2)_y + (1 - \cos\theta_{12})\mathbf{S}_1^y\mathbf{S}_2^y$$

This corresponds to a Heisenberg-like interaction with strength $\cos\theta_{12}$, an Ising-like interaction of strength $(1 - \cos\theta_{12})$ and the y-component of a Dzyaloshinskii-Moriya interaction term with strength $\sin\theta_{12}$.
That behavior can also be seen in the coefficients in Eq. (6.5)- (6.8), since the Heisenberg and Ising term are real, while DM and remaining terms are imaginary before the k-space summation.

6.1 Spin Structure and Groundstate

For a better understanding of the analytical spin structure and therefore of the parameters controlling the exact form of each contributions to the groundstate, the four different interaction coefficients are plotted for different distances and two different SOC strengths in Fig. 13. For the weaker SOC of $\gamma = 0.1$, Heisenberg interaction completely dominates the RKKY interaction

over short distances, which is depicted in Fig. 13(a). It is mainly positive, but does oscillate a little bit into the negative regime, too, which means that ferromagnetic spin alignment is strongly favored. The DM interaction dominates the interaction starting from middle distances, from where the Ising interaction also gains in strength. DM is mainly negative and has a very similar phase to the Heisenberg interaction and both oscillations are damped in the same way. Interestingly, the damping is not monotone, because the third maximum of interaction strength is larger than the second one. That is due to the splitting of the total RKKY interaction strength onto the different spin structure components. Calculating the total interaction strength still yields a monotone damping.

With a stronger SOC, the damping becomes monotone and Heisenberg as well as DM become weaker and their relative magnitude is inverted for even shorter distances than before, as can be seen in Fig. 13(b). Although Heisenberg interaction still dominates for short distances leading to a parallel alignment of the two impurity spins, DM interaction determines the spin structure for middle distances of $d = 2 - 7$a, because the overall magnitude of the Heisenberg interaction decreases stronger than the magnitude of the DM interaction. Therefore, a stronger SOC leads to non-colinear spin alignment for middle distances, which is induced by the D_y term of DM. Additionally, the stronger SOC leads to a smaller phase shift between Heisenberg and DM and an increase of the Ising interaction terms I_z and I_y. That further narrows down the favored groundstate spin orientation and counteracts the DM interaction on some distances.

For longer distances, Heisenberg interaction is dominating again, while DM and Ising interaction become significantly weaker, leading to a parallel alignment again. This behavior is additionally visualized as the groundstate spin configuration in App. E in Fig. 28.

The numerical approach does not allow to single out the different coefficients, but it allows to determine the groundstate spin configuration.

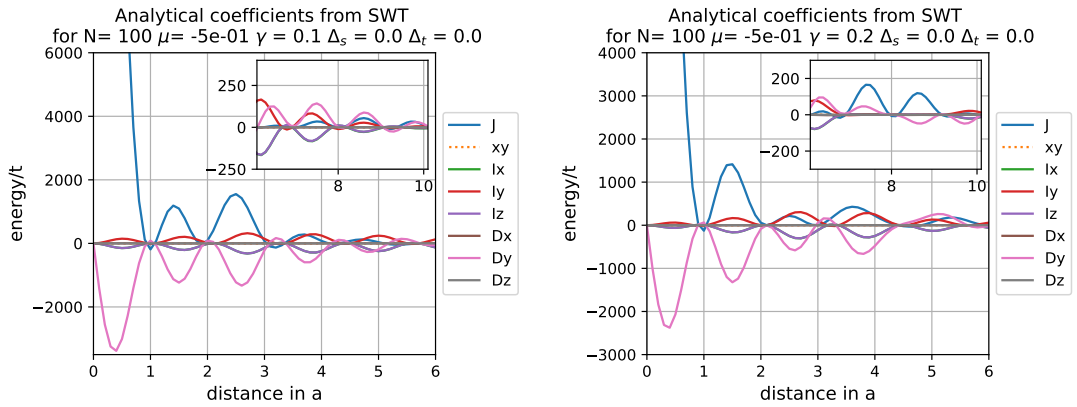

(a) (b)

Figure 13: Analytical results for spin structure coefficients of a normal metal with SOC for (a) weak SOC and (b) strong SOC. The inset shows longer distances, where the overall interaction strength decreases, and therefore, the details of the long range behavior would otherwise not be visible.

Fig. 14 presents the orientation of the impurity spins in the groundstate for different separation distances between them. The blue and the green arrows belong each to one of the impurities, respectively, and for parallel alignment the green arrow covers the blue arrow. As can be seen in Fig. 14, parallel and non-colinear alignment of the spins are present in the groundstate. For

shorter separation distances, there is an oscillation between these two configurations, while the oscillation vanishes for longer distances. That is as predicted by the analytical result.
Although not marked explicitly in this figure, there is some degeneracy to the groundstate in the numerical solution. All states belonging to one groundstate show the same relative angle towards each other, while their absolute orientation differs. Therefore the degeneracy is not completely lifted by the systems anisotropy caused by SOC.
As can be seen from the expressions for each of the interaction types in Eq. (6.5)- (6.8), a degeneracy in in the xy-plane is to be expected from the symmetry of $\mathbf{J}$ and $\overleftrightarrow{\Gamma}$. The DM terms, on the other hand, show differences for x- and y-direction, but only in that sense that they each couple differently to the z-direction. Therefore is the degeneracy in accordance with the analytical result.

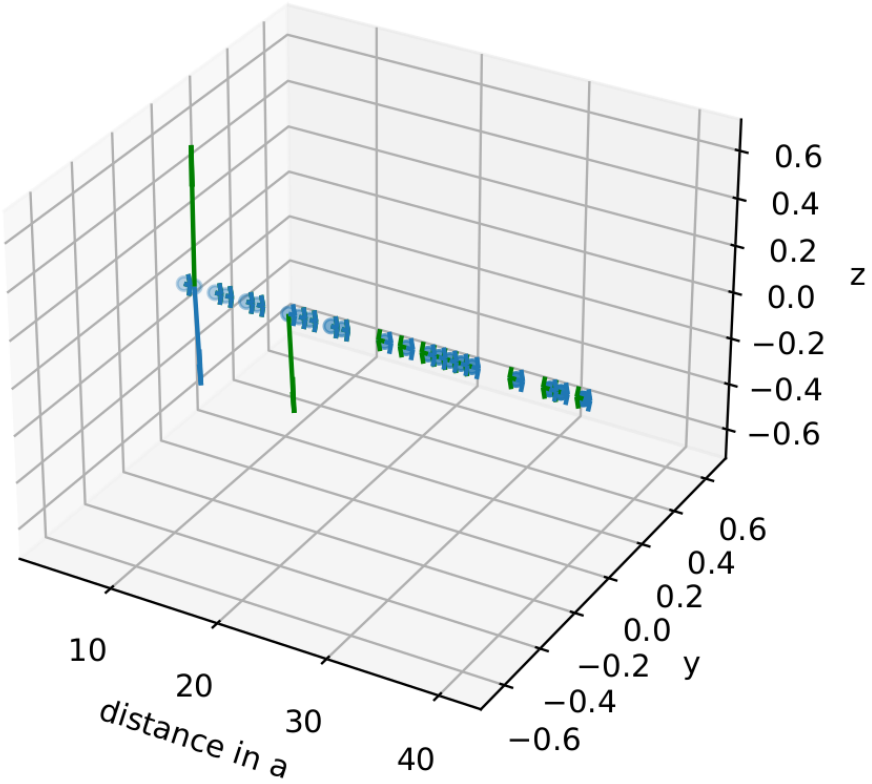

Figure 14: Numerical groundstate spin configuration for a normal metal with SOC $\gamma = 0.1$ and $\mu = 0.5$ for system size 120x15. The spin configuration changes with distance and shows an alternation between non-colinear and parallel spin alignment over distance.

Additional to the investigation of the separate analytical spin structure coefficients, the free energy of the system is determined based on them and the groundstate spin configuration is presented in Fig. 15. There the influence of the DM interaction after short distances becomes clearly visible, because non-colinear alignments dominate the groundstate. That is a difference to the numerical solution, where the DM seems to be weaker in comparison to the other coefficients, which might be due to finite size effects.

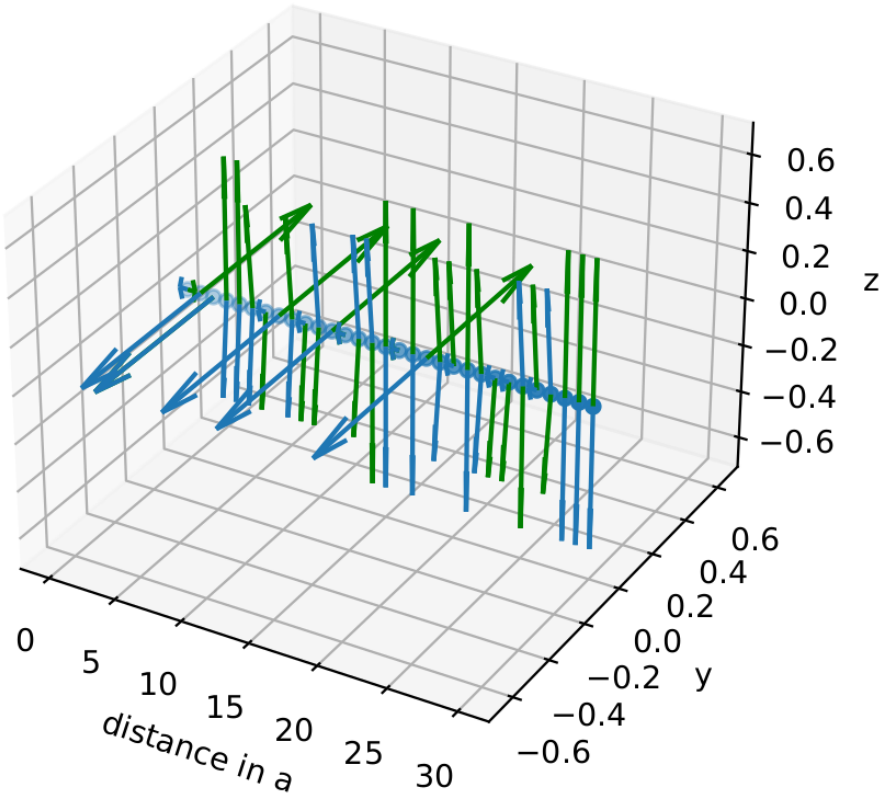

Figure 15: Analytical groundstate spin configuration for a normal metal with SOC $\gamma = 0.2$ and $\mu = 0.5$. The spin configuration changes with distance and shows an alternation between non-colinear and colinear spin alignment over distance.

7 Superconductor with SOC and RKKY

After the methods have been successfully tested on normal metal with and without SOC as well as on conventional superconductor, an unconventional superconductor is studied now. It's broken inversion symmetry, which results into Rashba SOC, leads to triplet pairing in addition to singlet pairing. The interactions within this non-centrosymmetric superconductor can be expressed by the following Hamiltonian:

$$H_{uSC} = H_{SOC} + H_{int} \tag{7.1}$$

The diagonalization of H_{SOC} is already known and written out in Eq. (6.4), therefore the attractive interaction between electrons H_{int} has to be added and the final Hamiltonian diagonalized. The RKKY interaction is going to be treated as a perturbation to that Hamiltonian again.
The attractive interaction term of the non-centrosymmetric superconductor is based on BCS theory and reads in helicity space

$$H_{int} = \sum_{k,k',q} \sum_{\alpha,\alpha',\beta,\beta'} -\frac{1}{2} V_{\alpha,\alpha',\beta,\beta'}(k,k',q) b^\dagger_{k,\alpha} b^\dagger_{-k+q,\beta} b_{-k'+q,\beta'} b_{k',\alpha'}$$

where α, β are helicity-band-indices and $V_{\alpha,\alpha',\beta,\beta'}(k,k',q) = \tilde{V}/t$ denotes the interaction strength. The SOC is assumed to be large compared to the size of the gaps, which suppresses interband hopping. Therefore, the helicity indices are set to $\alpha = \beta = \lambda$ and $\alpha' = \beta' = \lambda'$.
Since the phase space changes with the value of q and is maximal for $q = 0$, all other contributions are negligibly small for large enough SOC [50, 62].
This leads to the following expression for the interaction term

$$H_{int} = \sum_{k,k'} \sum_{\lambda,\lambda'} -\frac{1}{2} V_{\lambda,\lambda'}(k,k') b^\dagger_{k,\lambda} b^\dagger_{-k,\lambda} b_{-k',\lambda'} b_{k',\lambda'} \tag{7.2}$$

which allows for intraband pairing as well as pair-hopping.
Next, a mean-field approximation is done by introducing the average $a_{k,\lambda} = \langle b_{-k,\lambda} b_{k,\lambda} \rangle$ as done in Sec. 2.5.2. The deviation from this average is assumed to be small in the system, such that the approximation $b_{-k,\lambda} b_{k,\lambda} = a_{k,\lambda} + \delta_{k,\lambda}$ holds, and terms of order δ^2 can be disregarded.
This allows to rewrite the Hamiltonian (7.2) as

$$H_{int} = \sum_{k,k',\lambda,\lambda'} -\frac{1}{2} V_{\lambda,\lambda'}(k,k') \left[a^\dagger_{k,\lambda} b_{-k',\lambda'} b_{k',\lambda'} + a_{k',\lambda'} b^\dagger_{k,\lambda} b^\dagger_{-k,\lambda} - a^\dagger_{k,\lambda} a_{k',\lambda'} \right]$$

From that, the order parameter

$$\Delta_{k,\lambda} = \sum_{\lambda',k'} V_{\lambda,\lambda'}(k,k') a_{k',\lambda'}$$

can be defined, which is called gap in the BCS theory. It has a dependence on k, since it is defined in real space for nearest-neighbors only. Now, the Hamiltonian (7.2) can be further rewritten into the form

$$H_{int} = -\sum_{k,\lambda} \frac{1}{2} \left[\Delta_{k,\lambda} b^\dagger_{k,\lambda} b^\dagger_{-k,\lambda} + \Delta^\dagger_{k,\lambda} b_{-k,\lambda} b_{k,\lambda} \right] + \Delta_{k,\lambda} a^\dagger_{k,\lambda} \tag{7.3}$$

where the last term is constant and is going to be disregarded for now. The new characteristics of the gap $\Delta_{k,\lambda}$ are discussed in the next section.

7.1 Singlet and Triplet Pairing Interaction

The attractive interaction between electrons in a non-centrosymmetric superconductor does not only lead to spin-singlet pairs but also to spin-triplet pairs. The Hamiltonian for attractive electron interaction in the helicity basis is presented in Eq. 7.3 and reads

$$H_{int} = -\frac{1}{2}\sum_{k,\lambda}\left(\Delta_{k,\lambda} b^{\dagger}_{k,\lambda} b^{\dagger}_{-k,\lambda} + h.c.\right)$$

where the constant term is neglected, because it is only a constant energy shift.
The Hamiltonian including tight binding model and spin-orbit-coupling is diagonalized by fermionic operators in helicity space and its eigen-energies are symmetric in k. That allows to write the operation of the time-reversal operator $K = i\sigma_y K_0$ as $K|k,\lambda\rangle = t_{k,\lambda}|-k,\lambda\rangle$, where K_0 is the complex conjugation and it is acting on a state $|k,\lambda\rangle$ [62]. Here, the nontrivial phase factor $t_{k,\lambda}$ is defined for the eigenbasis in helicity space as

$$t_{k,\lambda} = \lambda\frac{\gamma_{k,x} - i\gamma_{k,y}}{|\gamma_k|}$$

and therefore depends on the chosen type of SOC. The phase factor allows to write the interaction potential and the gap as

$$\begin{aligned} V_{k,k',\lambda,\lambda'} &= t_{k,\lambda} t^{*}_{k',\lambda'} \tilde{V}_{k,k',\lambda,\lambda'} \\ \Delta_{k,\lambda} &= t_{k,\lambda}\tilde{\Delta}_{k,\lambda} \end{aligned} \tag{7.4}$$

That leaves the interaction potential and the gap even in k-space, because the phase factor $t_{k,\lambda}$ contains all parts odd in k. In addition, it is possible to split the gap in spin-space into positive and negative helicity parts

$$\begin{aligned} \Delta_{k,\sigma,\sigma'} &= \left[\left(\Delta_{s,k} + \mathbf{d}_k\sigma\right) i\sigma_y\right]_{\sigma,\sigma'} \\ \Delta_{s,k} &= \frac{\tilde{\Delta}_{k,+} + \tilde{\Delta}_{k,-}}{2} \\ \mathbf{d}_k &= \frac{\tilde{\Delta}_{k,+} - \tilde{\Delta}_{k,-}}{2}\frac{\gamma_k}{|\gamma_k|} = \Delta_{t,k}\frac{\gamma_k}{|\gamma_k|} \end{aligned}$$

which can be found when transforming between the two basis.
The resulting expression for the gap is a 2x2 matrix expressed in helicity basis variables for the different possible spin-configurations. Furthermore, the definition of $\mathbf{d}_k$ implies that only the orientation parallel to the SOC is allowed as discussed in Sec. 2.5.3.
In the case of Rashba-SOC, it is possible to specify the expression for $\mathbf{d}_k$ in terms of the SOC vector γ_k and the triplet-pairing Δ_t [66], so that the total gap reads in spin-space

$$\Delta_k = \begin{pmatrix} -i\frac{\Delta_{t,k}}{|\gamma_k|}(k_x + ik_y) & \Delta_{s,k} \\ -\Delta_{s,k} & i\frac{\Delta_{t,k}}{|\gamma_k|}(k_y - ik_x) \end{pmatrix}$$

which yields the same preferred triplet paring mechanism as predicted in Sec. 2.5.3. From this representation of the total gap, it also becomes clear that there are only singlet stemming from the s-wave gap and triplets (same spin pairs) stemming from the p-wave gap. There are no singlets from the p-wave gap, because the d_z component is zero since the symmetry breaking axis is chosen in that direction.

For a square lattice, the interaction potential can also be expressed as a more general 2x2 matrix of the structure [62]

$$\begin{aligned}\tilde{V}_{k,k',\lambda,\lambda'} &= \frac{1}{2}V_g\left(\sigma_0+\sigma_x\right)+\frac{1}{2}\lambda\lambda' V_{u,k,k'}\left(\sigma_0-\sigma_x\right)\\ &= \begin{bmatrix} \tilde{V}^d_{k,k',\lambda,\lambda'} & \tilde{V}^o_{k,k',\lambda,\lambda'} \\ \tilde{V}^o_{k,k',\lambda,\lambda'} & \tilde{V}^d_{k,k',\lambda,\lambda'} \end{bmatrix}\end{aligned}$$

where $V_{g[u]}$ represents the even [odd] parts of the interaction in spin-basis. The case of only singlet-pairing corresponds to $V_u = 0$ and $V_g \neq 0$.
Furthermore holds for a square lattice that SOC generally is $\gamma(\mathbf{k}) = \gamma_0\mathbf{k}$ and that an attractive interaction is most likely mediated by phonons, which leads to a k-independent even part V_g. Additionally, the resulting gap functions are isotropic in k-space, because phonons lead to local interactions in most cases. Nevertheless, the magnitudes of gaps corresponding to different helicity bands can generally be different and their difference depends on the strength of the spin-orbit coupling [62], because that leads to a difference in occupation of the two helicity bands. The ratio between the positive and negative helicity gap determines the ratio $|\mathbf{d}_k|/|\Delta_{s,k}|$ and suggests that for weak SOC singlet-pairing dominates while triplet-pairing dominates for strong SOC. Those two cases have different gap symmetries, namely s-wave dominated or p-wave dominated for weak and strong SOC, respectively.
Taking the triplet-pairing into account, as done in this section, alters the shape of the gap expected to be seen in the density of states. For singlet pairing, there is one region close to $E = 0$ where the density of states becomes zero. It is clearly visible for a large enough attractive potential U and the typical shape can be seen in Fig. 4. The spin splitting by SOC leads to a splitting of the gap into spin-up and spin-down parts, which give rise to an additional in-gap peak when added together as is illustrated in Fig. 16. A singlet gap does not feature such peaks and is most comparable to the spin-down gap of Fig. 16.

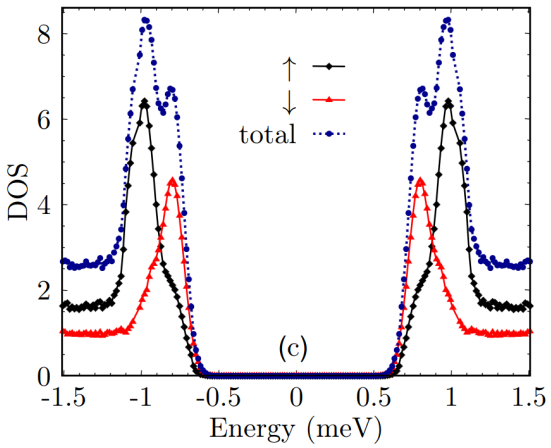

Figure 16: General expected behavior for a triplet gap. The spin-up and spin-down gaps are slightly shifted with respect to each other, which leads to a second peak inside the gap. Graph taken from [67].

Since the triplet-pairing mode allows for non-zero spin of Cooper pairs, these Cooper pairs can potentially influence the RKKY interaction. Non-zero spin Cooper pairs have a different movement behavior then singlet electrons, which have been the only mediating spins in a superconductor without SOC. Therefore it is expected that the presence of triplet Cooper pairs alters the RKKY

interaction between two impurity spins, in addition to the changes already caused by the SOC itself.

7.2 Diagonalization

Combining all individual terms of the Hamiltonian, the non-centrosymmetric superconductor can be described by

$$\begin{aligned} H_0 &= H_{kin} + H_{pot} + H_{SOC} + H_{int} \\ &= \sum_{k,\lambda} \frac{1}{2} \phi_k^\dagger \begin{bmatrix} \xi_{k,\lambda}\sigma_0 & i\Delta_{k,\lambda}\sigma_y \\ -i\Delta_{k,\lambda}^\dagger \sigma_y & -\xi_{k,\lambda}\sigma_0 \end{bmatrix} \phi_k + \sum_k \xi_k \end{aligned} \tag{7.5}$$

with the basis vectors $\phi_k^\dagger = (b_{k,\lambda}^\dagger, b_{-k,\lambda}^\dagger, b_{k,\lambda}, b_{-k,\lambda})$ and ϕ_k its complex conjugate. In addition, it is used that time reversal symmetry is preserved $\epsilon_k = \epsilon_{-k}$.
This matrix can easily be diagonalized and has eigenvalues

$$E_{k,\lambda}^{\pm} = \pm\sqrt{\xi_{k,\lambda}^2 + |\Delta_{k,\lambda}|^2}$$

The components of the eigenvectors are

$$\begin{aligned} \eta_{k,\lambda} &= \frac{E_{k,\lambda} + \xi_{k,\lambda}}{\sqrt{(E_{k,\lambda} + \xi_{k,\lambda})^2 + |\Delta_{k,\lambda}|^2}} \\ \nu_{k,\lambda} &= \frac{-\Delta_{k,\lambda}}{\sqrt{(E_{k,\lambda} + \xi_{k,\lambda})^2 + |\Delta_{k,\lambda}|^2}} \end{aligned}$$

where $E_{k,\lambda} = E_{k,\lambda}^+$ Combining the two eigenvectors result in the transformation matrix P between d and b operators

$$P_{k,\lambda}^\dagger = \begin{bmatrix} \eta_{k,\lambda} & \nu_{k,\lambda} \\ -\nu_{k,\lambda}^\dagger & \eta_{k,\lambda} \end{bmatrix}$$

where the eigenvectors are in the columns of P.
The diagonalized Hamiltonian can therefore be expressed in the form of a Fermi-gas

$$H_0 = \sum_{k,\lambda} \left[E_{k,\lambda}(d_{k,\lambda}^\dagger d_{k,\lambda} - d_{-k,\lambda}^\dagger d_{-k,\lambda}) \right] + \frac{|\Delta|^2}{V} + \sum_k \xi_k - \sum_k E_k \tag{7.6}$$

where $d^{[\dagger]}$ is the annihilation [creation] operator for the quasi-particles that diagonalize the total Hamiltonian. They are defined via the transformation from the helicity basis with matrix $P_{k,\lambda}$, which contains the eigenvectors as columns.

$$\begin{pmatrix} d_{k,\lambda} \\ d_{-k,\lambda}^\dagger \end{pmatrix} = \begin{bmatrix} \eta_{k,\lambda} b_{k,\lambda} + \nu_{k,\lambda} b_{-k,\lambda}^\dagger \\ -\nu_{k,\lambda}^\dagger b_{k,\lambda} + \eta_{k,\lambda} b_{-k,\lambda}^\dagger \end{bmatrix} \tag{7.7}$$

The anti-commutation-relations of the d-operators are fermionic again, since $P_{k,\lambda}$ is unitary.

7.3 Andreev Reflection

Besides free energy and gap equation, the LDOS of the p-wave superconductor is of interest. As a first test for the numerical approach for this system and as a first aid to characterize it, a special edge effect between superconductor to other materials or vacuum is investigated. This certain effect is called Andreev reflection, which was discovered by Andreev in 1964 [68] and by de Gennes and Saint-Jaimes in 1963-64 [69].
It describes originally the phenomenon that an electron with energy $E < \Delta$ (E relative to Fermi energy) can not be transmitted into a superconductor in the form of a single electron, since it can not overcome the potential barrier imposed by the superconducting gap. This electron can only be transmitted into the superconductor as a quasi-particle, which in turn requires the transmission of two electrons with opposite spin. Consequently, an electron with opposite spin at energy $-E$ must disappear from the normal-metal side of the interface. This looks like the reflection of a hole with opposite spin, approximately opposite momentum and energy to the initial electron that is to be transmitted into the superconductor [70, 71].
Rephrased this phenomenon can be described as an electron (hole) approaching a material, where there is a gap while there is no gap in its material of origin. That leads to the reflection of the electron (hole) as a hole (electron), while a Cooper pair is formed in the material with energy gap [5].
These reflections are also present within unconventional superconductors and as shown by Eschrig et al. [71] in a superconducting system that allows for triplet pairing, the surface states are strongly influenced by the relative magnitude of the singlet and triplet gap order parameter Δ_s and Δ_t, respectively.
To see that, the surface or boundary conditions in wave function formalism are defined by setting the wave function to zero at the boundary. Based on that the bound state condition can be expressed in dependence of singlet and triplet gap as well as the energy of the system and a proportionality constant $\xi \leq 1$ [72]. This bound state condition reads

$$\begin{aligned}\sqrt{(\Delta_1^2 - E^2)(\Delta_2^2 - E^2)} &= \frac{1-\xi}{1+\xi}(E^2 + \gamma\Delta_1\Delta_2) \\ \xi &= 1 \quad \text{for} \quad \Theta_c < |\Theta_2| \leq \pi/2 \\ \xi &= \frac{\sin^2(\frac{1}{2}[\Theta_1 + \Theta_2])}{\cos^2(\frac{1}{2}[\Theta_1 - \Theta_2])} \quad \text{for} \quad |\Theta_2| \leq \Theta_c\end{aligned}$$

with $\cos\Theta_1 = k_{1x}/k_1$ and $\cos\Theta_2 = k_{2x}/k_2$, and the critical angle $\Theta_C = \arcsin(k_1/k_2)$.
Therefore, the proportionality constant depends on the relative magnitude of singlet and triplet gap. The bound state condition reveals that only for $|\Theta_2| \leq \Theta_c$ and $\gamma = 1$ zero-energy states are possible. Consequently, they do only appear when the triplet gap is larger than the singlet gap $\Delta_s < \Delta_t$. Exactly this Δ_t/Δ_s dependent zero-energy states, which are caused by Andreev reflections, are visible in Fig. 17. With rising triplet gap $\Delta_t = V$, the LDOS at zero energy rises strongly at the edge of the system and eventually forms a clear peak.

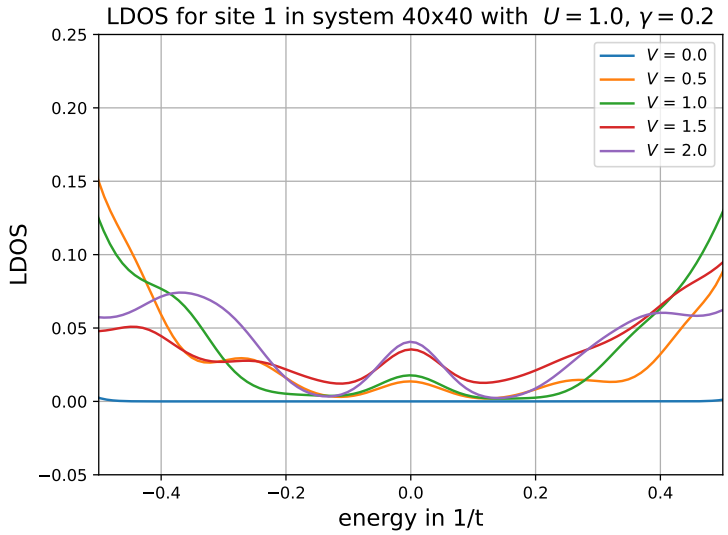

Figure 17: LDOS for the edge of an unconventional superconductor in the p-wave regime. With increasing triplet pairing strength, the amount of zero-energy states increases because of Andreev reflections [68, 72].

7.4 YSR States

Just as there are zero-energy states due to Andreev interaction at the edges of a non-centrosymmetric superconductor, there also are YSR states inside the gap present as impurity spins in non-centrosymmetric superconductors. These in-gap YSR states can be used to characterize p-wave superconductors into topological and non-topological by analyzing their number, energy and spin polarization. Furthermore, they allow to determine the direction of $\mathbf{d}$ for the triplet pairing [73]. Therefore the YSR states for a p-wave superconductor are investigated further here. According to Kim et al., YSR states are not only to be expected in normal metals with SOC, but also in non-centrosymmetric superconductors [74]. There the number and position of YSR bound states depends on the potential of the magnetic impurity, the SOC and the superconducting gap. The latter is relevant, because the energy of the bound states can be given most precise with respect to the superconducting gap in absence of impurities and because the bound states are visible inside the superconducting gap.

The s-wave dominated case has three potential bound states with energies

$$\begin{aligned} \frac{|E_{1,2}|}{\Delta_s} &= \frac{\alpha^2 - J_0^2 J_1^2 \pm \alpha^{(3/2)} \sqrt{(J_0^2 - J_1^2)^2 + (\alpha - 1)(J_0 - J_1)^4}}{\alpha^2 (1 + (J_0 - J_1)^2) + 2\alpha J_0 J_1 + J_0^2 J_1^2} \\ \frac{|E_3|}{\Delta_s} &= \frac{1 - J_1^2}{1 + J_1^2} \end{aligned} \tag{7.8}$$

where $\alpha = 1 + \gamma^2$. The impurity potential J_l can have different angular momenta l. Note that only two of the three states are possibly degenerate, but split by SOC. Additionally, the impurity potential J is of quadratic order, which means that the bound states do not depend on the sign of the impurity potential.

When the superconductor is dominated by p-wave superconductivity, the possible energies of bound

states become

$$\begin{aligned}\frac{|E_{4,5}|}{|\Delta_t|} &= \frac{1+J_1J_0}{\sqrt{(1+J_0^2)(1+J_1^2)}} \pm |\gamma| \frac{(J_0-J_1)^2}{(1+J_0^2)(1+J_1)^2} \\ \frac{|E_{6,7}|}{|\Delta_t|} &= \frac{1}{\sqrt{(1+J_1^2)}} \pm |\gamma| \frac{J_1^2}{(1+J_1^2)}\end{aligned} \tag{7.9}$$

which are four possible states. Those states are both degenerate, but split in the presence of SOC. Two of the states actually depend on the sign of J, because they appear in linear order.
In the system investigated here, the impurities are the isotropic local spins. Therefore, only the part of the potential, which corresponds to vanishing angular momentum, is relevant here. That means $J_0 \neq 0$, while $J_1 = 0$, and the expected bound states are

$$\begin{aligned}\frac{|E_{1,2}|}{\Delta_s} &= \frac{\alpha^2 \pm \alpha^{(3/2)}\sqrt{J_0^4 + (\alpha-1)J_0^4}}{\alpha^2(1+J_0^2)} \\ \frac{|E_3|}{\Delta_s} &= 0 \\ \frac{|E_{4,5}|}{|\Delta_t|} &= \frac{1}{\sqrt{(1+J_0^2)}} \pm |\gamma| \frac{J_0^2}{(1+J_0^2)} \\ \frac{|E_{6,7}|}{|\Delta_t|} &= 1\end{aligned} \tag{7.10}$$

Therefore, two bound states are expected to be visible in the s-wave non-centrosymmetric superconductor. The same holds true for the p-wave case, although the states are expected to have different energies. The explicit influence of SOC strength and RKKY interaction strength on the YSR state energies are depicted in Fig. 18, where three main trends are visible. For the singlet dominated case, the SOC strength does not seems to have any influence on the YSR energies, which can be seen from the constant solid lines in blue and orange. This can be understood from the fact that the majority of Cooper pairs does not have any net spin and therefore is not influenced by the SOC as long as the SOC does not break the Cooper pairs. However, the RKKY interaction strength does have an influence on the second energy for the singlet dominated case. Just as for the two energies of the triplet dominated case, an increasing RKKY interaction strength leads to a decrease of the YSR energy.
Furthermore does the SOC strength have an influence on the YSR energies of the triplet dominated case. While an increasing SOC leads to an increasing energy for E_4, it leads to a decrease in E_5. Physically, this reflects the change in the quasi-particle excitations with changing gap symmetry. These changes cause the decrease with increasing RKKY interaction strength, too. The decrease differs a little for the two energies and is slightly stronger for E_5 then for E_4, which leads to an effective splitting of those two energies with increasing RKKY.

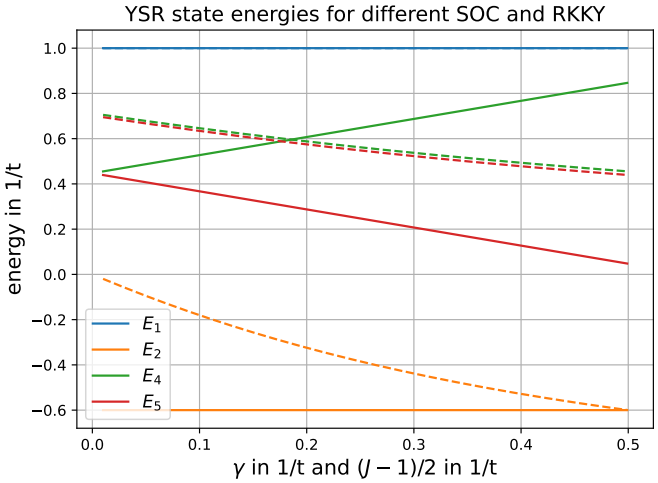

Figure 18: Dependence of YSR state energies on SOC strength γ (solid line) and RKKY interaction strength J (dashed line).

Additional to the different behaviors under change of SOC and RKKY interaction strength, the LDOS at the YSR energies differs for the triplet and singlet dominated case. While the LDOS is dependent on the distance from the impurity in both cases, it is generally higher as can be seen in Fig. 10. There the singlet and triplet dominated case depicted in the left and right plot, respectively. The singlet pairing is chosen quite high in the triplet dominated case, too, because otherwise in-gap YSR states are difficult to identify since other states would overlap.
In the singlet dominated case, the highest in-gap peaks are seen at a distance of two sites from the impurity at energies below the Fermi-level. The lower energy states are in general more clearly visible, because they have a higher relative difference to the effective gap of the system than the positive energy states.
For the triplet dominated case, the two most prominent peaks are at the impurity site and on its nearest neighbor. Those peaks are caused by the triplet gap Δ_t, which influences the LDOS at the impurity directly and at the neighboring site as expected based on Eq. 7.10. For sites further away from the impurity, these states that belong to $E_{6,7}$ are still present but seem to vanish in this plot, since they are moving into the energy regime where the gap of the impurity site ends. The remaining peaks behave very similar to the ones of the singlet dominated case, although their magnitude is significantly smaller.
For both cases, the magnitude seems to inversely depend on the RKKY interaction strength, which is also oscillating in a non-centrosymmetric superconductor as going to be investigated later on.
Additionally, to the increase in LDOS at the YSR state energy, there also is an increase in the LDOS at the opposite side of the gap. This contains two peaks and a lower but finite LDOS in between them. The peaks get higher and closer to each other with increasing triplet pairing.
There are basically no effects of increasing triplet pairing at the site of the impurity visible.

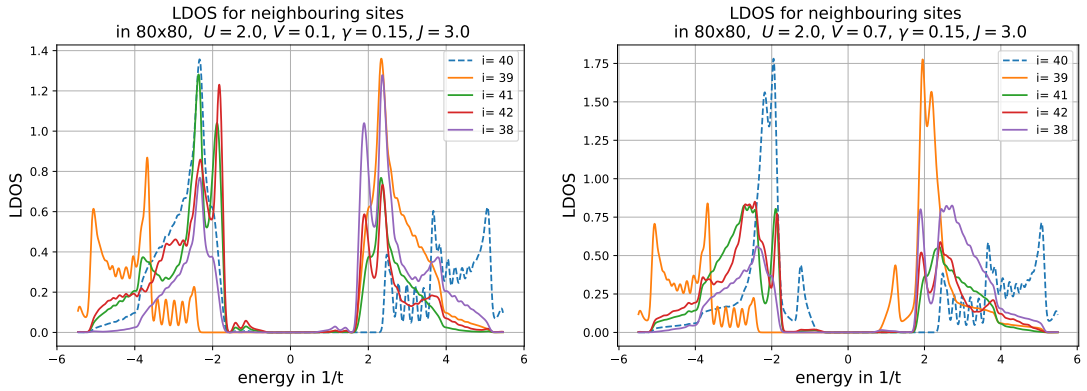

(a) (b)

Figure 19: YSR states in non-centrosymmetric superconductor. There are four in-gap states visible in (a) s-wave and (b) p-wave dominated case, which oscillate in energy and LDOS with increasing distance to the impurity sites (dashed lines).

Note here that the YSR states occur because of the same local spin-spin interaction that gives rise to RKKY interaction. Therefore, the RKKY interaction strength influences the YSR states and assumably vice-versa.

7.5 Effective Interaction including RKKY

After having investigated the superconductor at the edges and with one spin impurity, the focus is now set on the RKKY interaction between two impurities. The starting formulation of RKKY interaction in non-centrosymmetric superconductors is the same formulation as introduced in Sec. 2.1. Therefore the local spin-interaction term

$$H_{RKKY} = \sum_{\sigma,\sigma',k,k'} \sum_{i} \frac{J}{N} e^{i(k-k')r_i} (\mathbf{S}_i \cdot \vec{\sigma}_{\sigma,\sigma'}) c^\dagger_{k,\sigma} c_{k',\sigma'}$$

is treated as a perturbation to the system and firstly is transformed into helicity basis by means of Eq. (6.2):

$$H_{RKKY} = \sum_{k,k',i,\lambda,\lambda'} T^{\gamma}_{i,k,k',\lambda,\lambda'} b^\dagger_{k,\lambda} b_{k',\lambda'}$$

where $T_{\gamma,k,k',i,\lambda,\lambda'}$ contains all pre-factors. The exact expression for T for a general SOC can be found in App. B and Sec. 6.
After transforming it further into the eigenbasis of the unperturbed Hamiltonian using Eq. (7.7), the RKKY-interaction reads:

$$H_{RKKY} = \sum_{i,k,k',\lambda,\lambda'} T^{\gamma}_{i,k,k',\lambda,\lambda'}$$
$$\left(\eta^\dagger_{k,\lambda}\eta_{k',\lambda'} d^\dagger_{k,\lambda} d_{k',\lambda'} + \nu_{k,\lambda}\nu^\dagger_{k',\lambda'} d_{-k,\lambda} d^\dagger_{-k',\lambda'} - \nu_{k,\lambda}\eta_{k',\lambda'} d_{-k,\lambda} d_{k',\lambda'} - \eta^\dagger_{k,\lambda}\nu^\dagger_{k',\lambda'} d^\dagger_{k,\lambda} d^\dagger_{-k',\lambda'}\right)$$

In order to obtain the Hamiltonian describing the effective interaction of the system including the perturbation, a Schrieffer-Wolff-transformation is applied once more. Following the procedure as

explained in Sec. 3.2, the commutator $[S, H_0]$ is computed using the ansatz:

$$S = \sum_{\substack{i,k,k' \\ \lambda,\lambda'}} \left(A^{\gamma}_{\substack{i,k,k' \\ \lambda,\lambda'}} d^{\dagger}_{k,\lambda} d_{k',\lambda'} + B^{\gamma}_{\substack{i,k,k' \\ \lambda,\lambda'}} d_{-k,\lambda} d^{\dagger}_{-k',\lambda'} + C^{\gamma}_{\substack{i,k,k' \\ \lambda,\lambda'}} d_{-k,\lambda} d_{k',\lambda'} + D^{\gamma}_{\substack{i,k,k' \\ \lambda,\lambda'}} d^{\dagger}_{k,\lambda} d^{\dagger}_{-k',\lambda'} \right) \tag{7.11}$$

Afterwards, the requirement $H_{RKKY} + i[S, H_0] = 0$ is applied to it. The calculation can be found in Appendix C.2 and leads to the following coefficients:

$$\begin{aligned}
A^{\gamma}_{\substack{i,k,k' \\ \lambda,\lambda'}} &= i \sum_i T^{\gamma}_{i,k,k',\lambda,\lambda'} \frac{\eta_{k,\lambda}\eta_{k',\lambda'}}{E_{k,\lambda} - E_{k',\lambda'}} \\
B^{\gamma}_{\substack{i,k,k' \\ \lambda,\lambda'}} &= -i \sum_i T^{\gamma}_{i,k,k',\lambda,\lambda'} \frac{\nu^{\dagger}_{k,\lambda}\nu_{k',\lambda'}}{E_{-k,\lambda} - E_{-k',\lambda'}} \\
C^{\gamma}_{\substack{i,k,k' \\ \lambda,\lambda'}} &= i \sum_i T^{\gamma}_{i,k,k',\lambda,\lambda'} \frac{\nu^{\dagger}_{k,\lambda}\eta_{k',\lambda'}}{E_{-k,\lambda} + E_{k',\lambda'}} \\
D^{\gamma}_{\substack{i,k,k' \\ \lambda,\lambda'}} &= -i \sum_i T^{\gamma}_{i,k,k',\lambda,\lambda'} \frac{\eta_{k,\lambda}\nu_{k',\lambda'}}{E_{k,\lambda} + E_{-k',\lambda'}}
\end{aligned} \tag{7.12}$$

Based on that, the commutator $[S, H_{RKKY}]$ is calculated and the effective Hamiltonian is formulated.
The expectation value of the effective Hamiltonian $H_{eff} = H_0 - i[S, H_{RKKY}]$ is

$$\begin{aligned}
\langle H_{eff} \rangle &= \langle H_0 \rangle - i \langle [S, H_{RKKY}] \rangle \\
&= E_0 - i \sum_{\substack{i,k,k' \\ \lambda,\lambda'}} \sum_{\substack{j,q,q' \\ \beta,\beta'}} \langle \Big[A_{i,k,k',\lambda,\lambda'} d^{\dagger}_{k,\lambda} d_{k',\lambda'} + B_{i,k,k',\lambda,\lambda'} d_{-k,\lambda} d^{\dagger}_{-k',\lambda'} \\
&+ C_{i,k,k',\lambda,\lambda'} d_{-k,\lambda} d_{k',\lambda'} + D_{i,k,k',\lambda,\lambda'} d^{\dagger}_{k,\lambda} d^{\dagger}_{-k',\lambda'} \quad , \\
&\eta_{q,\beta}\eta_{q',\beta'} d^{\dagger}_{q,\beta} d_{q',\beta'} + \nu^{\dagger}_{q,\beta}\nu_{q',\beta'} d_{-q,\beta} d^{\dagger}_{-q',\beta'} - \nu^{\dagger}_{q,\beta}\eta_{q',\beta'} d_{-q,\beta} d_{q',\beta'} - \eta_{q,\beta}\nu_{q',\beta'} d^{\dagger}_{q,\beta} d^{\dagger}_{-q',\beta'} \Big] \rangle
\end{aligned} \tag{7.13}$$

and a more detailed form is presented in Appendix D.
The effective Hamiltonian contains terms of different spin-structures, which originate from the factors A, B, C, D and T only, because they contain the product $\mathbf{S}_i \cdot \vec{\sigma}_{\sigma,\sigma'}$ with σ being a spin index again.

7.6 Analytical Spin Structure

The spin structure of the effective Hamiltonian is determined in order to allow for statements about the preferred spin configuration of the impurity spins. Since all terms contain factors of the type $\Lambda^{\gamma}_{\substack{j,q,q' \\ \beta,\beta'}} T^{\gamma}_{i,k,k',\lambda,\lambda'}$, where $\Lambda = A, B, C, D$, the individual parameter combinations for helicity and momentum are going to determine the effective spin-structure.
While the spin-structure for a simple normal metal with RRKY is of Heisenberg- type, it gets more complicated with more included interactions. For a conventional superconductor without SOC but with spin-splitting due to an external magnetic field, a mixture of Ising and Heisenberg like spin-terms is present [5]. For a normal metal with SOC, the spin-structure contains Heisenberg and Dzyaloshinskii–Moriya like spin-interactions as well as interactions of type $\mathbf{S}_i \cdot \overleftrightarrow{\Gamma} \cdot \mathbf{S}_i$

[15]. Therefore it is possible that the spin-structure for a non-centrosymmetric superconductor is a combination of Heisenberg, Ising, Dzyaloshinskii–Moriya and tensor-product like terms.
The symmetry of the system limits the symmetry of the spin configurations. Since $\hat{n} = \hat{z}$ is chosen as symmetry breaking axis in the Rashba-type SOC, the z-axis is the only special axis in the system. No edge-effects are taken into consideration in this analytical approach, and the underlying superconductor is fully isotropic by choice of the potentials t, μ, V, U, which all do not depend on their position in the superconductor. That leads to a possible degeneracy of the groundstate spin-configurations.
As the transformation between spin- and helicity-basis in Eq.(6.2) shows, each helicity-basis operator contains a spin-up and a spin-down operator regardless of their helicity. Consequently, all spin-combinations are possible in the first place and are weighted and canceled solely based on the energy terms associated with them as well as the dependencies of momenta to each other.
Evaluating the expression of the commutator $[S, H_{RKKY}]$ leads to two distinct possible parameter combinations for helicity and momentum:

$$\begin{aligned} &(1st) \quad (i,k,k',\lambda,\lambda') \quad \text{with} \quad (j,k',k,\lambda',\lambda) \\ &(2nd) \quad (i,k,k',\lambda\lambda') \quad \text{with} \quad (j,-k,-k',\lambda,\lambda') \end{aligned}$$

In order to determine the effective spin structure of the non-centrosymmetric superconductor with RKKY-interaction, each term in $\langle H_{eff} \rangle$ (Eq. (7.13)) has to be evaluated individually. The resulting spin structure contains Heisenberg, Ising, DM and remaining terms, which are labeled $J, \mathbf{I}, \mathbf{D}, \overleftrightarrow{\Gamma}$ in accordance with Sec. 6 and are found to be

$$J_{i,j,k,k'} = 2F^{+++}_{k,k'} \tag{7.14}$$

$$\mathbf{I}_{i,j,k,k'} = \begin{pmatrix} m+m^* \\ -(m+m^*) \\ i(m-m^*) \end{pmatrix} F^{+--}_{k,k'} - \begin{pmatrix} 2\Phi_2 \\ 2\Phi_2 \\ \Phi_2+\Phi_2^* \end{pmatrix} G^{+--}_{k,k'} + \begin{pmatrix} -\left((\Phi_1')^2+(\Phi_1^*)^2\right) \\ (\Phi_1')^2+(\Phi_1^*)^2 \\ 1+\Phi_2^2 \end{pmatrix} G^{+++}_{k,k'} \tag{7.15}$$

$$\begin{aligned} \mathbf{D}_{i,j,k,k'} = &\begin{pmatrix} i\left(\Phi_1^*+\Phi_1\right)F^{-+-}_{k,k'} - i\left(\Phi_1'+(\Phi_1')^*\right)F^{--+}_{k,k'} \\ \left(\Phi_1^*-\Phi_1\right)F^{-+-}_{k,k'} + \left(\Phi_1'-(\Phi_1')^*\right)F^{--+}_{k,k'} \\ 0 \end{pmatrix} \\ &+ \begin{pmatrix} i\left(\Phi_1^*+\Phi_2\Phi_1'\right)G^{-+-}_{k,k'} - i\left(\Phi_1'+\Phi_2\Phi_1^*\right)G^{--+}_{k,k'} \\ \left(\Phi_1^*-\Phi_2\Phi_1'\right)G^{-+-}_{k,k'} + \left(\Phi_1'-\Phi_2\Phi_1^*\right)G^{--+}_{k,k'} \\ 0 \end{pmatrix} \end{aligned} \tag{7.16}$$

$$\overleftrightarrow{\Gamma}_{i,j,k,k'} = \begin{pmatrix} 0 & i(m^*-m)F^{+--}_{k,k'} + i\left((\Phi_1')^2-(\Phi_1^*)^2\right)G^{+++}_{k,k'} & 0 \\ i(m^*-m)F^{+--}_{k,k'} + i\left((\Phi_1')^2-(\Phi_1^*)^2\right)G^{+++}_{k,k'} & 0 & 0 \\ 0 & 0 & 0 \end{pmatrix} \tag{7.17}$$

for a non-centrosymmetric superconductor. The following short hand notation for the energy terms F, G is used:

$$\begin{aligned} F^{\pm\pm\pm}_{k,k'} &= E_1^{++}(k,k') \pm E_1^{--}(k,k') \pm E_1^{+-}(k,k') \pm E_1^{-+}(k,k') \\ G^{\pm\pm\pm}_{k,k'} &= E_2^{++}(k,k') \pm E_2^{--}(k,k') \pm E_2^{+-}(k,k') \pm E_2^{-+}(k,k') \end{aligned}$$

The energy terms $E_{1,2}^{\pm\pm}(k,k')$ consist of the sum of all prefactor combinations that yield a non-zero contribution to $\langle H_{eff}\rangle$. They take the following form

$$\begin{aligned}
E_1^{\lambda,\lambda'}(k,k') =& |\eta_{k,\lambda}|^2|\eta_{k',\lambda'}|^2\frac{f(E_{k,\lambda})-f(E_{k',\lambda'})}{E_{k',\lambda'}-E_{k,\lambda}} + |\nu_{k,\lambda}|^2|\nu_{k',\lambda'}|^2\frac{f(E_{k,\lambda})-f(E_{k',\lambda'})}{E_{k',\lambda'}-E_{k,\lambda}}\\
&- |\nu_{k,\lambda}|^2|\eta_{k',\lambda'}|^2\frac{f(E_{k,\lambda})+f(E_{k',\lambda'})}{E_{k',\lambda'}+E_{k,\lambda}} + |\eta_{k,\lambda}|^2|\nu_{k',\lambda'}|^2\frac{f(E_{k,\lambda})-f(E_{k',\lambda'})}{E_{k',\lambda'}+E_{k,\lambda}}\\
E_2^{\lambda,\lambda'}(k,k') =& \eta^\dagger_{k,\lambda}\eta_{k',\lambda'}\nu_{-k,\lambda}\nu^\dagger_{-k',\lambda'}\frac{f(E_{k,\lambda})-f(E_{k',\lambda'})}{E_{k',\lambda'}-E_{k,\lambda}} - \eta^\dagger_{-k,\lambda}\eta_{-k',\lambda'}\nu_{k,\lambda}\nu^\dagger_{k',\lambda'}\frac{f(E_{k,\lambda})-f(E_{k',\lambda'})}{E_{k',\lambda'}-E_{k,\lambda}}\\
&+ \nu_{k,\lambda}\nu^\dagger_{-k,\lambda}\eta_{k',\lambda'}\eta_{-k',\lambda'}\frac{f(E_{k,\lambda})+f(E_{k',\lambda'})}{E_{k',\lambda'}+E_{k,\lambda}} + \eta^\dagger_{k,\lambda}\nu^\dagger_{k',\lambda'}\nu_{k,k\lambda}\eta_{k',\lambda'}\frac{f(E_{k,\lambda})-f(E_{k',\lambda'})}{E_{k',\lambda'}+E_{k,\lambda}}
\end{aligned}$$

In addition the phases Φ and m are short hand notation for

$$\begin{aligned}
\Phi_1 &= \frac{\gamma_{k,x}+i\gamma_{k,y}}{|\gamma_k|}\\
\Phi_2 &= \frac{(\gamma_{k,x}-i\gamma_{k,y})(\gamma_{k',x}+i\gamma_{k',y})}{|\gamma_k|\,|\gamma_{k'}|}\\
m = \Phi_1'\Phi_1 &= \frac{(\gamma_{k,x}\gamma_{k',x}-\gamma_{k,y}\gamma_{k',y}+i\gamma_{k',x}\gamma_{k,y}+i\gamma_{k,x}\gamma_{k',y})}{|\gamma_k|\,|\gamma_{k'}|}
\end{aligned}$$

Putting all the components together the overall spin structure of the system reads

$$\langle H_{eff}\rangle = \left(\frac{J}{N}\right)^2\sum_{k,k',i,j} e^{i(k-k')R}\left((J+\mathbf{I})\,\mathbf{S}_i\cdot\mathbf{S}_j + \mathbf{D}\,(\mathbf{S}_i\times\mathbf{S}_j) + \mathbf{S}_i\overleftrightarrow{\Gamma}\mathbf{S}_j\right) \tag{7.18}$$

where R is the distance between the impurities again. In the case of $\Delta = 0$, no superconductivity, only terms with factors of F survive, which changes the spin structure of a superconductor with SOC to the spin structure of a normal metal with SOC (compare Eq. (6.5)- (6.8)). It is not possible, however, to take the limit of vanishing SOC, because the energies and coefficients do not only depend explicitly on the SOC strength γ, but also indirectly. As required by basics algebraic relations, the spin structure is real and symmetric.
Just as in the case for a normal metal with SOC, the spin structure of a superconductor with SOC comprises all four possible spin interactions. The Heisenberg J is basically the same in all four investigated systems, since only the energies are adjusted to the present system.
The Ising term exists in both systems with SOC and in the unconventional superconductor it gains an additional term. The DM interaction term has a similar form to the normal metal with SOC, although its terms are slightly different in the unconventional superconductor due to additional terms. These terms have, however, the same pattern as the terms equal to the normal metal case. The change in the tensor $\overleftrightarrow{\Gamma}$ is very much alike. The components of the normal metal case are to be found in the superconducting case, too, but there are additional terms.
Overall, the spin structure of a superconductor with SOC has the same structure as a normal metal with SOC and is just expanded by some additional terms with the same symmetry characteristics.

7.6.1 Analytical Groundstate Spin Configuration

As a first step to evaluating the analytically derived spin structure, the individual components are plotted over distance in Fig. 20. There, the cases of singlet and triplet non-centrosymmetric superconductor are distinguished. Both have in common, that the Heisenberg interaction is dom-

inating for short distances. Its exact value is cut in order to increase the visibility of the remaining coefficients over longer distances, but the Heisenberg interaction is one order of magnitude larger than all other coefficients for short distances. The interaction strength of $\overleftrightarrow{\Gamma}$ is one to two orders of magnitude smaller than the other interactions and therefore its behavior is only barely visible. The same holds true for the D_x and D_z components of the DM interaction, which is in strong contrast to the D_y component that is the second strongest interaction for short distances. Nevertheless, the damped oscillation of interaction strength is visible for all coefficients in both cases, which further verifies the found spin structure. The damping is similarly strong for singlet and triplet, although the exact oscillation differs.

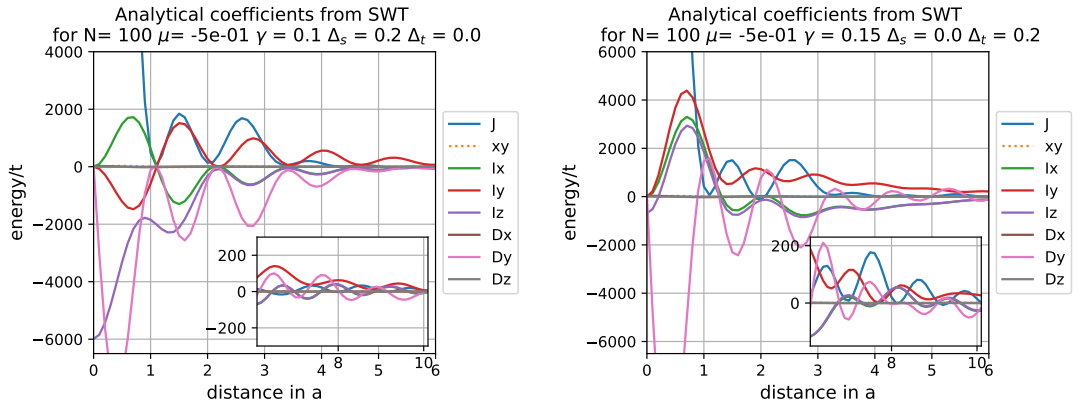

(a) singlet

(b) triplet

Figure 20: Analytically determined spin structure coefficients of a non-centrosymmetric superconductor, for the singlet (s-wave) case in (a) and the triplet (p-wave) case in (b).

For the singlet case depicted in Fig. 20(a), Heisenberg interaction dominates the interaction for short distances up to a distance of $d = 1$a. At that point the I_z Ising term is the strongest before DM interaction with D_y becomes strongest. Both these interaction favor anti-parallel spin alignment, since they are always negative, while the Heisenberg interaction always favors parallel alignment.

This clear preference of one certain alignment is not present for the second strongest interactions I_x and I_y. Both oscillate around zero and always have the opposite sign of each other and a similar magnitude, which is to be expected since the system is symmetric in the xy-plane. However, the I_y component has the largest magnitude for long distances and is therefore expected to dominate the interaction there. It has a positive sign for long distances and therefore favors parallel alignment in the y-direction, while the x- and y-direction are controlled by the D_y term of DM.

In the triplet case, there is only the Heisenberg interaction that keeps the same sign for all distances and favors only parallel alignment. All other components oscillate around zero in different ways, as can be seen in Fig. 20(b). The D_y component of DM interaction is again having a significant influence on the spin structure, even more than in the singlet case. Depending on the SOC strength it is even of the same order of magnitude as the Heisenberg interaction and therefore even more relevant on the short distances. Its defining role remains for distances between $d = 1$a to $d = 3$a leading to a groundstate spin configuration that prefers a non-colinear alignment of the two spins. Only after these middle distances, the Ising interaction with I_y starts to be of comparable size to the DM term. Therefore, the spin structure for long distances is expected to show anti-parallel

alignment in y-direction. In z-direction, the influence of DM and Ising are competing, while the x-direction is still dominated by DM.
Overall, the spin structure for the triplet case is stronger influenced by DM interaction than the singlet case.
In order to understand the changes in Ising interaction better, it is calculated for different singlet and triplet gap sizes. The results in Fig. 21 indicated, that an increasing gap corresponds to an increasing Ising interaction strength, although the exact changes and values depend on the dominating gap symmetry. In the s-wave dominated case presented in Fig. 21(a), the I_x and I_y components behave nearly anti-symmetric, while the I_z component is showing a completely different behavior. It shows an increasingly deep minimum with larger singlet gap for very short distances, but becomes more similar for all gap sizes with increasing distances. The same long distance behavior is true for the x and y components.
In the p-wave dominated case, the I_z and I_x component behave very similar as can be seen in Fig. 21(b). Although I_x grows slightly stronger with increasing triplet gap size, they show the qualitatively same behavior and converge towards each other for long distances. The I_y component grows with increasing triplet gap size, too, but is generally larger than the other components. Additionally, it is purely positive and therefore always favors a FM ordering, while the other two components are switching from FM ordering for short distances to AFM ordering on longer distances. On very long distances $d > 9.5$a, all three components are converging towards each other and eventually change sign.
Consequently, Ising interaction becomes increasingly important for the total spin structure with increasing superconducting gap, but it still originates from SOC.

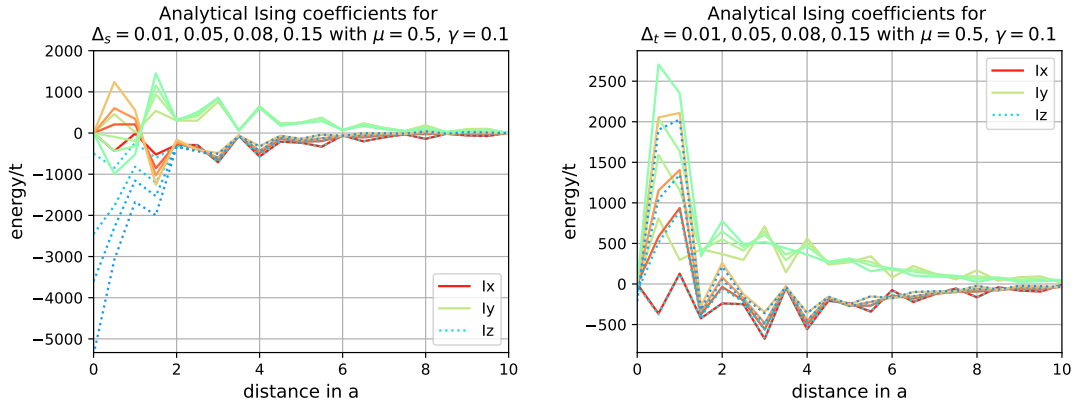

(a) (b)

Figure 21: Comparison of the three Ising components in an unconventional superconductor with dominating s-wave (a) and p-wave (b) gap symmetry. The respective gap is gradually increased from $\Delta = 0.01$ to $\Delta = 0.15$, while the system size is 100x100.

As a third case, a superconductor with equally stronger singlet and triplet pairing is investigated. Its spin structure coefficients are plotted in Fig. 22, where the influence of the pairing strength is visible immediately because of the differences in DM and Ising between Fig. 22(a) and 22(b). A stronger pairing leads to a stronger DM and a weaker Ising interaction, while the oscillation behavior stays nearly the same. As for all cases discussed so far, the Heisenberg interaction dominates the small distance interaction as well as it appears again in the long distance interaction. The middle distances are not as clearly dominated by one interaction, but are rather a complicated

interplay of Heisenberg, Ising and DM terms.

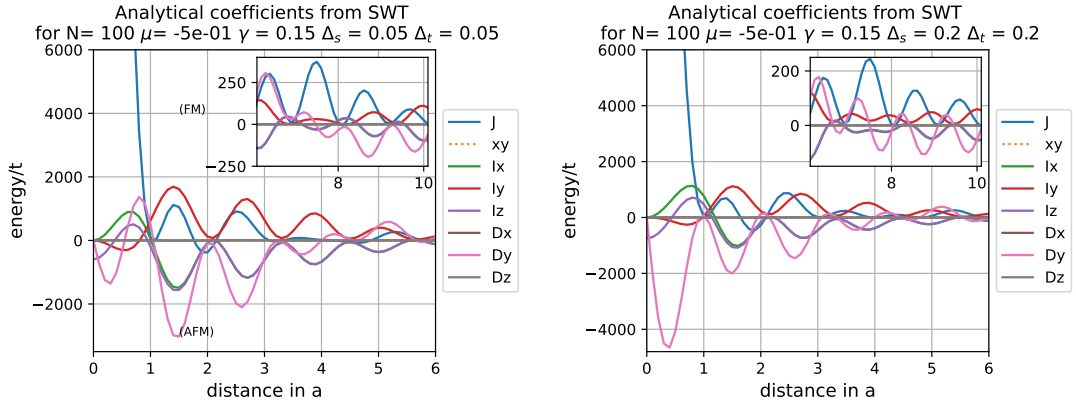

(a) (b)

Figure 22: Analytically determined spin structure coefficients of a non-centrosymmetric superconductor for (a) weak and (b) strong singlet and triplet pairing. The system size is 100x100 for both cases.

In all of the systems with $\Delta_t \neq 0$, there is an additional AFM bias visible, which stems from the fact that the triplet Cooper pairs contribute to the mediation of RKKY interaction.
The behavior of the analytically found spin structure components is also visualized as the groundstate spin configuration in App. E in Fig. 29, where the groundstate was determined by finding the spin configuration that minimizes the free energy from Eq. 7.18.

7.7 Numerical Groundstate Spin Configuration

The numerical groundstate spin configuration is determined with the approach presented in Sec. 3.3. Since the dominating gap symmetry depends on the strength of SOC, the singlet and triplet dominated case are both investigated. The ratio Δ_s/Δ_t is taken to be of order 10 or 1/10, respectively, to ensure a clear distinction between s- and p-wave symmetry.
The singlet dominated case is presented in Fig. 23. Just as for conventional superconductor, the oscillation between FM and AFM ordering is fast for small distances but decays quickly for increasing distance. It does not stop completely for the current system, which might be because of the SOC. Since the SOC causes an alternation in the oscillation for normal metals, it is expected to have an influence in superconductors, too, even when they are still of s-wave symmetry.
The orientation of the spins is mostly parallel in x-direction, but for short distances there are also non-colinear configurations to be found. In some configurations, the spins are parallel to each other, but not to x- or y-direction. This mixture occurs due to the influence of DM and Ising interaction and is replaced by colinear spins along the x-axis for longer distances.

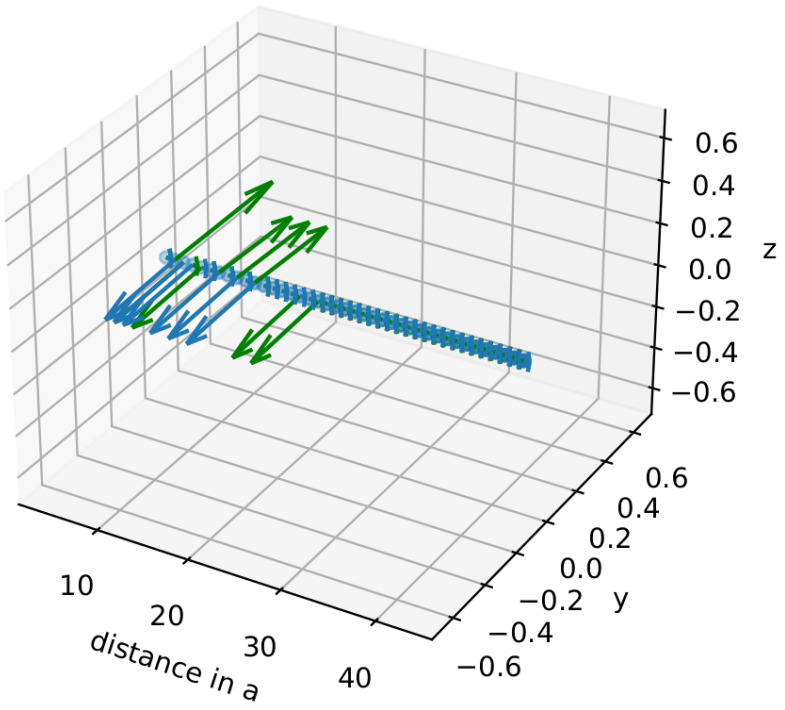

Figure 23: Numerical groundstate spin configuration of an s-wave superconductor with $\gamma = 0.2$ for 80 lattice sites.

The groundstate spin configuration for a p-wave superconductor is presented in Fig. 24, where to different system sizes are compared. In both cases, the spin alignment oscillation does barely change over the distances investigated. For distances up to $d = 21$a, the results for the groundstate spin configuration are non-degenerate, which means that only one groundstate is identified within the numerical accuracy. For longer distances, there are 26 possible groundstates found numerically and therefore only the short distances are of relevance here.
The mostly parallel ordering can be understood by looking at the mediators of RKKY interaction. In normal metals, only the conduction electrons are transport spin information between the impurities. Electrons are a part of the quasi-particles which mediate RKKY interaction in singlet superconductors and the other part of these quasi-particles are holes. In triplet superconductors, there are two information carriers. On the one hand, the same quasi-particles as in singlet superconductors contribute to the information transport, and on the other hand, the triplet Cooper pairs are also mediating RKKY interaction. That leads to a change in the movement behavior of the information carriers, which are partially able to travel significant longer distances, which is reflected in the changed oscillation behavior of the RKKY interaction strength. Additionally, there is a clear preference for alignment along the y-axis in the square system, while the x-axis is preferred in the rectangular system. This difference stems from finite size effects and shows the sensibility of the numerical solution. Nevertheless, it is in accordance with the analytical model, since Heisenberg interaction does not prefer a specific direction and the components of Ising interaction are of competing magnitudes.
For short distances in the rectangular system, there is one spin configuration that is non-colinear and the spins have nearly opposite orientation as depicted in Fig. 24(b). This stems from the short domination of DM interaction. DM interaction depends, in turn, on the exact gap structure and size, since the amount of Cooper pairs with net-spin decreases with decreasing triplet gap size, which leads to a slightly altered oscillation behavior. Less Cooper pairs correspond to a lower

chance that spin information gets mediated between the two impurity spins, because there are less probabilities that one Cooper pair gets in contact with both impurities. Since this probability does not only depend on the amount of possible attempts aka. information carrying particles, but also on the distance between the impurities, a weaker triplet pairing leads to an earlier damped oscillation. And since finite size effects tend to suppress the triplet gap, the non-colinear groundstate spin configuration is not visible in the square system in Fig. 24(a).
Overall, the numerical results for a p-wave superconductor suggest a very similar behavior to a normal metal, except that the information transport can happen over significantly longer distances and the alignment along x-axis is strongly favored.

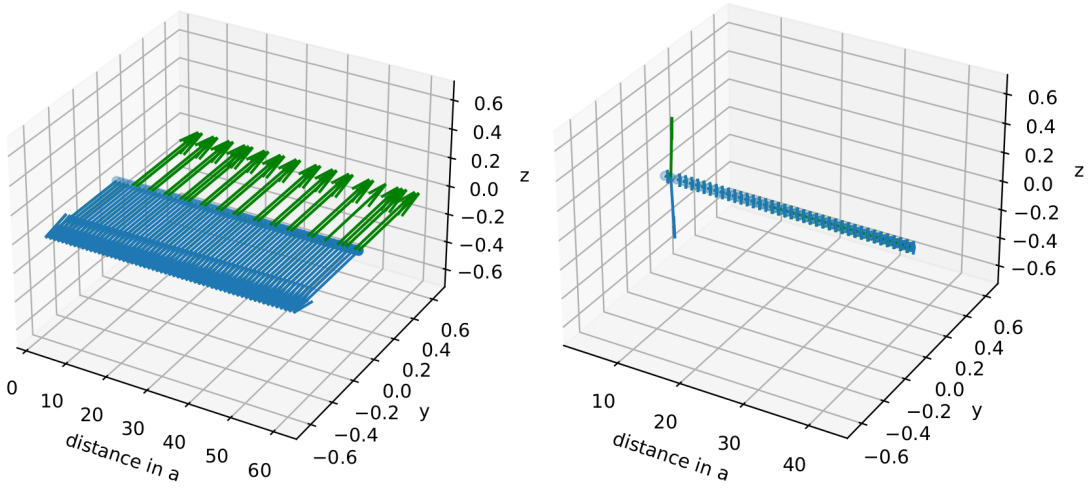

Figure 24: Numerical groundstate spin configuration of a p-wave superconductor with $\gamma = 0.1$ and $\Delta_t = 0.1$ (a) for system size 80x80 and (b) for system size 120x15. Finite size effects and the dominance of Ising and Heisenberg interaction are visible.

As in the normal metal with SOC case, the analytically determined groundstate is also plotted in the same way as the numerical groundstate. In Fig. 25, the three different cases are presented: singlet- and triplet dominated as well as mixed superconductivity. All feature anti-parallel alignment along the y-axis for the majority of distances, which stems from the Ising interaction. Furthermore, are there non-colinear alignments for several distances in all three systems, but their position and exact orientation differ. In the singlet dominated case in Fig. 25(a), there are more non-colinear alignments than in the other two systems. It is also visible that the mixed system in Fig. 25(c) shows a mixture of the features from singlet- and triplet-dominated systems. It shows the more constant groundstate configuration in the middle distances as in the triplet-dominated case in Fig. 25(b), while the configurations themselves show more similarity to the singlet-dominated case.
The distances with the most non-colinear configurations are longer, which is as expected from the coefficients discussed earlier. The numerical solution presented in Fig. 23 and 24 shows less of the non-colinear states and only on short distances. There are also non-colinear states on short distances in the analytical solution, which suggests that the numerical solution has more accuracy for short distances. That might be due to finite size effects, since they show more influence on weaker phenomena and RKKY interaction weakens with distance.

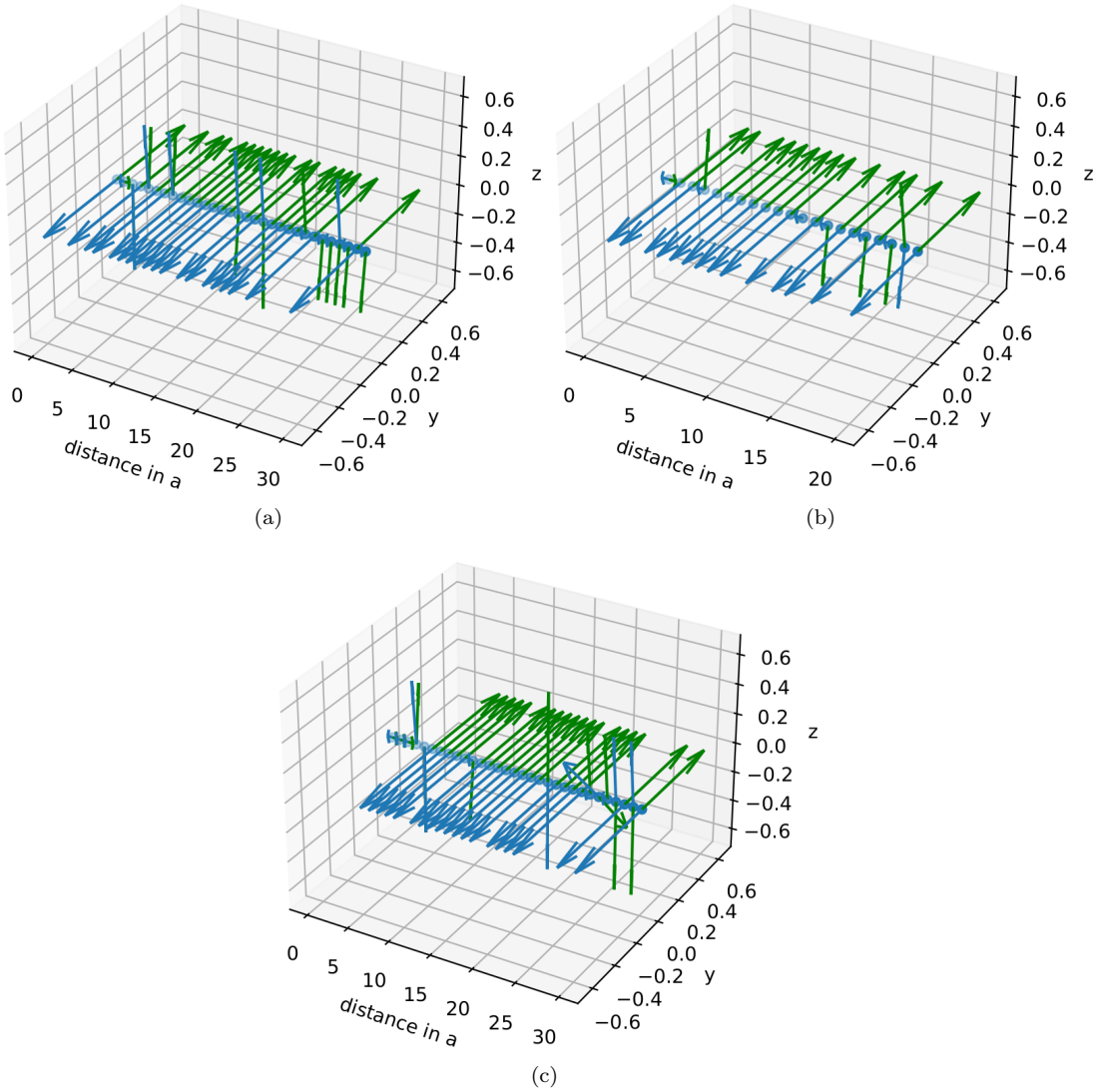

Figure 25: Analytical groundstate spin configuration of an unconventional superconductor with $\gamma = 0.1$ for (a) singlet- and (b) triplet-dominated superconductivity, as well as (c) mixed. The gap are either zero or $\Delta = 0.2$ in all cases.

8 Discussion

The spin structure of an unconventional superconductor with Rashba SOC shows a combination of normal metal and conventional superconductor characteristics, as can be shown with analytical and numerical calculations. The results of the analytical approach are going to be discussed first and the numerical results later on, and the used methods are critical examined, too.

In a normal metal, the RKKY interaction is of Heisenberg type and oscillates between ferromagnetic (FM) and anti-ferromagnetic (AFM) ordering (Fig. 7). When superconductivity is introduced into the system, the gap in the density of states (DOS) suppresses the AFM part of the still Heisenberg-like RKKY interaction (Fig. 12). The larger the gap is, the stronger the FM part of RKKY interaction is suppressed, too, leading to a faster decay in total RKKY interactio strength. The RKKY interaction gains additional Ising and DM interaction terms as well as interactions between the x and y components, when a Rashba SOC is considered. For the normal metal case, the oscillation between FM and AFM ordering driven by Heisenberg interaction remains, and DM also oscillates between those two orderings (Fig. 13). Especially on short distances, the Heisenberg interaction is still dominating the system, although the DM is of competing magnitude. An increasing SOC strength leads to an increasing Ising interaction, which is purely FM in y-direction and purely AFM in z-direction. It becomes of the same order as DM on middle distances, and the DM influence also increases with increasing SOC strength for those distances. As expected because of the increase in Ising and DM interaction, the Heisenberg interaction strength generally decreases with increasing SOC strength. Nevertheless, Heisenberg interaction dominates the interaction on long distances again, leaving only short and middle distances with potentially non-colinear spin alignment.

For the unconventional superconductor, three different cases are investigated: s-wave, p-wave and a mixture of those two. All three cases have Heisenberg, Ising, DM and xy-interaction terms, just as the normal metal with SOC system. In an s-wave superconductor (Fig. 20(a)), the Heisenberg term is purely FM and the DM term is purely AFM, as expected, because of the present gap structure. The x and y components of the Ising term are oscillating between FM and AFM ordering and have the same magnitude, while having opposite phase. That also makes the x component of Ising interaction more significant than in the previous systems, where it is one order of magnitude smaller. Additionally, the z component of Ising is the largest in the s-wave superconductor and of nearly the same magnitude as the already very strong DM interaction. Therefore, the Ising interaction takes a significantly more influential role in the unconventional s-wave superconductor than in normal metal or conventional superconductor cases. This can also be seen in Fig. 21(a), where the influence of the gap size on Ising shows a clear correlation. An increasing gap size leads to an increase in Ising interaction strength. That makes the spin structure of the impurity spins colinear for most distances.
In a p-wave superconductor, the Ising interaction becomes even stronger with increasing triplet gap and all its three components are in phase now (Fig. 21(b)). But while the y component is staying purely FM, the other two components oscillate between FM and AFM ordering. There is no physical explanation for this correlation between gap size and Ising interaction yet. Even in the normal metal case, there is no complete phenomenological explanation for the Ising interaction, but the form of the correlation suggests, nevertheless, two causalities. Since the Ising term only

exists for systems with SOC, specifically Rashba SOC in this thesis, the fundamental reason for the Ising is to be expected in the broken inversion symmetry. That also explains the special and more complicated behavior of the I_z component, which is in the direction of the symmetry breaking axis. Furthermore, the superconducting gap, regardless of its symmetry, enhances the Ising interaction strength, which suggests an interplay between broken inversion symmetry and Cooper pairs as well as quasi-particles. For the triplet Cooper pairs, this enhancement is explainable by their non-vanishing net-spin, which is interlinked with the broken inversion symmetry of the system, but the exact form is not directly visible from the correlations found in this thesis. However, the larger significance of Ising interaction in unconventional superconductors compared to normal metals can be expected based on the analytical form of the Ising term, which gains two additional terms in case of superconductivity.
DM and Heisenberg interaction are also oscillating between FM and AFM, which means that the p-wave case shares more similarities with the normal metal case than with the s-wave case (Fig. 20(b)). That is due to the change in gap structure, since the triplet pairing adds states to the gap edges. The gap led to the suppression of AFM ordering in the first place, but the edge states counteract this effect. Additionally, there are in-gap YSR states that further counteract the suppression of AFM ordering, such that the p-wave case includes it again. The triplet Cooper pairs are also the reason for the purely FM z component of Ising interaction, because they contribute to the mediation of RKKY interaction in addition to quasi-particles. In contrast to the quasi-particles, they are not losing their spin information due to the superconductivity and therefore behave more like quasi-particles in normal metals.
In the case of s- and p-wave gaps having the same size (Fig. 22), a mixture of the pure s- and p-wave characteristics are visible. All spin structure terms oscillate between FM and AFM, and the Ising interaction keeps its dominating role. For an increasing gap, the Ising interaction becomes a little weaker, but the oscillation between FM and AFM becomes even clearer. That is because an increasing gap does not only increase the singlet gap structure, but also the triplet gap structure. Consequently, the characteristics of a conventional superconductor become more visible, but the influence of the triplet gap is growing at the same time.

Two types of bound states are identified numerically for different systems in this thesis. Firstly, there are Andreev states for the edges of an unconventional superconductor (Fig. 17). They appear for systems with a triplet gap as large as or larger than the singlet gap, which proves the implemented BdG to work as expected.
Secondly, for conventional and unconventional superconductor, bound states and YSR states are found close to the impurity sites (Fig. 10), respectively. Their existence and position haven been predicted by Kim et al. and they behave exactly accordingly [74]. The position depends on the type of gap structure and on RKKY and SOC strength, which both have different influence on the position depending on the gap structure. Those differences occur because of the different net-spin of Cooper pairs as more thoroughly explained in Sec. 7.4. Overall, it is expected that these states influence the effective RKKY interaction and may lead to differences between numerical and analytical groundstate spin configurations.

The numerical groundstate for normal metals and conventional superconductors fully agrees with the analytically predicted pure Heisenberg interaction, as well as with the modifications due to chemical potential and superconducting gap.

With introducing SOC to a normal metal, the movement behavior of information carriers, which means that the electrons in normal metals mediate RKKY interaction differently depending on the SOC. As suggested by the analytical results, the numerical groundstate spin configuration of a normal metal with SOC exhibits not only FM and AFM ordering, but also non-colinear spin alignments that originate in DM (Fig. 14). The oscillation behavior suggests the expected long range behavior.
The expected influence of YSR states on RKKY interaction fits with the found groundstates for conventional and unconventional superconductors. In both cases, there is only FM and AFM ordering regardless of the gap structure, but the oscillation behavior changes with gap structure. While the oscillations for the s-wave superconductor are strongly damped and therefore relatively short ranged, they show longer range behavior for p-wave superconductors (Fig. 23 and 24). This differences stem from the different possible information carriers as explained in more detail in Sec. 7.7.
Just as for the normal metal with SOC, non-colinear spin alignment was also expected to occur in unconventional superconductors, but the DM appears to be too weak in relation to Heisenberg and Ising interaction in order to produce such an orientation.

As a third part of investigation, analytical and numerical results were compared more directly, but determining the groundstate spin configuration based on the analytical coefficients. This was only done for the systems with SOC, since in the isotropic systems there is only Heisenberg interaction. These direct comparisons underline the influence of finite size effects on the numerical solution, but generally show that the differences between the systems persist nonetheless. The allow to understand the interplay of the competingly strong Ising and DM interaction better, since the groundstate is strongly influenced by the effectively strongest spin structure coefficient. That reveals how much the enhanced Ising interaction suppresses non-colinear alignment in superconducting systems, while the groundstate spin configuration in a normal metal is non-colinear for nearly all distances.

All analytical results were obtained using the Schrieffer-Wolff transformation (SWT), which is a tool in quantum many-body theory for studying the effective Hamiltonian of a system with two energy scales. It is often used to study the RKKY interaction between magnetic impurities in a metal, where the system contains a high-energy scale (associated with the exchange interaction between the magnetic moments) and a low-energy scale (associated with the conduction electrons), which is exactly the case here. One of the main strengths of the SW transformation is its ability to derive an effective Hamiltonian that describes the low-energy physics of the system, which can simplify the theoretical analysis. The effective Hamiltonian obtained through the SWT can also provide physical insights into the underlying physics of the system, such as the role of quantum fluctuations and collective excitations. Another strength of the SWT is its ability to handle systems with strong correlations and non-trivial geometries, where other methods such as mean-field theory or perturbation theory may not be applicable. The SWT can be particularly useful in systems with impurities, where the impurities can strongly affect the electronic structure and the transport properties of the system. However, there are also some weaknesses associated with the SWT. One is the high sensitivity to the choice of perturbation parameter that controls the strength of the high-energy scale interactions, because a poor choice of perturbation parameter may result in an ineffective transformation or an inaccurate effective Hamiltonian. Another potential limita-

tion of the SWT is its sensitivity to the choice of basis set used to represent the operators in the Hamiltonian. A different choice of basis set may lead to a different effective Hamiltonian, which can affect the accuracy of the theoretical predictions.
Overall, the SWT is a powerful tool for investigating the RKKY interaction in metals with magnetic impurities. Since the studied systems fit well to the SWT approach and the perturbation parameter and basis set were chosen carefully, the obtained results form this analytical approach are considered reliable. There is one more short coming in the SWT performed in this thesis, which is the loss of information about the feedback between impurities and the LDOS. Consequently, it is not possible to study bound states or modifications of the gap due to RKKY interaction and spin impurities. That is where the numerical approach becomes necessary and relevant.

For the numerical approach, the Bogoliubov-de Gennes transformation (BdG) is used, which is a theoretical framework for studying superconductivity and related phenomena, including RKKY interaction. The transformation allows for the description of the quasi-particle excitations in a superconductor, which arise due to the formation of Cooper pairs. One of the main strengths of the BdG is its ability to accurately capture the effects of superconductivity on the electronic structure of a material, including the formation of the superconducting energy gap, and the modification of the density of states near the Fermi level. This makes it a useful tool for investigating the behavior of the RKKY interaction in superconductors, which is affected by the presence of the superconducting condensate and the modification of the electronic structure. Another strength of the BdG is its ability to capture the spatial variation of the RKKY interaction, which is important for understanding the behavior of magnetic impurities in superconductors and related phenomena, such as the formation of YSR states. However, there are also some weaknesses associated with the BdG transformation. One potential limitation is that the BdG transformation is a mean-field theory and may not capture certain quantum fluctuations and other non-mean-field effects that can be important in some materials, such as strongly correlated electron systems. That is, however, not a problem for the studied systems in this thesis. Another limitation of the BdG is the computational cost associated with its application to large systems and the potential need to solve self-consistency equations. Although the self-consistency equations were omitted due to time limitation, the computational costs are still high and consequently the maximum feasible system size had to be kept smaller than desired. That leads to finite size effects influencing the numerically determined groundstate spin structures and constant pairing potentials for all system sites. Therefore the following numerical results are preliminary for the spin configuration, but can be trusted for the YSR states, because they are not as prone to be influenced by finite size effects. Additionally, numerical accuracy limits the distinction between energy levels such that only differences of larger than order 10^{-10} give reliable results for groundstate configurations. Those short-comings are also visible in comparison to the analytically determined groundstate spin configurations.

Based on all previously presented results, the RKKY interaction of an unconventional superconductor can be understood as a mixture of the RKKY interaction in normal metals with SOC and superconductors. It exhibits analytically the same structure as the former, while numerically showing great resemblance with the latter. That might offer the possibility of a longer range control of more complex spin structure than in normal metals without any external fields. Furthermore, the groundstate of an unconventional superconductor is non-degenerate for short to middle distances as suggested by the numerical results, and therefore it allows for more accuracy than a normal

metal, which exhibits several possible groundstates due to its high symmetry.

To determine the groundstate spin configuration in a non-centrosymmetric superconductor experimentally and therefore testing the presented results, a spin-polarized scanning tunneling microscopy (STM) analysis of the material $CePt_3Si$ with added spin impurities can give further insights. Such experiments would also allow to study the predicted YSR states in more detail as previous experiments have already shown [75, 76]. The good resolution and spatial accuracy also allow to study spin configurations influenced by RKKY interaction explicitly.
On the analytical side, the next step would be to implement a self-consistent approach to the BdG methods. That would allow to study the influence of the RKKY interaction on the superconductor. Additionally, a more advanced theory for YSR states that involves the coupling of electrons to the impurities in l=2 channel [77] could be interesting to implement and study. Although, the combination of BdG and SWT allows to study more phenomena than just one by itself and consequently gives a complete mean-field picture of the studied system, it might also be of interest to compare the presented results that were obtained using SWT to results obtained by Green's functions, because they allow to see more details about YSR states and are easier to generalize to more SOC types.
Conclusively, the RKKY interaction in non-centrosymmetric superconductors is similar to the RKKY interaction in normal metals with SOC, but has a higher tunability and a more accurate groundstate for short to middle distances, when studied with a mean-field approach.

References

1. Ipcc, C. C. *et al.* Mitigation of climate change. Contribution of working group III to the fifth assessment report of the intergovernmental panel on climate change. *Cambridge University Press, Cambridge, United Kingdom and New York, NY, USA* (2014).
2. Masson-Delmotte, V. *et al.* Contribution of working group I to the sixth assessment report of the intergovernmental panel on climate change. *Climate Change 2021: The Physical Science Basis* (2021).
3. Balatsky, A. V., Vekhter, I. & Zhu, J.-X. Impurity-induced states in conventional and unconventional superconductors. *Reviews of Modern Physics* **78,** 373 (2006).
4. Wu, M.-K. *et al.* Superconductivity at 93 K in a new mixed-phase Y-Ba-Cu-O compound system at ambient pressure. *Physical review letters* **58,** 908 (1987).
5. Ghanbari, A. *RKKY interaction and coexistence with magnetism in superconducting systems* PhD thesis (2022), 171.
6. Aristov, D.N., Maleyev, S.V. & Yashenkin, A.G. RKKY interaction in layered superconductors with anisotropic pairing. *Zeitschrift für Physik B Condensed Matter.*
7. Mackenzie, A. P. & Maeno, Y. The superconductivity of Sr 2 RuO 4 and the physics of spin-triplet pairing. *Reviews of Modern Physics* **75,** 657 (2003).
8. Bauer, E. *et al.* Heavy fermion superconductivity and magnetic order in noncentrosymmetric C e P t 3 S i. *Physical review letters* **92,** 027003 (2004).
9. Tietjen, F. *What are superconductors?* 2023. https://www.youtube.com/watch?v=gDXhhQ5qWIY.
10. Tietjen, F. *Finjat97/Ma-RKKY-Linder: Masteroppgave about RKKY interaction in superconductors supervised by Jacob Linder* https://github.com/finjat97/MA-RKKY-Linder.git.
11. Rudermann, M.A. & Kittel, C. Indirect Exchange Coupling of Nuclear Magnetic Moments by Conduction Electrons. *physical review* (1954).
12. Yosida, K. Magnetic properties of Cu-Mn alloys. *Physical Review* **106,** 893 (1957).
13. Kasuya, T. A theory of metallic ferro-and antiferromagnetism on Zener's model. *Progress of theoretical physics* **16,** 45–57 (1956).
14. Black-Schaffer, A. M. RKKY coupling in graphene. *Physical Review B* **81,** 205416 (2010).
15. Valizadeh, Mohammad M. *Magnetic Interactions in the Spin-orbit Coupled Electron Gas* PhD thesis (University of Missouri, 2017).
16. Ashcroft, N. W. & Mermin, N. D. *Solid state physics* (Cengage Learning, 2022).
17. Kittel, C. & Fong, C.-y. *Quantum theory of solids* (Wiley, 1987).
18. Bruus, H. & Flensberg, K. *Many-body quantum theory in condensed matter physics: an introduction* (OUP Oxford, 2004).
19. Sudbø, Asle & Fossheim, Kristian. *Superconductivity - Physics and Applications* ISBN: 0-470-84452-3 (wiley, 2004).
20. Meissner, W. & Ochsenfeld, R. Ein neuer effekt bei eintritt der supraleitfähigkeit. *Naturwissenschaften* **21,** 787–788 (1933).
21. Abdul Hussein, A. A., Abdul Hussein, A. M. & Hasan, N. A. Study of the Properties of YBCO Superconductor Compound in Various Preparation Methods: A Short Review. *Journal of Applied Sciences and Nanotechnology* **3,** 65–79 (2023).

22. Otto, T. *Safety for Particle Accelerators* (Springer Nature, 2021).

23. Schwall, R. MRI-superconductivity in the marketplace. *IEEE Transactions on Magnetics* **23,** 1287–1293 (1987).

24. Ruede, F. *et al.* Highly sensitive and easy-to-use SQUID sensors. *Verhandlungen der Deutschen Physikalischen Gesellschaft* **43** (2008).

25. Sigrist, Manfred. *Introduction to Unconventional Superconductivity* ETH Zürich.

26. Mackenzie, A. & Maeno, Y. P-wave superconductivity. *Physica B: Condensed Matter* **280,** 148–153 (2000).

27. Onnes, H. K. *Further experiments with liquid helium. C. On the change of electric resistance of pure metals at very low temperatures etc. IV. The resistance of pure mercury at helium temperatures* in *KNAW, Proceedings* **13** (1911), 1910–1911.

28. Bardeen, J., Cooper, L. N. & Schrieffer, J. R. Theory of superconductivity. *Physical review* **108,** 1175 (1957).

29. Klam, Ludwig. *Unconventional properties of non-centrosymmetric superconductors* PhD thesis (2010). http://dx.doi.org/10.18419/opus-6766.

30. Griffiths, D. J. & Schroeter, D. F. *Introduction to quantum mechanics* (Cambridge university press, 2018).

31. Landau, L. D. & Lifshitz, E. M. *Quantum mechanics: non-relativistic theory* (Elsevier, 2013).

32. Johnson, M., Bloemen, P., Den Broeder, F. & De Vries, J. Magnetic anisotropy in metallic multilayers. *Reports on Progress in Physics* **59,** 1409 (1996).

33. Wu, M., Jiang, J. & Weng, M. Spin dynamics in semiconductors. *Physics Reports* **493,** 61–236 (2010).

34. Mills, D. L. & Rezende, S. M. Spin damping in ultrathin magnetic films. *Spin Dynamics in Confined Magnetic Structures II,* 27–59 (2003).

35. McGuire, T. & Potter, R. Anisotropic magnetoresistance in ferromagnetic 3d alloys. *IEEE Transactions on Magnetics* **11,** 1018–1038 (1975).

36. Nagaosa, N., Sinova, J., Onoda, S., MacDonald, A. H. & Ong, N. P. Anomalous hall effect. *Reviews of modern physics* **82,** 1539 (2010).

37. Dzyaloshinskii, I. *et al.* Thermodynamic theory of weak ferromagnetism in antiferromagnetic substances. *Sov. Phys. JETP* **5,** 1259–1272 (1957).

38. Moriya, T. Anisotropic superexchange interaction and weak ferromagnetism. *Physical review* **120,** 91 (1960).

39. Johnsen, L. G., Svalland, K. & Linder, J. Controlling the superconducting transition by rotation of an inversion symmetry-breaking axis. *Physical Review Letters* **125,** 107002 (2020).

40. Frigeri, P., Agterberg, D., Koga, A. & Sigrist, M. Superconductivity without Inversion Symmetry: MnSi versus C e P t 3 S i. *Physical review letters* **92,** 097001 (2004).

41. Rashba, E. Properties of semiconductors with an extremum loop. I. Cyclotron and combinational resonance in a magnetic field perpendicular to the plane of the loop. *Sov. Phys.-Solid State* **2,** 1109 (1960).

42. Aoki, D. *et al.* Unconventional superconductivity in UTe2. *Journal of Physics: Condensed Matter* **34,** 243002 (2022).

43. Shimizu, Y., Braithwaite, D., Aoki, D., Salce, B. & Brison, J.-P. Spin-triplet p-wave superconductivity revealed under high pressure in UBe 13. *Physical review letters* **122,** 067001 (2019).

44. Zhou, H. *et al.* Isospin magnetism and spin-polarized superconductivity in Bernal bilayer graphene. *Science* **375,** 774–778 (2022).

45. Chronister, A. M. *Nuclear Magnetic Resonance Investigations of the Highly Correlated Unconventional Superconductor Strontium Ruthenate* (University of California, Los Angeles, 2022).

46. Crépel, V. & Fu, L. Spin-triplet superconductivity from excitonic effect in doped insulators. *Proceedings of the National Academy of Sciences* **119,** e2117735119 (2022).

47. Yogi, M. *et al.* Evidence for novel pairing state in noncentrosymmetric superconductor CePt3Si: 29Si-NMR Knight shift study. *Journal of the Physical Society of Japan* **75,** 013709 (2006).

48. Tateiwa, N. *et al.* Novel pressure phase diagram of heavy fermion superconductor CePt3Si investigated by ac calorimetry. *Journal of the Physical Society of Japan* **74,** 1903–1906 (2005).

49. Bonalde, I. *et al.* Unusual behaviours and impurity effects in the noncentrosymmetric superconductor CePt3Si. *New Journal of Physics* **11,** 055054 (2009).

50. Samokhin, K., Zijlstra, E. & Bose, S. CePt 3 Si: An unconventional superconductor without inversion center. *Physical Review B* **69,** 094514 (2004).

51. Naskar, M., Mishra, P. K., Ash, S. & Ganguli, A. K. Superconductors with noncentrosymmetric crystal structures. *Bulletin of Materials Science* **44,** 1–16 (2021).

52. Wang, Y. *et al.* Phonon-mediated long-range attractive interaction in one-dimensional cuprates. *Physical Review Letters* **127,** 197003 (2021).

53. De Gennes, P.-G. & Pincus, P. A. *Superconductivity of metals and alloys* (CRC Press, 2018).

54. Zhu, J.-X. *Bogoliubov-de Gennes method and its applications* (Springer, 2016).

55. Cyrot, M. Ginzburg-Landau theory for superconductors. *Reports on Progress in Physics* **36,** 103 (1973).

56. Schrieffer, J. R. & Wolff, P. A. Relation between the anderson and kondo hamiltonians. *Physical Review* **149,** 491 (1966).

57. Bravyi, S., DiVincenzo, D. P. & Loss, D. Schrieffer–Wolff transformation for quantum many-body systems. *Annals of physics* **326,** 2793–2826 (2011).

58. Ambegaokar, V. & Griffin, A. Theory of the Thermal Conductivity of Superconducting Alloys with Paramagnetic Impurities. *Phys. Rev.* **137,** A1151–A1167. https://link.aps.org/doi/10.1103/PhysRev.137.A1151 (4A 1965).

59. Ghanbari, A. & Linder, J. RKKY interaction in a spin-split superconductor. *Physical Review B* **104,** 094527 (2021).

60. Shiba, H. Classical spins in superconductors. *Progress of theoretical Physics* **40,** 435–451 (1968).

61. Galitski, V. & Larkin, A. Spin glass versus superconductivity. *Physical Review B* **66,** 064526 (2002).

62. Samokhin, K. & Mineev, V. Gap structure in noncentrosymmetric superconductors. *Physical Review B* **77,** 104520 (2008).

63. Mukherjee, Soumya P. & Curnoe, Stephanie H. Superconductivity in non-centrosymmetric LaNiC2. *Physica C: Superconductivity* **499** (2014).

64. Imamura, H., Bruno, P. & Utsumi, Y. Twisted exchange interaction between localized spins embedded in a one-or two-dimensional electron gas with Rashba spin-orbit coupling. *Physical Review B* **69,** 121303 (2004).

65. Gong, M., Qian, Y., Yan, M., Scarola, V. W. & Zhang, C. Dzyaloshinskii-Moriya interaction and spiral order in spin-orbit coupled optical lattices. *Scientific Reports* **5,** 1–8 (2015).

66. Ikegaya, S., Rui, W. B., Manske, D. & Schnyder, A. P. Tunable Majorana corner modes in noncentrosymmetric superconductors: Tunneling spectroscopy and edge imperfections. *Physical Review Research* **3.** https://doi.org/10.1103%2Fphysrevresearch.3.023007 (2021).

67. Ghosh, S. K. *et al.* Quantitative theory of triplet pairing in the unconventional superconductor LaNiGa 2. *Physical Review B* **101,** 100506 (2020).

68. Andreev, A. The thermal conductivity of the intermediate state in superconductors (1964).

69. De Gennes, P. & Saint-James, D. Elementary excitations in the vicinity of a normal metal-superconducting metal contact. *Phys. Letters* **4** (1963).

70. Blonder, G., Tinkham, m. M. & Klapwijk, k. T. Transition from metallic to tunneling regimes in superconducting microconstrictions: Excess current, charge imbalance, and supercurrent conversion. *Physical Review B* **25,** 4515 (1982).

71. Eschrig, M. Spin-polarized supercurrents for spintronics: a review of current progress. *Reports on Progress in Physics* **78,** 104501 (2015).

72. Eschrig, M., Iniotakis, C. & Tanaka, Y. Theoretical aspects of Andreev spectroscopy and tunneling spectroscopy in non-centrosymmetric superconductors: a topical review. *arXiv preprint arXiv:1001.2486* (2010).

73. Kaladzhyan, V., Bena, C. & Simon, P. Characterizing p-wave superconductivity using the spin structure of Shiba states. *Physical Review B* **93,** 214514 (2016).

74. Kim, Y., Zhang, J., Rossi, E. & Lutchyn, R. M. Impurity-induced bound states in superconductors with spin-orbit coupling. *Physical review letters* **114,** 236804 (2015).

75. Yazdani, A., Jones, B., Lutz, C., Crommie, M. & Eigler, D. Probing the local effects of magnetic impurities on superconductivity. *Science* **275,** 1767–1770 (1997).

76. Heinrich, B. W., Pascual, J. I. & Franke, K. J. Single magnetic adsorbates on s-wave superconductors. *Progress in Surface Science* **93,** 1–19 (2018).

77. Von Oppen, F. & Franke, K. J. Yu-Shiba-Rusinov states in real metals. *Physical Review B* **103,** 205424 (2021).

A RKKY Caused Band Splitting in Superconductor

As explained in detail for the normal metal in Sec. 4, an increase in the RKKY interaction strength, leads to a split in energy bands at the impurity sites. This change influences the LDOS at the sites between the impurities, too, which leads to a shift in free energy. Since the shift depends on the relative orientation of the impurity spins, its leads to a shift from favored parallel to favored anti-parallel alignment of the impurity spins. That is visible in the following plots and the exact same phenomenon as in the normal metal.
Therefore the RKKY interaction strength in superconducting systems is again restricted to $J \in [0, 4t)$.

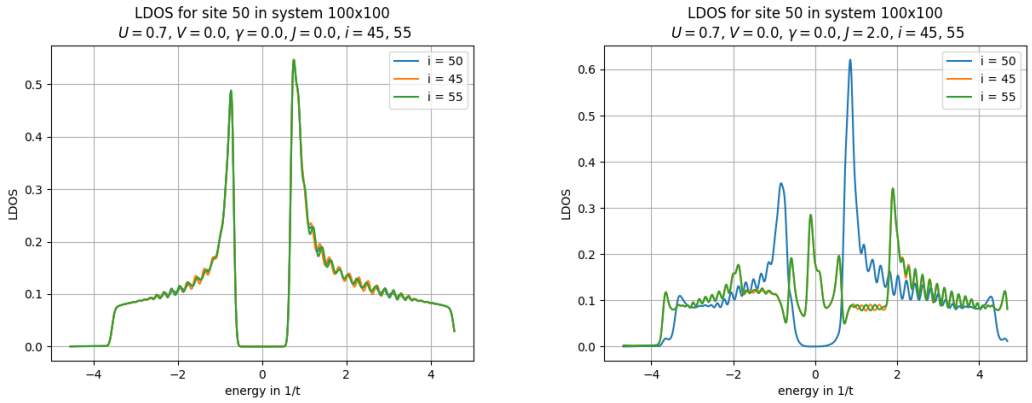

(a) Spin structure for SC with RKKY $J = 2$ (no SOC) (b) Spin structure for SC with RKKY $J = 5$ (no SOC)

Figure 26: Bands are splitting

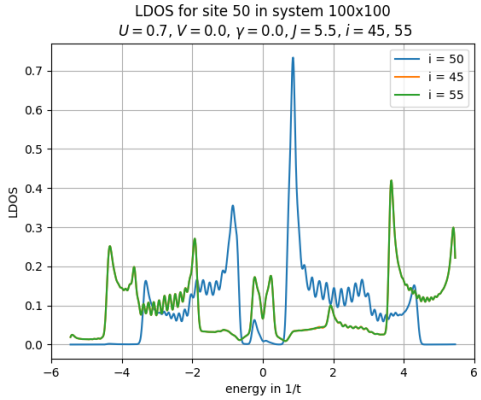

(a) Spin structure for SC with RKKY $J = 2$, with SOC

Figure 27: Bands do not overlap any longer

B Basis Transformation Coefficient

arrows ($\uparrow$, $\downarrow$) correspond to spin (up, down), while + and − correspond to positive and negative helicity, respectively

$$H_{RKKY} = \sum_{\substack{i,k,k' \\ \lambda,\lambda',\sigma,\sigma'}} \frac{J}{N} \frac{e^{i(k-k')r_i}}{2\sqrt{|\gamma_k||\gamma_{k'}|}} \begin{bmatrix} S_z & (S_x - iS_y)\frac{\gamma_{k',x}+i\gamma_{k',y}}{|\gamma_{k'}|} \\ (S_x+iS_y)\frac{\gamma_{k,x}-i\gamma_{k,y}}{|\gamma_k|} & -S_z \frac{(\gamma_{k',x}+i\gamma_{k',y})(\gamma_{k,x}-i\gamma_{k,y})}{|\gamma_k||\gamma_{k'}|} \end{bmatrix}_{\sigma,\sigma'} \tag{B.1}$$
$$\times \begin{bmatrix} \sqrt{|\gamma_k|+\sigma\gamma_{k,z}}\sqrt{|\gamma_{k'}|+\sigma'\gamma_{k',z}} & \sigma'\sqrt{|\gamma_k|+\sigma\gamma_{k,z}}\sqrt{|\gamma_{k'}|-\sigma'\gamma_{k',z}} \\ \sigma\sqrt{|\gamma_k|-\sigma\gamma_{k,z}}\sqrt{|\gamma_{k'}|+\sigma'\gamma_{k',z}} & \sigma\sigma'\sqrt{|\gamma_k|-\sigma\gamma_{k,z}}\sqrt{|\gamma_{k'}|-\sigma'\gamma_{k',z}} \end{bmatrix}_{\lambda,\lambda'} b^\dagger_{k,\lambda} b_{k',\lambda'}$$

for Rashba-type SOC the expression simplifies to

$$H_{RKKY} = \sum_{\substack{i,k,k' \\ \lambda,\lambda',\sigma,\sigma'}} \frac{J}{N} \frac{e^{i(k-k')r_i}}{2\sqrt{|\gamma_k||\gamma_{k'}|}} \begin{bmatrix} S_z & (S_x - iS_y)\frac{\gamma_{k',x}+i\gamma_{k',y}}{|\gamma_{k'}|} \\ (S_x+iS_y)\frac{\gamma_{k,x}-i\gamma_{k,y}}{|\gamma_k|} & -S_z \frac{(\gamma_{k',x}+i\gamma_{k',y})(\gamma_{k,x}-i\gamma_{k,y})}{|\gamma_k||\gamma_{k'}|} \end{bmatrix}_{\sigma,\sigma'} \tag{B.2}$$
$$\times \sqrt{|\gamma_k||\gamma_{k'}|} \begin{bmatrix} 1 & \sigma' \\ \sigma & \sigma\sigma' \end{bmatrix}_{\lambda,\lambda'} b^\dagger_{k,\lambda} b_{k',\lambda'}$$
$$= \sum_{\substack{i,k,k' \\ \lambda,\lambda',\sigma,\sigma'}} \frac{J}{N} \frac{e^{i(k-k')r_i}}{2} \Bigg[S_z - \lambda\lambda' S_z \frac{(\gamma_{k',x}+i\gamma_{k',y})(\gamma_{k,x}-i\gamma_{k,y})}{|\gamma_k||\gamma_{k'}|}$$
$$+\lambda'(S_x - iS_y)\frac{\gamma_{k',x}+i\gamma_{k',y}}{|\gamma_{k'}|} + \lambda(S_x+iS_y)\frac{\gamma_{k,x}-i\gamma_{k,y}}{|\gamma_k|}\Bigg]$$

C Commutator

The calculation of the following commutator is based on the following identity of commutator and anti-commutator for four arbitrary operators A, D, C, D:

$$[AB, CD] = AD\{B, C\} - BD\{A, C\} + CA\{B, D\} - CB\{A, D\} \tag{C.1}$$

The calculation are performed for a non-centrosymmetric superconductor and the limit of non-superconductivity can be taken. With using the anti-commutation relations of the $d^{[\dagger]}$-operators, this commutator reads:

$$\begin{aligned}
[S, H_0] = \sum_{i,k,k',\lambda,\lambda',q,\beta} & \Big[A_{i,k,k',\lambda,\lambda'} d^\dagger_{k,\lambda} d_{k',\lambda'} + B_{i,k,k',\lambda,\lambda'} d_{-k,\lambda} d^\dagger_{-k',\lambda'} \\
& + C_{i,k,k',\lambda,\lambda'} d_{-k,\lambda} d_{k',\lambda'} + D_{i,k,k',\lambda,\lambda'} d^\dagger_{k,\lambda} d^\dagger_{-k',\lambda'}, E_{q,\beta} d^\dagger_{q,\beta} d_{q,\beta}\Big] \\
= \sum_{i,k,k',\lambda,\lambda',q,\beta} & A_{i,k,k',\lambda,\lambda'} E_{q,\beta} \left(d^\dagger_{k,\lambda} d_{q,\beta} \delta_{q,k'} \delta_{\beta,\lambda'} - d^\dagger_{q,\beta} d_{k',\lambda'} \delta_{q,k} \delta_{\beta,\lambda}\right) \\
& + B_{i,k,k',\lambda,\lambda'} E_{q,\beta} \left(d^\dagger_{q,\beta} d_{-k,\lambda} \delta_{q,-k'} \delta_{\beta,\lambda'} - d^\dagger_{-k',\lambda'} d_{q,\beta} \delta_{q,-k} \delta_{\beta,\lambda}\right) \\
& + C_{i,k,k',\lambda,\lambda'} E_{q,\beta} \left(d_{-k,\lambda} d_{q,\beta} \delta_{q,k'} \delta_{\beta,\lambda'} - d_{k',\lambda'} d_{q,\beta} \delta_{q,-k} \delta_{\beta,\lambda}\right) \\
& + D_{i,k,k',\lambda,\lambda'} E_{q,\beta} \left(d^\dagger_{q,\beta} d^\dagger_{k,\lambda} \delta_{q,-k'} \delta_{\beta,\lambda'} - d^\dagger_{q,\beta} d_{-k',\lambda'} \delta_{q,k} \delta_{\beta,\lambda}\right) \\
= \sum_{i,k,k',\lambda,\lambda'} & A_{i,k,k',\lambda,\lambda'} \left(E_{k',\lambda'} - E_{k,\lambda}\right) d^\dagger_{k,\lambda} d_{k',\lambda'} + B_{i,k,k',\lambda,\lambda'} \left(E_{-k',\lambda'} - E_{-k,\lambda}\right) d_{-k,\lambda} d^\dagger_{-k',\lambda'} \\
& + C_{i,k,k',\lambda,\lambda'} \left(E_{k',\lambda'} - E_{-k,\lambda}\right) d_{-k,\lambda} d_{k',\lambda'} + D_{i,k,k',\lambda,\lambda'} \left(E_{-k',\lambda'} + E_{k,\lambda}\right) d^\dagger_{k,\lambda} d^\dagger_{-k',\lambda'}
\end{aligned} \tag{C.2}$$

D Expectation Value of Effective Hamiltonian

It is used that $\langle H_0 \rangle = E_0$ is the expectation-value in the groundstate of the unperturbed system and $f(x)$ is the Fermi-Dirac distribution. λ, λ' are helicity indices and k, k' are momenta. In addition, i, j are the positions of the impurity spins, which are introduced with the RKKY-interaction.

$$\begin{aligned}\langle H_e f f \rangle = E_0 + \sum_{i,j,k,k',\lambda,\lambda'} & A_{i,k,k',\lambda,\lambda'} a_{j,k',k,\lambda',\lambda} \left(f(E_{k,\lambda}) - f(E_{k',\lambda'})\right) \\ & - A_{i,k,k',\lambda,\lambda'} b_{j,-k,-k',\lambda,\lambda'} \left(f(E_{k,\lambda}) - f(E_{k',\lambda'})\right) \\ & - B_{i,k,k',\lambda,\lambda'} b_{j,k',k,\lambda',\lambda} \left(f(E_{-k,\lambda}) - f(E_{-k',\lambda'})\right) \\ & + B_{i,k,k',\lambda,\lambda'} a_{j,-k,-k',\lambda,\lambda'} \left(f(E_{-k,\lambda}) - f(E_{-k',\lambda'})\right) \\ & - C_{i,k,k',\lambda,\lambda'} d_{j,k',k,\lambda',\lambda} \left(f(E_{-k,\lambda}) + f(E_{k',\lambda'})\right) \\ & - C_{i,k,k',\lambda,\lambda'} d_{j,-k,-k',\lambda,\lambda'} \left(f(E_{-k,\lambda}) + f(E_{k',\lambda'})\right) \\ & + D_{i,k,k',\lambda,\lambda'} c_{j,k',k,\lambda',\lambda} \left(f(E_{k,\lambda}) + f(E_{-k',\lambda'})\right) \\ & - D_{i,k,k',\lambda,\lambda'} c_{j,-k,k',\lambda,\lambda'} \left(f(E_{k,\lambda}) + f(E_{-k',\lambda'})\right)\end{aligned} \tag{D.1}$$

where the coefficients a, b, c, and d are defined as

$$\begin{aligned} a_{j,k,k',\lambda,\lambda'} &= \eta^\dagger_{k,\lambda} \eta_{k',\lambda'} \\ b_{j,k,k',\lambda,\lambda'} &= \nu_{k,\lambda} \nu^\dagger_{k',\lambda'} \\ c_{j,k,k',\lambda,\lambda'} &= \nu_{k,\lambda} \eta_{k',\lambda'} \\ d_{j,k,k',\lambda,\lambda'} &= \eta^\dagger_{k,\lambda} \nu^\dagger_{k',\lambda'} \end{aligned}$$

E Analytical Groundstate Spin Configuration

The spin configuration for a normal metal and a superconductor, each with SOC, is determined analytically and the following graphs depict the spins in 3d.

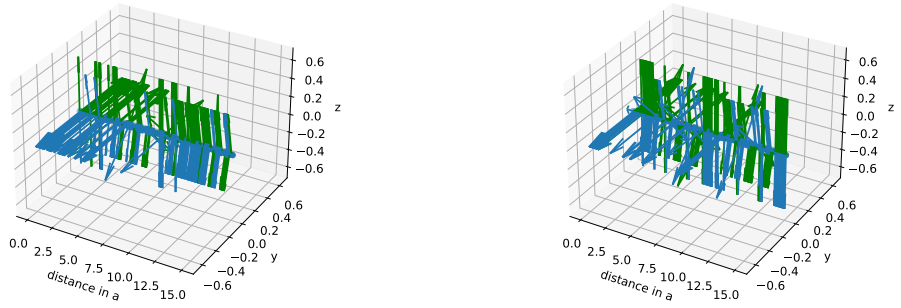

(a) weak SOC

(b) strong SOC

Figure 28: Normal metal with SOC, analytical

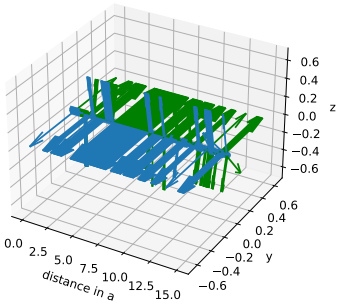

(a) singlet

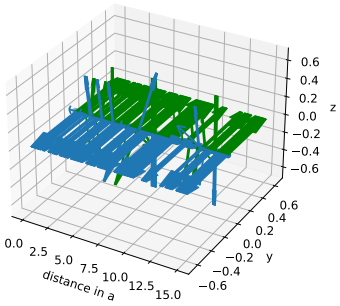

(b) triplet

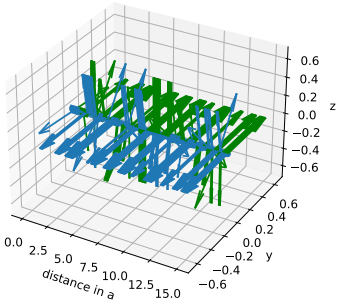

(c) mixed

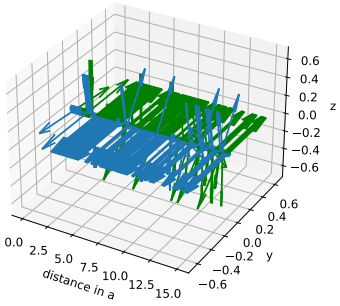

(d) mixed

Figure 29: Superconductor with SOC, analytical

F Poster

This poster was presented on the DPG March Meeting 2023 in Dresden as part of the poster session on low temperature physics. Thank you to the Department of Physics at NTNU for covering my travel expenses.

RKKY interaction in non-centrosymmetric superconductors

FINJA TIETJEN, JACOB LINDER

Acknowledgements

The design of this poster was inspired by Dr. Andreas T. G. Janssønn.

Previous important work on RKKY in conventional superconductors was done by Dr. Atousa Ghanbari.

Motivation

When RKKY interaction between two impurity spins in known materials is understood, one can determine properties of new materials based on RKKY interaction there. Additionally, the impurity spins can in turn be controlled by the material around them resulting in controllable information bits on atomic scale. Recent interest in unconventional superconductors leads to increased interest of RKKY in superconductors without inversion symmetry, where RKKY has not been studied yet.

Method

The analytical solution via Schrieffer-Wolff transformation is complemented by the numerical solution via Bogoliuobov - de Gennes formalism and exact diagonalization.

$$H = -t \sum_{\langle i,j\rangle,\sigma} c^\dagger_{i,\sigma} c_{j,\sigma} - \mu \sum_{i,\sigma} c^\dagger_{i,\sigma} c_{i,\sigma} + \sum_{\sigma,\sigma',\langle i,j\rangle} \vec{\gamma}\cdot\vec{n}\left(\vec{d}_{i,j}\times\vec{\sigma}_{\sigma,\sigma'}\right) c^\dagger_{i,\sigma} c_{j,\sigma'} - \sum_{\langle i,j\rangle,\sigma,\sigma'} V^{\sigma,\sigma'}_{ij} c^\dagger_{i,\sigma} c_{i,\sigma} c^\dagger_{j,\sigma'} c_{j,\sigma'}$$

tight binding Hamiltonian with spin orbit coupling and attractive electron interaction

Result

$$\langle H_{eff}\rangle = \sum \left[J\vec{S}_i\cdot\vec{S}_j + \vec{I}\,\vec{S}_i\cdot\vec{S}_j + D_x(S_{i,y}S_{j,z} - S_{i,z}S_{j,y}) + D_y(S_{i,z}S_{j,x} - S_{i,x}S_{j,z}) + \vec{S}_i\cdot\overleftrightarrow{\Gamma}\cdot\vec{S}_j \right] + E_0$$

The effective Hamiltonian contains Heisenberg, Ising, Dzyaloshinskii-Moriya and further spin interactions.
The coefficients depend on the spin orbit coupling strength and energy distribution of the system.

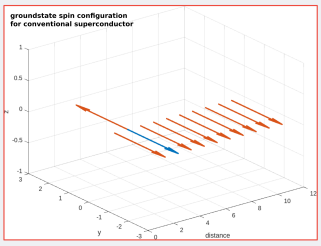

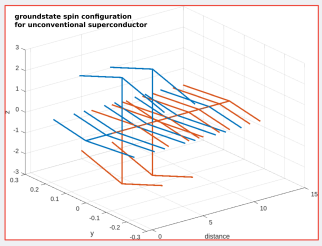

Conclusion

The analytically obtained spin structure suggests additional terms in an unconventional superconductor compared to a normal metal with spin-orbit-coupling and a conventional superconductor.
The exact numerical solution agrees with the analytical result and shows the existence of bound states at the impurities.

Further insights will be obtained by solving the gap equation selfconsistently.

contact email: finjat@stud.ntnu.no

Center for Quantum Spintronics
DEPARTMENT OF PHYSICS, NTNU, NO-7491 TRONDHEIM, NORWAY

G EinsteinSlam

The EinsteinSlam took place during the DPG SKM Spring Meeting 2023 in Dresden. It was part of the evening program and attracted an audience of around 800 people. There were five participants that each talked about their most resent research, after having three coaching sessions about the science slam together. The audience voted the winner with their applause, and I got second place. The two following pictures are to illustrate the style of the presentation, while a video of the science slam is going to be uploaded by DPG to YouTube.

(a) Finja (me)

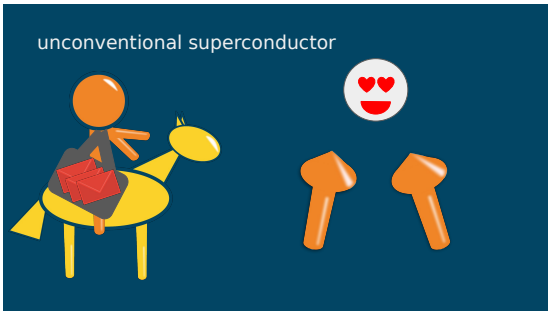

(b) part of the presentation

Figure 30: Impressions from the EinsteinSlam of the DPG 2023.

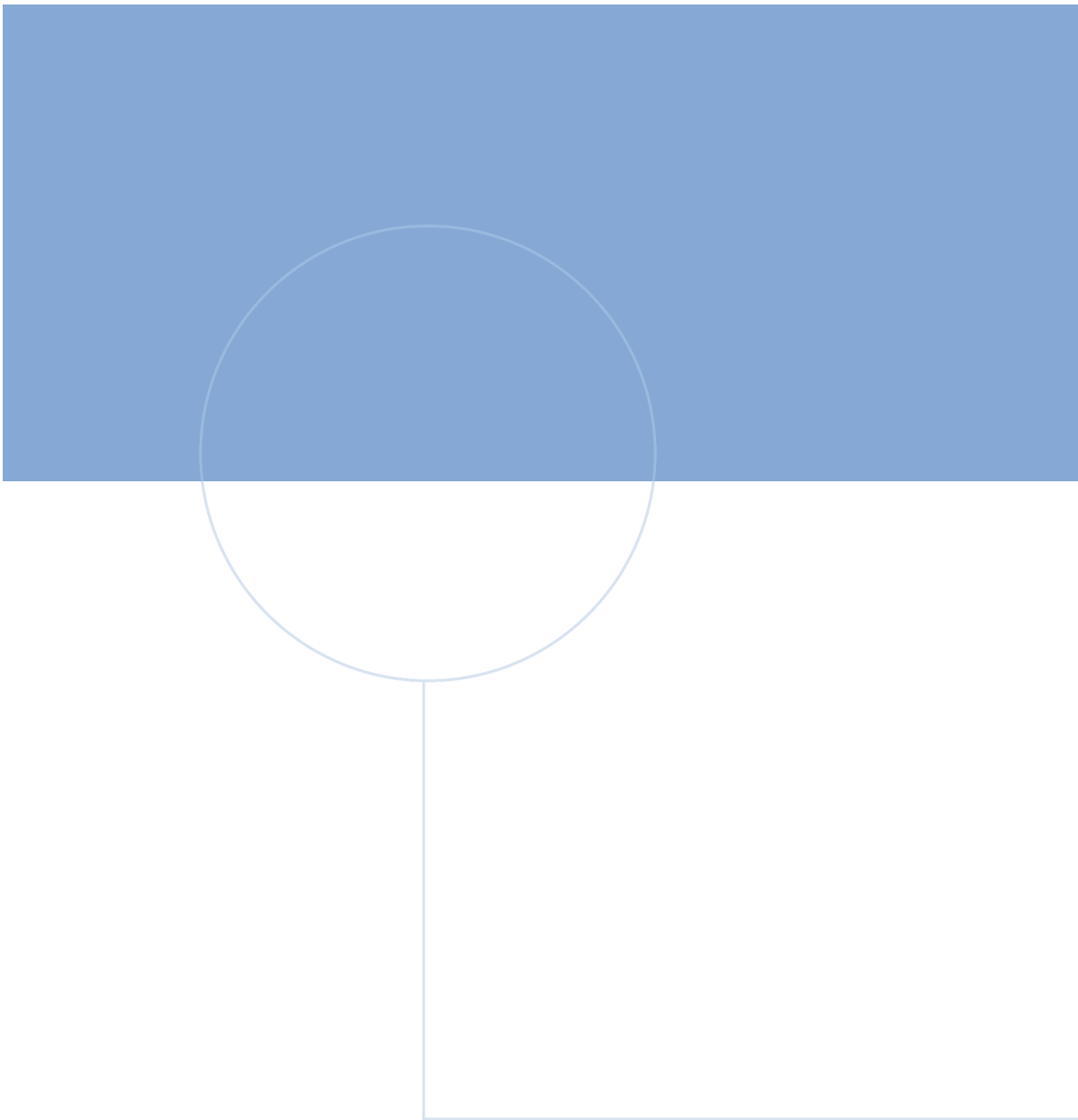

NTNU

Norwegian University of
Science and Technology